BERICHTE
aus dem MARUM und dem Fachbereich Geowissenschaften der Universität Bremen

No. 297

Kopf, A., Asshoff, K., Belke-Brea, M., Bergenthal, M., Bohrmann, G., Bräunig, A., Düssmann, R., Feseker, T., Fleischmann, T., Franke, P.D., Geprägs, P., Hammerschmidt, S., Heesemann, B., Herschelmann, O., Hüpers, A., Ikari, M.J., Kaszemaik, K.M., Kaul, N., Kimura, T., Kitada, K., Klar, S., Lange, M., Madison, M., Mai, A.H., Noorlander, C., Pape, T., Rehage, R., Reuter, C., Reuter, M., Rosiak, U.D., Saffer, D.M., Schmidt, W., Seiter, C., Spiesecke, U., Stachowski, A., Takanori, O., Tryon, M., Vahlenkamp, M., Wei, J., Wiemer, G., Wintersteller, P., Zarrouk, M.K.

Report and preliminary results of R/V SONNE cruise SO222

MEMO

MeBo drilling and in situ Long-term Monitoring in the Nankai Trough accretionary complex, Japan

Leg A: Hong Kong, PR China, 09.06.2012 – Nagoya, Japan, 30.06.2012
Leg B: Nagoya, Japan, 04.07.2012 – Pusan, Korea, 18.07.2012

Berichte, MARUM – Zentrum für Marine Umweltwissenschaften, Fachbereich Geowissenschaften, Universität Bremen, No. 297, 121 pages, Bremen 2013

ISSN 2195-9633

Berichte aus dem MARUM und dem Fachbereich Geowissenschaften der Universität Bremen

published by

MARUM – Center for Marine Environmental Sciences
Leobener Strasse, 28359 Bremen, Germany
www.marum.de

and

Fachbereich Geowissenschaften der Universität Bremen
Klagenfurter Strasse, 28359 Bremen, Germany
www.geo.uni-bremen.de

The "Berichte aus dem MARUM und dem Fachbereich Geowissenschaften der Universität Bremen" appear at irregular intervals and serve for the publication of cruise, project and technical reports arising from the scientific work by members of the publishing institutions.

Citation:

Kopf, A., Asshoff, K., Belke-Brea, M., Bergenthal, M., Bohrmann, G., Bräunig, A., Düssmann, R., Feseker, T., Fleischmann, T., Franke, P.D., Geprägs, P., Hammerschmidt, S., Heesemann, B., Herschelmann, O., Hüpers, A., Ikari, M.J., Kaszemaik, K.M., Kaul, N., Kimura, T., Kitada, K., Klar, S., Lange, M., Madison, M., Mai, A.H., Noorlander, C., Pape, T., Rehage, R., Reuter, C., Reuter, M., Rosiak, U.D., Saffer, D.M., Schmidt, W., Seiter, C., Spiesecke, U., Stachowski, A., Takanori, O., Tryon, M., Vahlenkamp, M., Wei, J., Wiemer, G., Wintersteller, P., Zarrouk, M.K. Report and preliminary results of R/V SONNE cruise SO222. MEMO: MeBo drilling and in situ Long-term Monitoring in the Nankai Trough accretionary complex, Japan. Leg A: Hong Kong, PR China, 09.06.2012 – Nagoya, Japan, 30.06.2012. Leg B: Nagoya, Japan, 04.07.2012 – Pusan, Korea, 18.07.2012. Berichte, MARUM – Zentrum für Marine Umweltwissenschaften, Fachbereich Geowissenschaften, Universität Bremen, No. 297, 121 pages. Bremen, 2013. ISSN 2195-9633.

An electronic version of this report can be downloaded from:
http://nbn-resolving.de/urn:nbn:de:gbv:46-MARUM9

Printed copies can be ordered from: Monika Bachur, MARUM – Center for Marine Environmental Sciences, University of Bremen, Leobener Strasse, 28359 Bremen, Germany
Phone: (49) 421 218-65516 - Fax: (49) 421 218-9865516 - e-mail: MBachur@marum.de

For editorial concerns please contact reports@marum.de

Table of Contents

Personnel aboard R/V *Sonne*

Leg A:

Dr. Achim Kopf (MARUM), Chief scientist
Markus Bergenthal (MARUM), MeBo
Uwe Rosiak (MARUM), MeBo
Kai Kaszemeik (MARUM), MeBo
Steffen Klar (MARUM), MeBo
Christian Seiter (MARUM), MeBo
Werner Schmidt (MARUM), MeBo
Ralf Düssmann (MARUM), MeBo
Adrian Stachowksi (MARUM), MeBo
Uli Spiesecke (MARUM), MeBo
Cornelis Noorlander (MARUM), MeBo
Matthias Lange (MARUM), CPT
Dr. Matt Ikari (MARUM), Physical properties
Dr. Andre Hüpers (MARUM), Sedimentology
Maximilian Vahlenkamp (Univ. Bremen), Sedimentology
Takanori Ojima (AORI, Univ. Tokyo), Sedimentology
Dr. Norbert Kaul (Univ. Bremen), Heat flow
Bernd Heesemann (Univ. Bremen), Heat flow
Jiangong Wei (Univ. Bremen), Core lab, IR imagery
Timo Fleischmann (MARUM), Core Lab, Observatories
Sebastian Hammerschmidt (MARUM), Core Lab, Observatories
Dr. Thomas Pape (Univ. Bremen), Gas chemistry, gas hydrates
Patrizia Geprägs (Univ. Bremen), Gas chemistry, gas hydrates
Dr. Michael Tryon (SCRIPPS), Inorganic geochemistry, Flowmeters
Anja Bräunig (Univ. Bremen), Inorganic/organic geochemistry

Leg B:

Dr. Achim Kopf (MARUM), Chief scientist
Christian Reuter (MARUM), ROV
Christian Seiter (MARUM), ROV
Michael Reuter (MARUM), ROV
Philipp Franke (MARUM), ROV
Oliver Herschelmann (MARUM), ROV
Marcel Zarrouk (MARUM), ROV
Ralf Rehage (MARUM), ROV
HoangAnh Mai (MARUM), ROV
Maximilian Vahlenkamp (Univ. Bremen), Sedimentology
Maria Belke-Brea (MARUM), CPT, Sedimentology
Timo Fleischmann (MARUM), Core Lab, Observatories
Sebastian Hammerschmidt (MARUM), Core Lab, Observatories
Dr. Tomas Feseker (Univ. Bremen), Heat flow
Kira Asshoff (Univ. Bremen), Heat flow
Toshinori Kimura (JAMSTEC) Observatories, DONET
Dr. Kazuya Kitada (JAMSTEC) Observatories, DONET
Patrizia Geprägs (Univ. Bremen), Gas chemistry
Dr. Paul Wintersteller (Univ. Bremen), Mapping
Dr. Gerhard Bohrmann (MARUM), Gas flares, gas hydrates
Melissa Madison (UCA), Organic geochemistry
Anja Bräunig (Univ. Bremen), Inorganic chemistry

Participating institutions

DFG-Excellence Cluster MARUM
University Bremen
Leobener Strasse
28359 Bremen --- GERMANY

Univ. Bremen,
Department of Geosciences
Klagenfurter Strasse
28359 Bremen --- GERMANY

Earthquake and Tsunami Research Project for Disaster Prevention
Japan Agency for Marine-Earth Science and Technology (JAMSTEC)
2-15 Natsushima-cho
Yokosuka, 237-0061 --- JAPAN

Ocean Research Institute
The University of Tokyo
1-15-1 Minamidai
Nakano, Tokyo 164-8639 --- JAPAN

SCRIPPS Institution of Oceanography
University of California, San Diego
9500 Gilman Drive
92093 La Jolla --- USA

Abstract

Approximately 90% of the seismic moment on Earth is released in often devastating subduction zone earthquakes (EQs). In the Integrated Ocean Drilling Program (IODP), the study of seismogenesis along an active convergent margin plays a key role in the form of a multi-expedition effort named "NanTroSEIZE" (Nankai Trough Seismogenic Zone Experiment). To date, eight expeditions (IODP Expeditions 314-316, 319, 322, 326, 332-333) drilled 12 sites along a transect from the incoming plate across the frontal accretionary prism to the forearc basin. Two holes are currently equippe dwith long-term instruments (C0002, C0010). The project Sonne SO222 MEMO, **Me**Bo drilling & in situ long-term **Mo**nitoring offshore Japan (Nankai Trough Accretionary Prism), aims to extend the long-term monitoring efforts to active mud volcanoes in the northern Kumano Basin. These features carry gas hydrates and deep-seated fluids, most likely tapping into the seismogenic zone at a depth of several km below seafloor, and are also overlying an area of high strains and a locked plate boundary-thrust. Cruise SO222 sampled both mud volcanoes and background sediments and installed long-term monitoring devices in key locations.

The main results of the two legs SO222A and SO222B include:

- The discovery of 5 new, previously not reported mud volcanoes, so that there are 13 MVs in the Kumano Basin now;
- Gas hydrate presence in many of the features;
- Enigmatic pore fluid signatures with high B, Li and Sr, but low Mg in the pore waters, suggesting deep-seated fluid origin;
- Successful installation of of 4 MeBo borehole observatories in a total of six holes drilled in appx. 2 km water depth;
- Successful installation of six CAT flowmeters on the most active mud volcanoes in the Kumano field;
- Successful operation on so-called MeBoCORK observatories with ROV Quest;
- Recovery of gravity and MeBo cores as well as TV grab that contain a suite of clasts in the mud breccias that span the range from soft to hard rocks and cover all grain size classes of sedimentary rocks, but also comprise magmatic materials and deformed rocks;
- Gas composition attests a biogenic origin for the majority of the mud domes visited;
- Heat flow data attest active flow in at least some of the mud domes; however,
- No active venting was neither observed by acoustic techniques nor by direct observation with ROV or TV-grab.

2. Introduction

The Nankai Trough, Japan (Fig. 1A) is one of the best-studied subduction systems on Earth, and has emerged as one key focus of earthquake research since NanTroSEIZE was set up. We here reiterate the scientific rationale of CORK (Circulation Obviation Retrofit Kit) instruments, and then introduce the regional geology (3.1), the results from NanTroSEIZE drilling operations (3.2), and the main objectives of the BMBF-funded MEMO project using RV *Sonne* during expedition SO222 (3.3), where simple CORK instruments were deployed.

Long-term *in situ* hydrologic and geophysical measurements in borehole observatories have been recognized as a key element in the IODP Initial Science Plan [*IODP*, 2001], and are also mentioned prominently in the new IODP Science Plan "Discovering Earth's Hidden Frontiers through Scientific Ocean Drilling" for 2013-2023. The time series of data provided by long-term observatories are critical toward understanding strain and fault slip at plate boundaries, the fluxes of volatiles and chemical budgets at subduction systems, and the role of fluids in mechanical, chemical, biological, and thermal processes beneath the seafloor. Over the past several years, long-term observations of pore pressure, temperature, and fluid chemistry in sealed ODP/IODP boreholes have produced a wealth of data that have significantly advanced our understanding of subseafloor deformation and hydrogeology. For example, monitoring of pore pressure and temperature coupled with continuous sampling of pore waters for chemical analysis have provided constraints on fluid flow systems associated with globally significant transport of heat and solutes [e.g., *Davis & Becker*, 1994, 2001, 2002; *Becker et al*., 2004; *Fisher et al*., 1997]. Direct measurement of ambient pore pressure attested the key role of fluids in impacting fault mechanical behaviour [e.g., *Foucher et al*., 1997; *Becker et al*., 1997]. The analysis of tidally-driven pressure changes has provided a powerful means to quantify formation and fluid elastic and hydrologic properties in many settings – and potentially to resolve changes in formation properties associated with strain events [e.g., *Becker & Davis*, 2003].

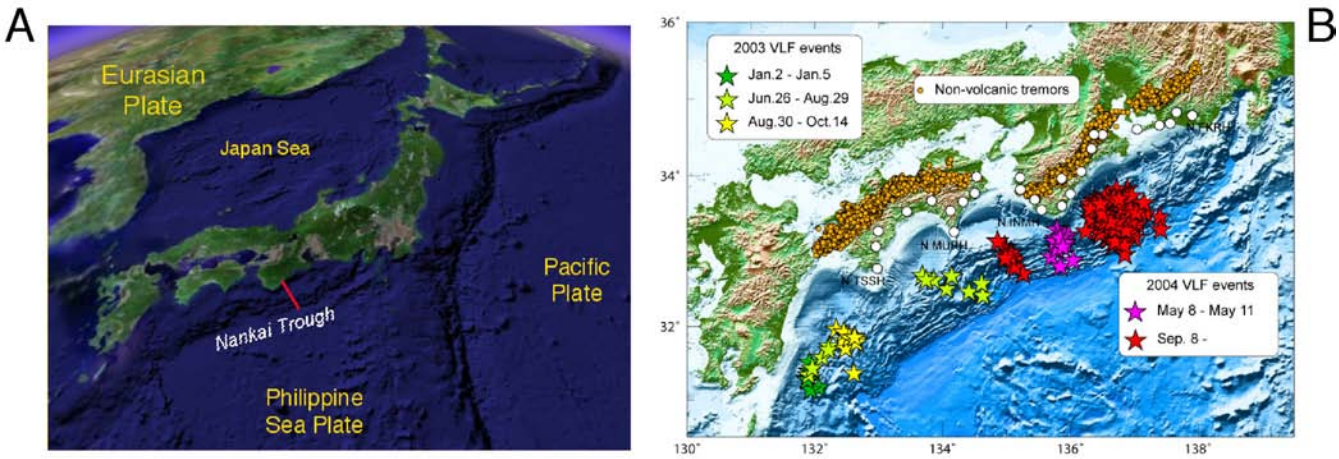

Figure 1: **A**) Satellite view of the island of Japan with the Nankai Trough drilling area marked. **B**) Locations of VLF earthquakes (M 3.5-4.4) in the Nankai Trough in 2003-2004 [from *Obara & Ito*, 2005]. Focal mechanisms and locations for the events off Kii Peninsula are consistent with reverse faulting within the accretionary wedge.

Recent observations of fluid pressure transients have been linked to both coseismic and interseismic deformation [*Husen & Kissling*, 2001; *Davis et al*., 2001, 2006], highlighting the potential to characterize patterns of strain accumulation and release through the seismic cycle. These transients cover a wide range of temporal scales and reinforce seismological and geodetic observations that indicate e.g., episodic slow slip [e.g., *Rogers & Dragert*, 2003; *Obara et al*., 2004], aseismic creep [*Davis et al*., 2006], and earthquakes with an anomalously large low-frequency source component [e.g., *Obara & Ito*, 2005; *Obara et al*., 2004; *Ito & Obara*, 2006] (see also Fig. 1B). Seafloor observations of fluid expulsion have also documented links between subduction zone seismicity and hydrologic processes in the shallow subsurface [*Brown et al*., 2005]. Although such studies have locally provided exciting *in situ* observations, a quantitative understanding of the relationship between fault slip processes and associated strain, pore pressure, and fluid flow in the surrounding sediment (and crust) has been lacking both detail and wide spatial coverage. To overcome these deficits, a network of collocated observatories for pore pressure, seismicity, and strain is needed [*Davis et al*., 2006].

When translated to the Nankai Trough subduction zone (Fig. 2A), two CORK systems are presently in operation along the Muroto transect, Central Nankai (Sites 808 and 1173, open circles). In addition, two borehole observatories have very recently been installed along the Kii transect (Fig. 2B, Sites C0002 and C0010 – for details see below). Although the proposed new observatories to be installed with the MeBo drill rig are not part of the NanTroSEIZE operations *sensu stricto*, they aim at understanding the hydrologic behavior of the Japan subduction megathrust and use mud volcanoes juxtaposing deep-seated faults. Multi-phase, multi-expedition drilling off Cape Kii extends from the Kumano forearc basin all the way out to the subducting Philippine Sea Plate, and overlies a zone of coseismic slip along the plate boundary during the 1944 Tonankai M 8.2 earthquake, as defined by seismic waveform and tsunami inversions [*Tanioka & Satake*, 2001; *Ichinose et al*., 2003; *Kikuchi et al*., 2003] (Fig. 1B, shaded area). The series of drillsites serves to (i) characterize the subduction inputs (including basement) and penetrate both the plate boundary thrust and a mega-splay fault initiating from it in several locations and depth levels (see Fig. 2). Pore pressure monitoring in the observatories of some selected drill sites (C0002, C0009, C0010 curently envisaged) will achieve three main scientific objectives: (i) document ambient pore pressures at several depth intervals, (ii) provide constraints on formation elastic and hydraulic properties from the response to tidal loading at the seafloor, and (iii) record hydraulic transients related to strain and/or episodic fluid flow. Obtaining reliable measurements of ambient pore pressure will provide insight into hypotheses invoking fluids as a cause of mechanical weakness in faults and wall rock, and constrain regional scale models used to estimate pore pressures at greater depths [e.g., *Screaton et al.,* 2005]. Hydraulic transients can be used as a highly sensitive proxy for volumetric strain, and offer the opportunity to investigate the

relationship between fluid pressure, strain accumulation, and fault slip at an active margin [e.g., *Davis et al*., 2001, 2004, 2006]. All downhole pore pressure monitoring systems have to be complemented by high-resolution temperature monitoring as these data provide a simple means of controlling the integrity of the borehole seals at the seafloor as well as sensitive indicators of transient pore water flux events [*Heesemann et al*., 2006].

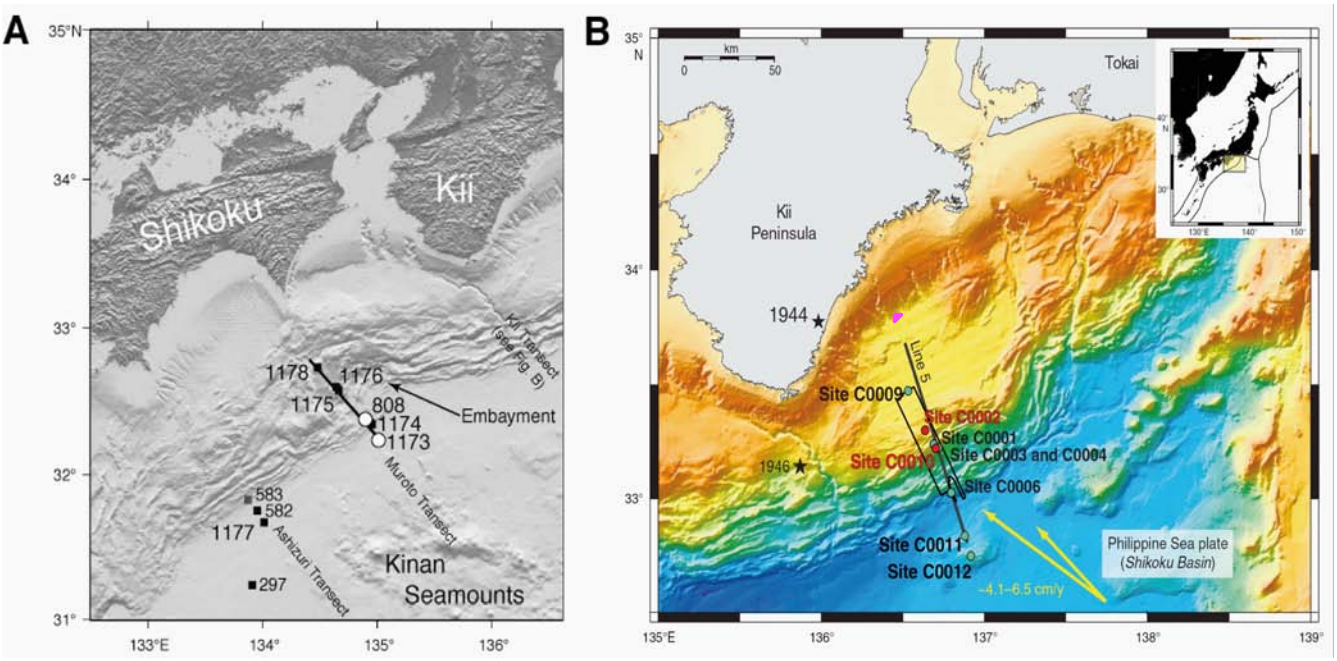

Figure 2: Location map showing locations of previous DSDP and ODP Nankai Trough drilling and planned NanTroSEIZE drillsites. **A**) Map of western (Cape Ashizuri transect) and central (Cape Muroto transect) Nankai drilling including site numbers. The open circles show present CORK installations. **B**) Map of NanTroSEIZE drill sites to date [from *Kopf et al., 2011*]. Data for this proposal will be obtained from the Kumano mud volcano field marked by the pink circle.

Given that pore water flux plays a crucial role in the pressure evolution, and added advantage would be to also use hydraulic pore pressure lines for fluid sampling. This has been done in ODP/IODP for two decades, and the majority of the boreholes CORKed and used for sampling were located in oceanic crust (or sediments overlying crust). Among the large number of scientific papers having originated from those observatories and fluid studies, three articles are of particular interest to the general scientific community and also of relevance for what is proposed for the MeBo CORKs (this proposal). One is a compilation of first-order scientific results spanning hydrogeological, physical and geochemical conclusions [*Kastner et al*., 2006]. The other paper highlights the evolution of CORK design and physical sensors, methods of submersible operation, and an outlook for future work and funding pathways [*Becker & Davis*, 2005]. The third manuscript focuses on fluid sampling capabilities and chemical sensors associated with CORK observatories during the past two decades [*Wheat et al*., in press] and outlines a number of pitfalls in this field which we aimed to avoid when deploying much simpler, smaller and affordable *MeBo CORK instruments (see Ch. 3.3)*.

In subduction zones, large volumes of sediment are underthrust and eventually undergo diagenetic, metamorphic, and magma generation processes. Sediment has been shown to re-emerge in arc volcanoes based on typical geochemical signatures such as Be isotope values or depletion of high field strength elements (HFSE) relative to light rare earth elements (LREE) and large ion lithophile elements (LILE) at the volcanic arc (e.g. Tera et al., 1986; Morris et al., 1990; Brenan et al., 1995; Plank and Langmuir, 1998; Elliot et al., 1997). Afterwards, part of the sediment residue continues to sink into the mantle and becomes one of the potential sources of mantle plumes and/or heterogeneities (e.g., Kogiso et al., 1997; Kamber and Collerson, 2000). Despite the improvements of geophysical investigation techniques and numerous DSDP and ODP expeditions, there is a clear lack of understanding of the physico-chemical processes attendant to the subduction of sediment. This is particularly true for the mechanical processes controlling the the location and frictional behaviour of the plate boundary fault, but also regarding processes of fluid-rock interaction, mineral transformation, and devolatilisation that affect chemical cycling as well as effective strength of these materials (e.g. Dia et al., 1995; Johnson & Plank, 1999; Bebout et al., 1999). In the so-called subduction factory, there is a fundamental difference between the inputs (i.e. incoming sediment and crust as well as material from frontal and basal subduction erosion) and outputs, most importantly accretion, underplating, fluid release, and arc and back-arc magmatism (Fig. 3). We suggest to regard mostly the fault-driven fluid release originating from the frontal and intermediate loop (Fig. 3), which will be quantified *in situ* using CAT fluxmeter systems (Tryon et al., 2001). Five of those systems were placed in key location in the northern part of the MedRidge during expedition P410 (Kopf et al., 2012) and are to be recovered during the cruise proposed here. The locations chosen were either surface outcrops of deep-seated faults or mud volcanoes believed to be actively emitting fuids from depth.

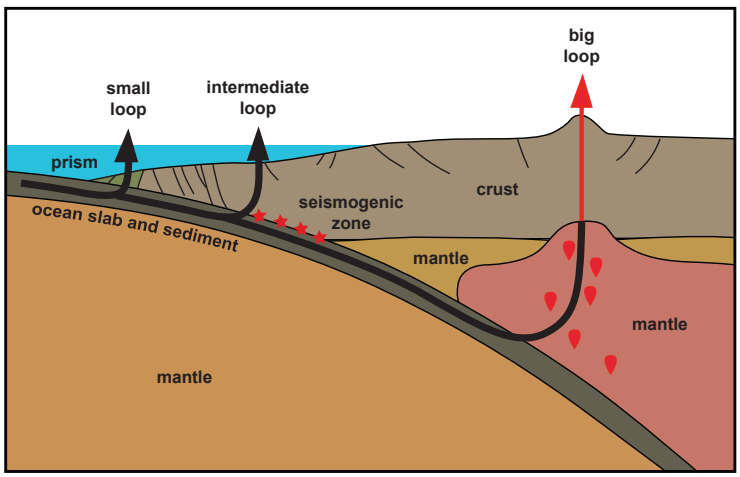

Figure 3: Schematic diagram of subduction zone devolitilisation in the frontal (short loop) as well as landward part of the forearc (intermediate loop) as well as the volcanic arc (big loop).

The interaction between solid sediment particles and trapped pore water has profound physical and chemical repercussions and starts immediately after deposition on the seafloor. Consolidation may only occur if the fluid pressure from the pores can dissipate; otherwise pore pressures build up and counteract cohesion and reduce the mechanical strength of the sediment. This has first been described by Hubbert & Rubey (1959) and ever since has been a matter of controversial debate (see e.g. Byerlee [1978] vs. Rice [1992]). In addition to the physical properties, chemistry of the solids and fluids is also affected after deposition (in particular the ad-/desorption processes on clay minerals). Both mechanical pore space reduction and diagenetic reactions cause a decrease in permeability. Processes active include clay mineral dehydration, alteration of biogenic opal, zeolite formation, dissolution of metastable mineral phases, to name just a few (see summary in Moore & Saffer, 2001). Such diagenetic to low-grade metamorphic processes may mobilise major (such as K, Na, Ca, Mg, Fe, S, and Si) and minor components (e.g. Cl, Ba, B, Sr, Cs, Li, Rb) as well as many other trace elements as a result of dissolution and mineral transformation processes (see summary in Guangzhi, 1996). The resulting supersaturated pore fluids may cause precipitation and hence significantly modify the fabric (Kawamura & Ogawa, 2004) as well as the strength and permeability of the sediment (Bjorlykke & Hoeg, 1997; Dewhurst et al., 1999), its mineralogy, and chemical composition of the pore fluid residue.

Mud volcanism has been demonstrated to be a global phenomenon, which is commonly associated with compressional tectonics and sediment accretion at convergent margins (see review by Kopf, 2002). Mud domes and diapirs frequently occur in marine subduction zones at the plate boundary near the toe of accretionary prisms (Henry et al., 1996), further landward in the forearc (Mascle et al., 1999), but also on land where collisional processes and deformation are more accentuated (Lavrushin et al., 1996). Irrespective of the tectonic compression, the main driving force of mud extrusion is the negative buoyancy of the clay-rich material at depth. Fluids may either be trapped as a result of high sedimentation rates or lateral influx into clay-bearing sediments, or may be generated *in situ* owing to processes such as mineral dehydration reactions and hydrocarbon generation at greater depth (e.g. Hedberg, 1974). Quiescent as well as catastrophic emission of greenhouse gases (mostly methane) accompanies extrusion and may contribute significantly to climate change (Higgins & Saunders, 1974; Kopf, 2002).

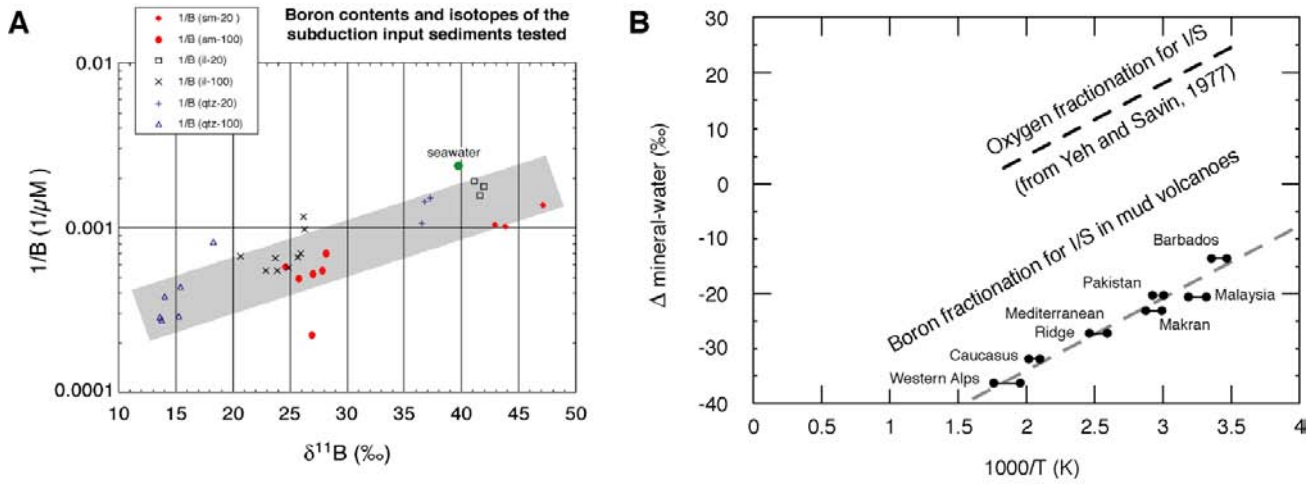

Figure 4: **a**) Results from B analysis on fluids and solid particles from hydrothermal deformation tests of smectite (sm)-, illite (il)- and quartz (qtz)-rich endmember sediments off Japan (from Kopf et al., 2002); b) Data compilation from MV study using B fractionation and paleo-T to estimate the depth of mud- and fluid mobilisation (from Kopf & Deyhle, 2002).

When returning to the subduction factory cycles (Fig. 3), mud volcanism and deep-seated faults may help illuminate the intermediate loop. Numerous authors have used the mobile element Boron and its stable isotope ratio ($\delta^{11}B$) to illuminate processes in the moderate T window of subduction zones (Spivack et al., 1987; You et al., 1993, 1996; Kopf et al., 2000; Deyhle & Kopf, 2001, 2002). These studies on natural samples and from hydrothermal experiments suggest that B is a powerful proxy with a wide variety of $\delta^{11}B$ values for different subduction inputs and related diagenetic reactions. Examples of the proponent's evolvement in these studies are given in Figure 4 and have been wrapped up in various publications (oral and as manuscripts; see Kopf & Deyhle, 2002; Deyhle & Kopf, 2001, 2002, 2005). The work attested that there are well-defined trends for B processes in selected silica systems such as clay-dominated ones (Kopf & Deyhle, 2002), but not in all of them (Deyhle & Kopf, 2005).

3. Regional geology

3.1. The Nankai Trough subduction zone

The Nankai Trough accretionary complex is formed by the northwestward subduction of the ~15 Ma Philippine Sea plate below the Eurasian plate along the Nankai Trough at ~65 km Myr-1 [*Miyazaki & Heki*, 2001] down an interface dipping 3°–7° [*Kodaira et al*., 2000] (Fig. 1). Nankai is a sediment-dominated subduction zone, much as the East Aleutian and Cascadia systems, characterized by repeated occurrence of great earthquakes of ~M_w 8.0 [*Ruff & Kanamori*, 1983]. Although the causative mechanisms remain poorly documented [*Byrne et al*., 1988; *Vrolijk*, 1990; *Hyndman et al*., 1997; *Moore & Saffer*, 2001; *Saffer & Marone*, 2003], the up-dip limit of the seismogenic zone at these margins is thought to correlate with a topographic break along the outer rise [e.g. *Byrne et al*., 1988, *Wang & Hu*, 2006]. Nankai is among the most extensively studied subduction zones in the world; it has been selected as a focus site for studies of seismogenesis based on the wealth of geological and geophysical data available, a long historical record of great (M>8.0) Eqs [e.g., *Ando*, 1975], and direct societal relevance of understanding tsunamis and earthquakes to the heavily populated coastal area. The region offshore the Kii Peninsula on Honshu Island has been identified as the best location for seismogenic zone drilling for several reasons. First, the rupture area of the most recent great earthquake, the 1944 M 8.2 Tonankai event, is well constrained by recent seismic and tsunami waveform inversions [e.g., *Tanioka & Satake*, 2001; *Ichinose*, 2003; *Kikuchi et al*., 2003]. A region of significant coseismic slip (1-2 m) is reachable by drilling with the DV *Chikyu*, which is currently limited to 2500 m water depth (Fig. 2b). Second, the region offshore Kii is generally typical of the Nankai margin in terms of heat flow and sediment on the incoming plate. Previous drilling (DSDP and ODP drilling on Legs 31, 131, and 190) offshore Cape Muroto on Shikoku Island (~150 km to the southwest) found anomalously high heat flow and lithostratigraphy associated locally with basement highs. Third, OBS campaigns and on land geodetic studies (though of short duration) indicate significant interseismic strain accumulation [e.g., *Miyazaki & Heki*, 2001; *Obana et al*., 2001].

3.2. The IODP NanTroSEIZE project

Nankai is a sediment-dominated subduction zone, and has been selected as a focus site for studies of seismogenesis based on the wealth of geological and geophysical data available, a long historical record of great (M>8.0) EQs [e.g., *Ando*, 1975], and direct societal relevance of understanding tsunamis and earthquakes to the heavily populated coastal area. Drilling into the seismogenic zone was advocated by an international group of proponents who submitted a Complex Drilling Proposal (CDP) with three major phases of operations. Phase 1 drilling targets the incoming sediments and

ocean crust to characterize their physical properties, composition, and state (pore pressure and temperature). Phase 2 is focused on the investigation of a major splay fault system implicated in coseismic rupture, and includes penetration of the fault at several depths ranging from ~1 to 3.5 km bsf. Phase 3 proposes to sample and instrument the plate interface at ca. 6 km bsf, in a region predicted to be both capable of generating seismogenic behaviour and in the zone of co-seismic slip in the 1944 Tonankai EQ.

Until now, the first two stages of NanTroSEIZE have been completed and the third one has started. Stage 1 of the NanTroSEIZE science plan included three coordinated non-riser drilling expeditions. Eight sites were drilled across the continental slope and rise offshore the Kii Peninsula, many within the inferred coseismic slip region of the 1944 Tonankai M 8.2 EQ. The first expedition to all of the Stage 1 drilling sites (**Exp 314: LWD transect**) used Logging While Drilling (LWD) to define physical properties, lithostratigraphy, and structural information in advance of coring operations. This was followed by the first CDEX coring expedition (**Exp 315: Mega-Splay Riser Pilot**) aimed at sampling the materials and characterizing *in situ* conditions within the accretionary wedge to a depth of 1 km bsf at Site C0001 across the deep "mega-splay" out-of-sequence thrust. This site also serves as a pilot hole for later Stage 2 riser drilling targeting the "mega-splay" fault at a depth of ~3-3.5 km bsf. A third non-riser expedition (**Exp 316: Shallow Megasplay and Frontal Thrusts**) targeted another shallow fault zone of the "mega-splay" system in the older accretionary prism (Site C0004) as well as the frontal thrust at the toe of the young accretionary prism (Sites C0006 and C0007).

The locations drilled by DV *Chikyu* during Stage 1 are Sites C0001 through C0008, as shown in shown in Figure 3B. The general results by Stage 1 drilling along the NanTroSEIZE transect are briefly summarised in an article for Scientific Drilling [*Tobin et al*., 2009] and can be found on the IODP website in full detail [see *Kinoshita et al*., 2009]. A hole seaward of the frontal splay fault revealed frequent mass wasting deposits, potentially related to (EQ-) activity of this out-of-sequence thrust [*Strasser et al*., 2009]. Other results from Stage 1 drilling reveal new insights into the stress history and temporal evolution of the Nankai forearc. First, there is no discontinuity in the depositional record between thick forearc basin sediments and the underlying Late Miocene accreted strata (C0002). Second, both borehole breakouts (LWD results) and the orientation of structural measurements on cores suggest a pattern of compression parallel to plate convergence in the wedge, trench-parallel extension above the branches of the mega-splay fault (in particular Site C0001), overlain by trench-orthogonal normal faults in the forearc and below, suggesting predominantly extensional stresses in the overriding accretionary system. Third, the fault zones are highly active given immense problems in borehole stability and core recovery at Sites C0001, C0004, and C0006. The initial Stage 1 shipboard data serve to put forward preliminary hypothesis on the displacement

history along the mega-splay and frontal thrust faults.

NanTroSEIZE Stage 2 operations with DV *Chikyu* took place in 2009 with **Exp 319** "Riser drilling and observatories" and **Exp 322** "Subduction Inputs". The drill holes of NanTroSEIZE Stage 2 are C0009 – C0012 (Fig. 3). Exp 319 aimed to conduct deep Riser drilling of a hole (C0009) through the Kumano Basin fill into old accreted strata of the Nankai wedge overlying the locked subduction thrust. Drilling added detail to the understanding of the history of the Kumano forearc basin, and indirectly the activity of the splay fault system over time. The updip-end of the splay fault was the focus of the second site of Exp 319, where a cased drillhole (C0010) was placed 3 km along-strike of C0004 (Fig. 2B, 5). This hole penetrated the shallow portion of the mega splay fault in appx. 420 mbsf (meters below sea floor), and terminated at appx. 560 mbsf. The interval where the fault zone was interpreted to be from LWD data had been prepared with a 22 m-long section of perforated casing screens, which allow fluids to enter the lower portion of the borehole [see *Saffer et al.*, 2009]. Hole C0010A was the first NanTroSEIZE hole where an observatory was deployed (Fig. 4). This temporary system represented the first simple observatory off Kii and measured P and T over time. The second Stage 2 expedition, **Exp 322**, followed immediately to characterise the input into the subduction system in the abyssal plain and on a topographic high, both represented by Sites C0011 and C0012.

Two more Stage 2 expeditions followed a year later: **Exp 332** exchanged the temporary mini-CORK observatory at C0010 with an upgraded system, and further deployed the first permanent CORK at Site C0002 (see Ch. 2.3.). Immediately afterwards, **Exp 333** completed what was not finished during **Exp 322** at Sites C0011 and C0012, and further drilled a hole into a mass-wasting complex on the upper slope of the Nankai margin (C0018).

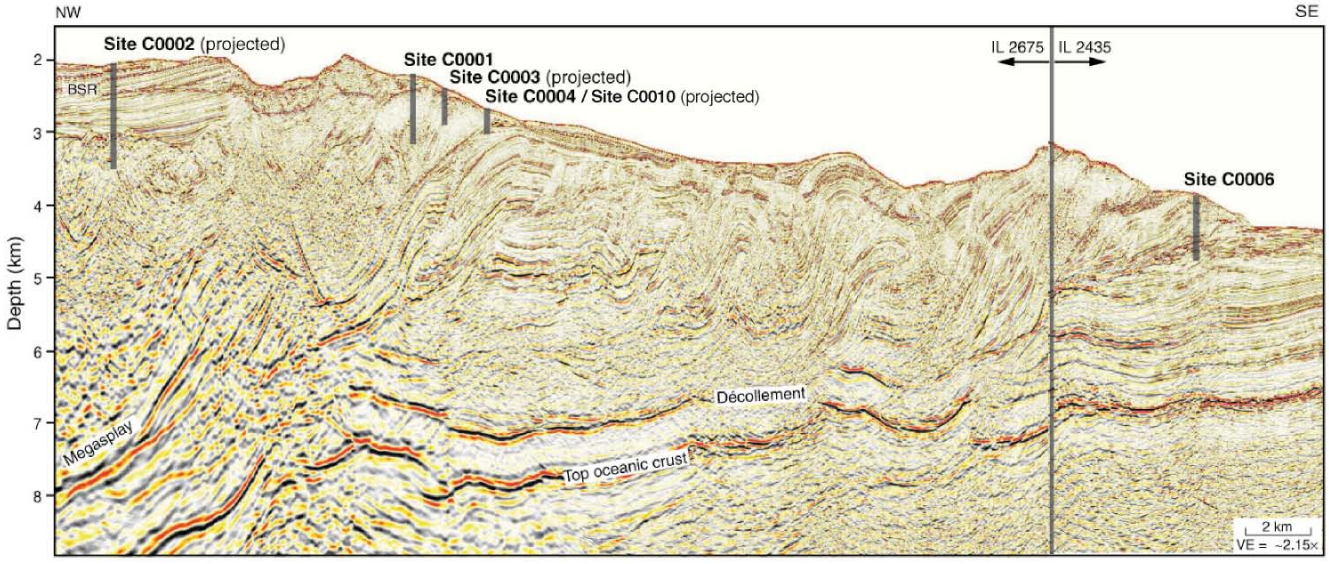

Figure 5: Seismic reflection profile across the NanTroSEIZE area including drillsites relevant for this proposal.

Expedition 332 has been the most successful NanTroSEIZE expedition to date where major milestones of the project were reached [*Kopf et al.*, 2011]. The cruise focused mainly on engineering work, including (1) the permanent observatory installation at Site C0002 in the outer Kumano Basin, at the location of planned future deep riser drilling, (2) the retrieval of a temporary mini-CORK observatory instrument installed during Exp 319 at Site C0010, which penetrates the shallow "mega-splay" fault in the mid-forearc, and installation of a new suite of temporary sensors, and (3) the deployment of an upgraded temporary observatory at Site C0010.

At Site C0002, a new hole was drilled with LWD and cased for placement of a Long-term borehole monitoring system (LTBMS). It comprises a CORK assembly with a hydrogeological unit measuring pressure at four depth levels as well as a broadband seismometer, volumetric strainmeter, tiltmeter, geophones, and a thermistor string (see Figs. 6, 7). The key goals include pore pressure monitoring in the upper accretionary prism (Unit IV), a series of measurements in the homogeneous sediments of Unit III (strain, tilt, seismicity, pressure) in the transition zone, and temperature and pressure in the overlying Kumano Basin sediments of Unit II. The string of the CORK assembly had a total length of 965 m and was carefully secured during deployment with centralizers, bands and straps to withstand the strong current.

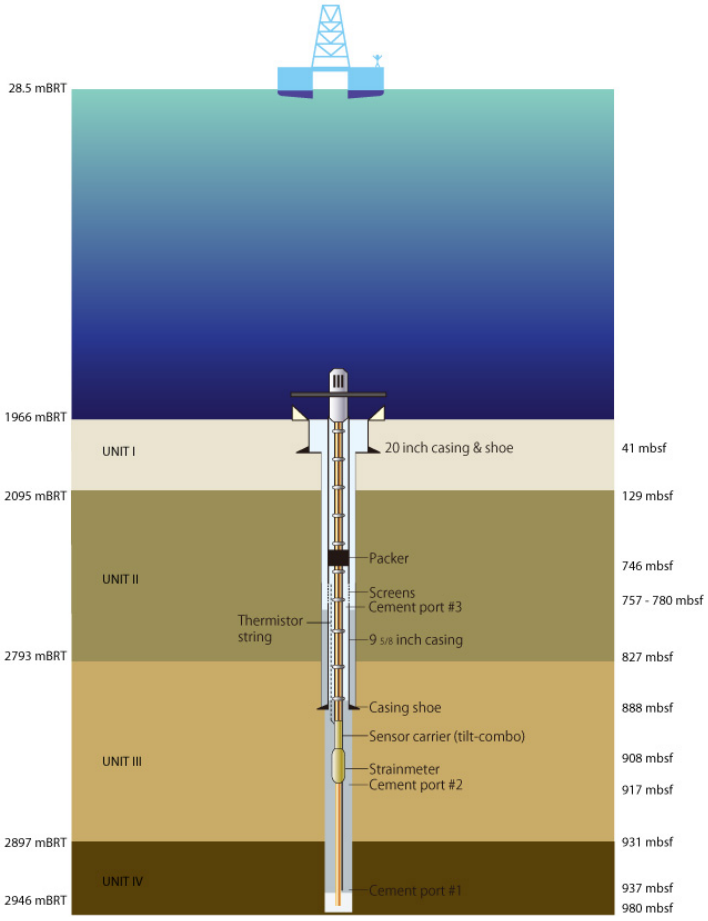

Figure 6: Schematic of the CORK assembly at Site C0002, as set during IODP Expedition 332.

The lower portion of the assembly is isolated against the overlying ocean body by a swellable packer at 746 mbsf. Part of the instrument string below was cemented (appx. 780-935 mbsf) to couple strainmeter and seismometer to the formation/casing. The CORK head was revisited prior and after cementing for system tests of the borehole instruments using the ROV, and all of these experiments were successful. The CORK is working in a self-contained (battery-driven) mode for some of the instruments, while others will be connected to external batteries in spring 2013. The long-term perspective is a connection of the system to the real-time seafloor cabled network DONET.

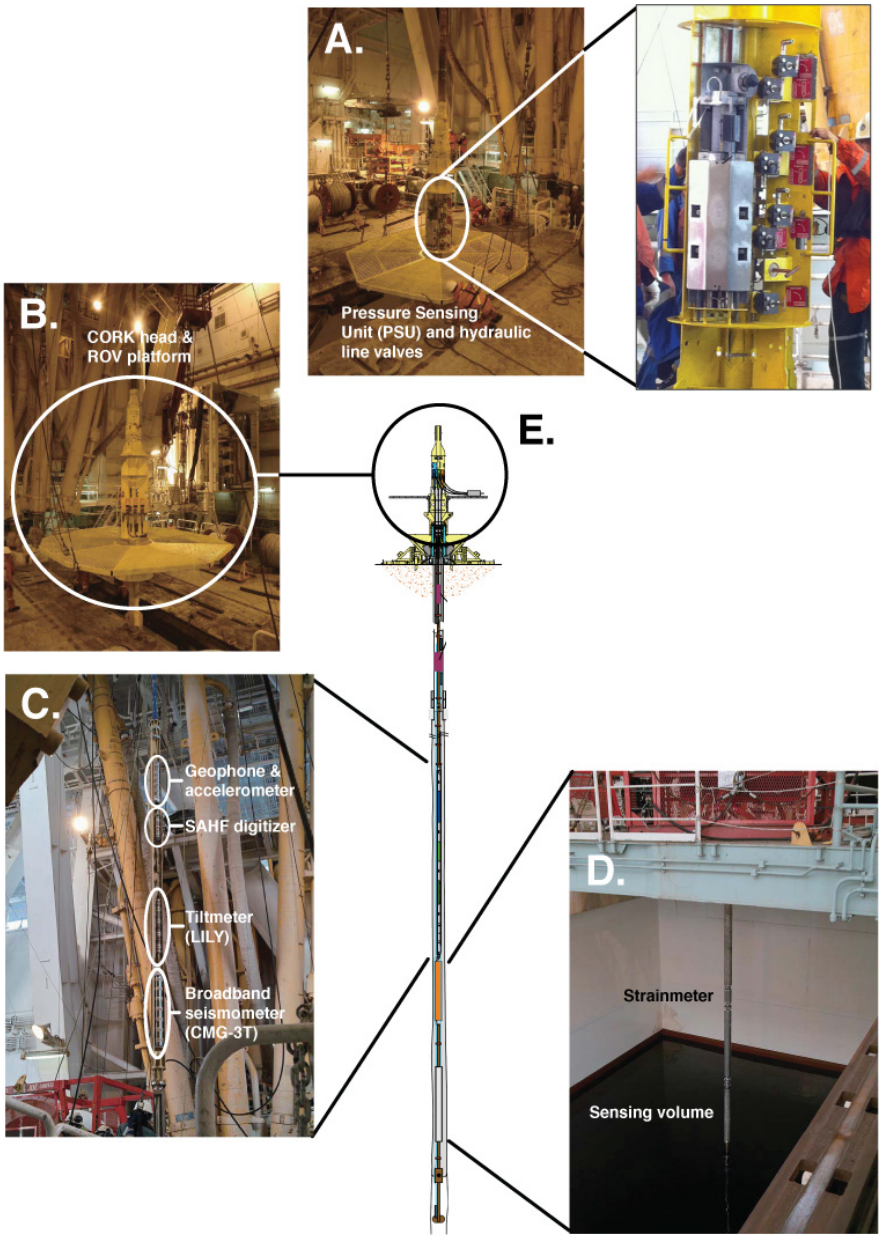

Figure 7: The sensors and placement on the LTBMS CORK observatory at Site C0002. The different sensor packages and their arrangement on the downhole and CORK head sections are shown in photographs taken during deployment. A. The Pressure Sensing Unit (PSU) an independent sensor array mounted on the CORK head. B. CORK head and ROV platform. C. Sensor carrier, with a geophone & accelerometer assembly, a stand-alone heat flow meter (SAHF) digitizer for the thermistor string, LILY tiltmeter, and a CMG-3T Guralp seismometer. D. Strainmeter and sensing volume. E. Cartoon diagram of the Site C0002 CORK observatory.

At Site C0010 further downslope, the focus was on exchanging the SmartPlug (Fig. 8) temporary "mini-CORK" with an upgraded GeniusPlug, both attached to a retrievable casing packer above the screened megasplay fault zone at Site C0010. SmartPlug recovery was successful despite the strong Kuroshio current, which can be attributed to an efficient reduction of vortex-induced vibration (VIV) on the drill string by attaching ropes. Times series data recovered from the self-contained instrument include seafloor and formation pressure as well as 4 independent temperature records from the fault zone and the overlying seafloor reference. Tentative analysis of those data proves the effective seal of the bridge plug, dampened pressure amplitudes in the tight, slightly overpressured formation, and identification of prominent earthquake and tsunami events in the 15-month record (23 Aug 2009 – 7 Nov 2010). Once the SmartPlug was secured, a GeniusPlug (named like that since, compared to the SmartPlug, it additionally comprises an osmo-sampler for 24 months of fluid sampling plus a FLOCS unit for microbiological research [*Orcutt et al*., 2010] in the splay fault) was deployed at C0010.

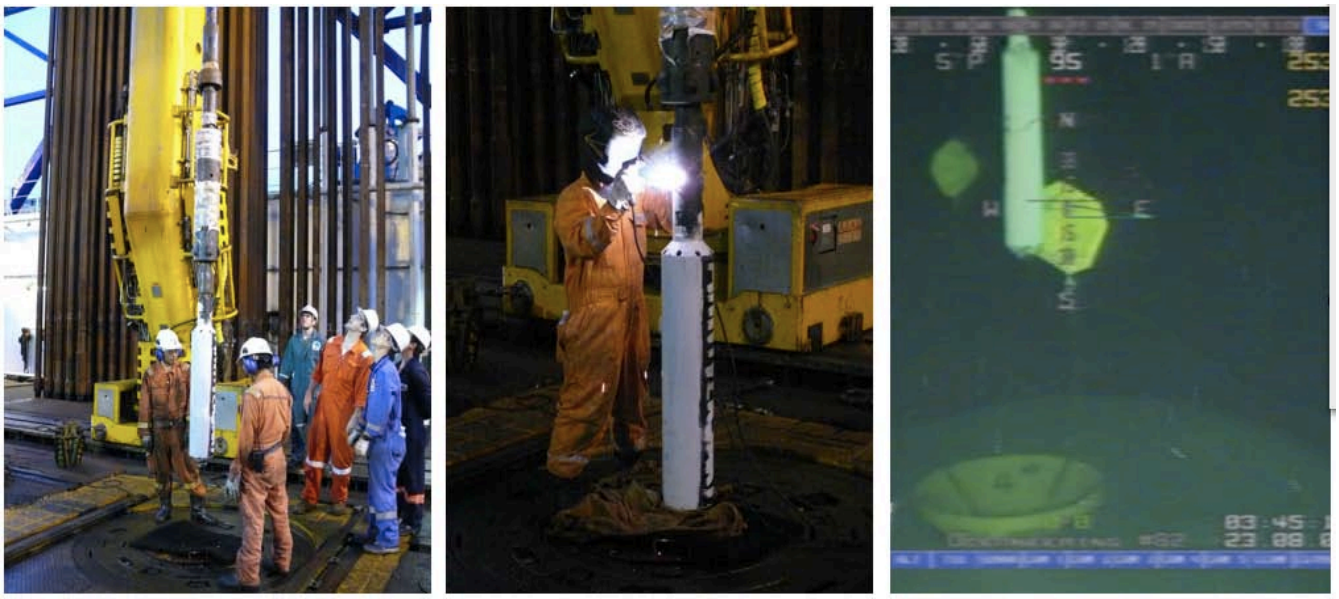

Figure 8: "Mini-CORK" observatory consisting of a retrievable Bridge Plug to separate the borehole from the overlying ocean water hydraulically (left, top), and a pore pressure instrument attached to bridge plug (left), additionally secured by tack-welding (middle), and at the drill string in appx. 2500 m waterdepth prior to re-entry of hole C0010A (right).

The SmartPlug record nicely shows an increase in pressure and decrease in temperature as the instrument is entering the water and being lowered towards and into the seafloor. Thereafter, equilibration starts, and data attest that the bridge plug effectively sealed the borehole, because upon re-entry of the drill string and latching onto the device during Expedition 332 the upward-looking P-sensor shows a strong fluctuation owing to displacement of borehole fluid whereas the downward-looking P-sensor encounters no such interference and remains at a near-constant value [*Kopf et al*., 2011]. A cursory review of the data identified multiple pressure and – to a lesser extent - temperature excursions that may be related to seismic events, although further detrending and processing of the data are required to filter the tidal signal and resolve pressure anomalies.

3.3. The MEMO project

The acronym MEMO stands for ***Me****Bo drilling and in situ long-term* ***mo****nitoring offshore Japan: Nankai Trough Accretionary Prism*. It is funded by the German Ministry for Education and Research (BMBF) and tied to two legs on RV *Sonne*.

As outlined above, the purpose of the NanTroSEIZE project is to study fault zone processes to gain a greater understanding of seismogenesis. One aspect of this is to investigate the role of fluids and fluid genesis as they are thought to play a major role in the transition from aseismic to seismogenic behavior. One of the expected outcomes of NanTroSEIZE stages 1 and 2 was to find evidence of long-distance travel of fluids along fault-controlled conduits. Such fluids would be expected from dehydration reactions at depth that drive up fluid pressures and, thus, fluid transport. Such fluids have been sampled at other convergent margins (e.g. Hensen et al., 2004), farther SW on the Nankai forearc (Moore et al., 2001), and to the north at the Japan trench forearc (e.g. Deyhle et al., 2003). These fluids carry with them a record of water-rock reactions occurring in the region of the transition from aseismic to seismogenic behavior. At this time, however, all fluids sampled during NanTroSEIZE appear to be entirely, or very nearly so, produced *in situ*. Given this enigmatic lack of evidence for deep-sourced fluids trenchward of the Kumano Basin, it seems prudent to seek such evidence arcward. Therefore, the purpose of the *MEMO* research program is to extend the fluid sampling arcward of the NanTroSEIZE transect into the northern Kumano Basin to test the following hypotheses:

- Much, if not most, of the chemically bound water released from depths corresponding to the transition from aseismic to seismogenic behavior are being transported via the subduction factory's intermediate loop (Fig. 3), i.e. upwards through the wedge via faults and the fractured upper plate.

- The Kumano Basin mud volcanoes tap these fluids and may provide insights on fluid genesis and pathways within the Nankai forearc.

- The mud volcanoes root deeply and, by providing hydraulic pathways, may allow to monitor EQ precursors if long-term instrumentation is installed in the most active regions of those features.

To this end, we will be carrying out a research cruise aboard the R/V *Sonne* (Project MEMO). During the project we will collect gravity and MeBo cores and install long-term monitoring instruments to test the above and other hypotheses regarding physico-chemical processes occurring within the Kumano Basin mud volcanoes, their roots, and their fluid sources at depth. The *MEMO* project has multiple objectives, many directly related to the NanTroSEIZE objectives, but also others more directly related to the ongoing investigation of the nature and global significance of mud volcanoes. The project is a collaboration between German, Japanese, and American scientists whose

investigations aim to answer the following questions:

- How stable (i.e., mechanically competent) are the forearc basin sediments and the extruded mudflows? What are the physical parameters of the sediment that control the slope stability and geometry of the mud volcanoes?
- Can we provide a chronology of activity by dating the individual mud flows interspersed with hemipelagic sediments of the dome flank (typical "Christmas tree" structure; e.g. Robertson et al., 1996)? Can these be related to paleo earthquakes?
- Is there evidence of deeply mobilized fluids? To what extent are the exotic chemical signatures of the Nankai prism further south and the Japan prism to the north, seen in the arcward regions of the Nankai forearc? Can we determine which processes release these fluids? Can such geochemical patterns originate from seismogenic depth (i.e., 6 km or more)?
- Can fresh water and characteristic oxygen isotope signatures be found, indicating that gas hydrates are decomposed in the active mud volcano (as is suggested by the broken BSR).
- Is the heat flow in the active mud volcano higher than in its inactive counterpart? How does this relate to the estimated temperatures in the Kumano basin where the NanTroSEIZE campaign will aim for their deepest borehole (Phase 3), some 5-7 km below the seafloor?
- Can one detect correlated regional seismicity, transient pore pressure changes, and fluid flow rate changes in the mud volcano? How do these compare to CORK measurements further south and other DONET stations in the neighbourhood?

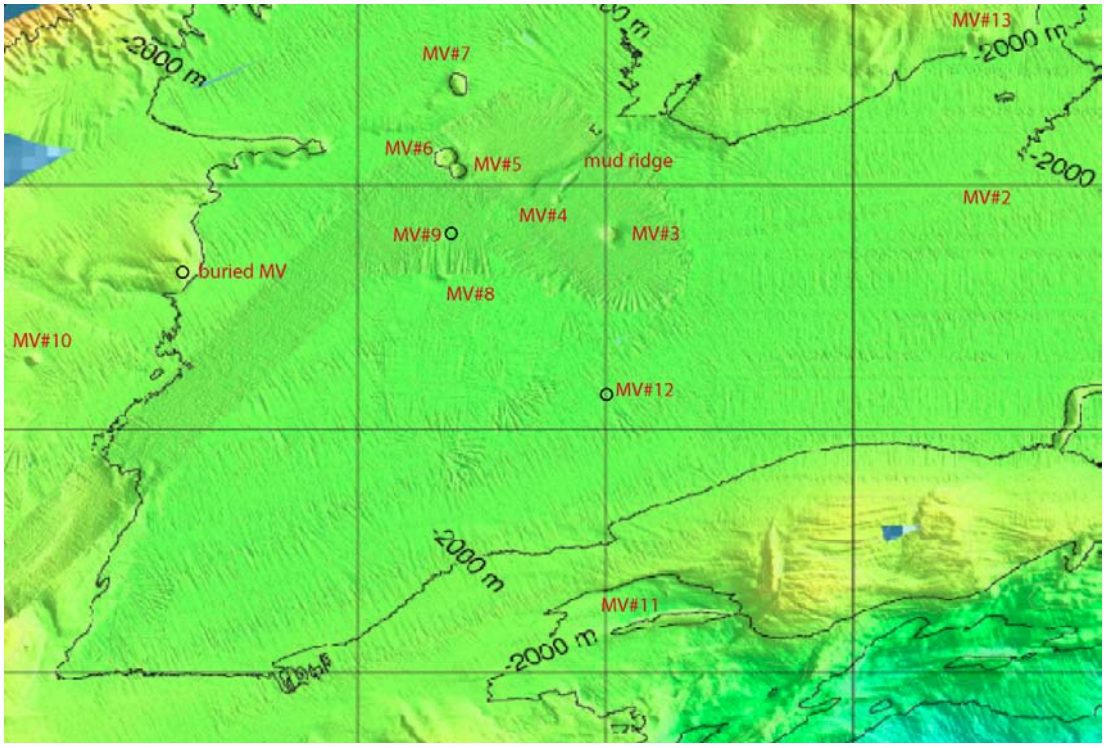

Figure 8: Most prominent mud volcanoes in the northern Kumano Basin.

The Kumano basin is ideal for this study for several reasons. First, it represents the northward prolongation of the NanTroSEIZE transect with a huge geophysical data set (e.g. 3D multi-channle seismic reflection data; Moore et al., 2009; Bangs et al., 2010) and several IODP drill holes in its southern (C0001, C0002) and central (C0009) part (Kinoshita et al., 2009; Saffer et al., 2010). Second, long-term information about seismicity and other phenomena is available from both seafloor installations (e.g. DONET cabled network; see Fig. 9) and IODP borehole observatories at Sites C0002 and C0010 (Kopf et al., 2011). Third, earlier investigations by D/V *Chikyu* as well as by ROV attested deep seated fluids and methane emission at e.g., MV #5 (Tsunogai et al., 2012).

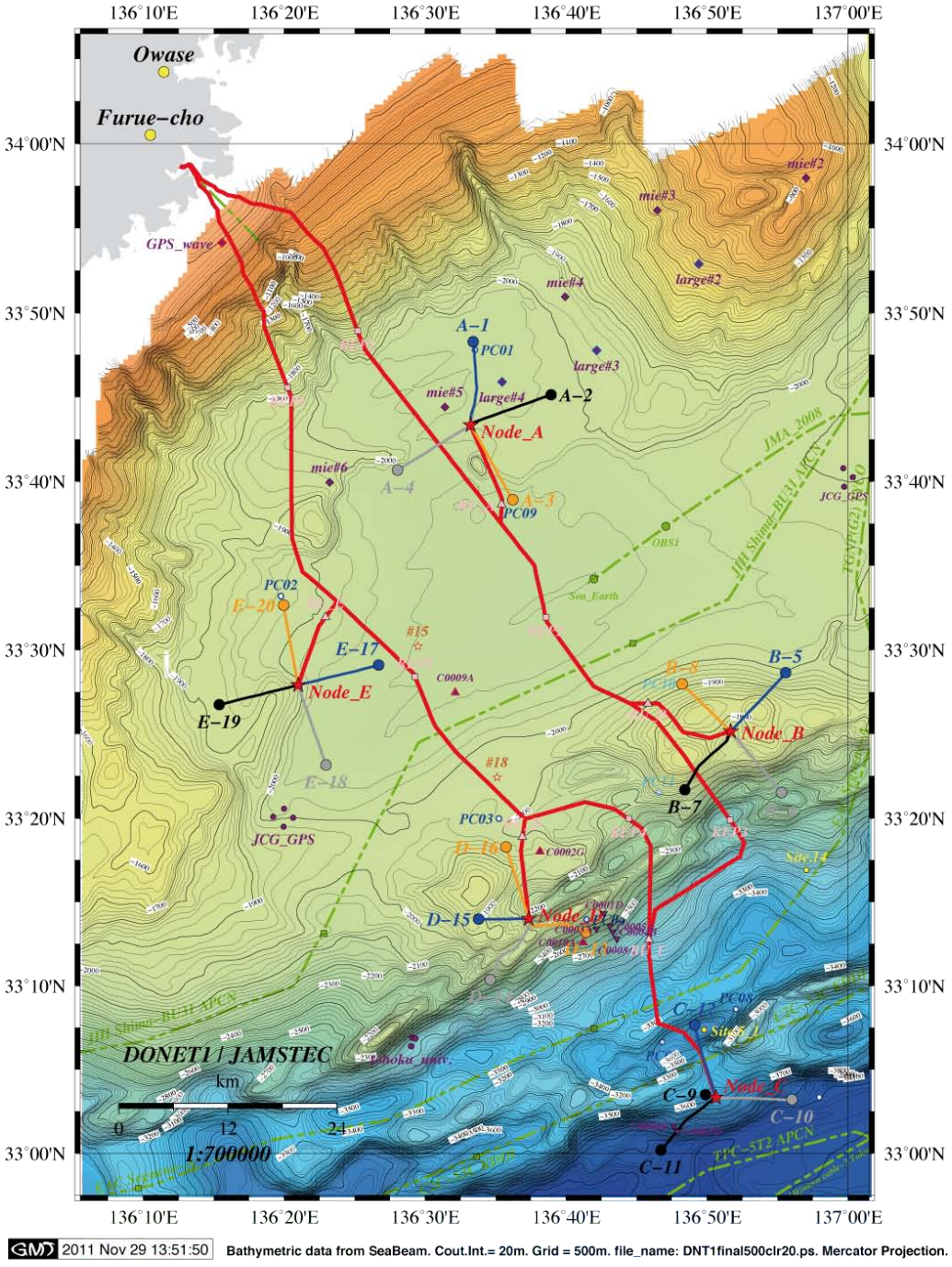

Figure 9: Layout of DONET cabled network in the northern Kumano Basin.

There are two fundamentally different objectives of the *MEMO* project:

1) The use of certain parameters to detect EQ precursors as well as co-seismic and post-seismic transients (P, T, geochemical variations in the pore water composition and flow rate) and their relationship to regional seismicity. This goal is to be achieved by long-term installations.

2) The study of mud volcanic products to assess the depth of origin of the solid (clay-mineral rich matrix, clasts) and the fluid phase (headspace gas, gas from gas hydrate dissociation, pore waters). This goal is to be reached using samples taken during cruise SO222.

Objective 1: Long-term observations of MV activity

MeBo instruments

It is well documented that pore pressure in boreholes responds to tectonic strain events in a range of settings, both onland (e.g. *Roeloffs*, 1996) and in subseafloor formations (e.g. *Davis et al*., 2001, 2004). Existing data indicate that such transient hydrologic events are common both at ridges and subduction complexes, having been observed in CORK systems, by seafloor seepage meters, and by changes in seismic velocity (e.g. *Davis et al*., 2001, 2004, 2006; *Husen & Kissling*, 2001; *Kastner et al*., 2005; *Kopf et al*., 2011). The pore pressure response to such events can be divided into two components: First, strain in the surrounding rock volume results in an initial change in pore pressure. The magnitude of this effect depends upon the compressibility of the rock (less compressible rock yields a larger pore pressure signal), and the magnitude of the strain signal (larger signals lead to larger pore pressure changes) (e.g. *Ge & Screaton*, 2005). Second, diffusion occurs in response to the initial strain-induced pore pressure changes, with a rate that scales with formation hydraulic diffusivity (the ratio of hydraulic conductivity to specific storage).

The first component, i.e. the pore pressure transients with time, will be monitored with MeBo borehole instruments, while the diffusion-related response can be characterised by geotechnical testing on core materials (see next section). The MeBo CORK instruments were designed to hydraulically decouple the drill string, which remains in the hole once it is completed as casing, from the overlying water body. This has been achieved by two fundamentally different designs, the MeBo CORKs and the MeBo-Plugs. The instruments have in common that their backbone-parameters are P and T, monitored in self-contained mode over time.

Onshore observations indicate that mud volcanoes tend to erupt before, during and shortly after large EQs (e.g. 1906 San Francisco EQ, 1960 Chile, EQ, 1964 Alaska EQ; see Panahi, 2005). In other areas, both the flow rate and composition of gaseous and aqueous fluids changes as a result of seismicity (Martinelli & Ferrari, 1991; Bagirov et al., 1996; Chigira & Tanaka, 1997; Mellors et al., 2003; Kopf et al., 2010). In the Caucasus collision zone with hundreds of active MVs, crustal and

mantle gas is released weeks prior to large EQs whereas the ionic composition of pore fluids changes a few days prior to the seismic event (Guliyev, 1992). Several changes produced by EQs have been proposed as MV triggers, including mud liquefaction (Manga et al., 2009) increased hydraulic permeability (e.g. Rojstaczer et al., 1995) and bubble nucleation or growth. Previous studies indicate that transient hydrologic events related to EQs are common in various geological settings and may be triggered in the near- or far-field (Chigira & Tanaka, 1997; Davis et al., 2004; Kopf et al., 2011). MVs are ideal stress indicators because of their fluid-rich nature and hydraulic connection to depth. They function similar to a valve; stress changes from deformation before, during and after EQs may be discernable as transients in pore pressure, fluid chemistry, and mud or gas discharge rates. Therefore, mud volcanoes and sites of active seepage (e.g. pockmarks) are well suited for monitoring strain and seismicity using a number of proxies: P, T, fluid chemistry, to name just a few. The governing process in changes of any of the above is elevated permeability as a result of seismic wave propagation (Elkhoury et al., 2006) and subsurface fluid flow, as documented onshore (e.g. Brodsky et al., 2003) and offshore (Johnson et al., 2000). Out of several available physical parameters, we rely largely on pore pressure (pP) and temperature (T), which are straightforward to measure with affordable, reliable transducers. *Pore pressure* functions as a strainmeter given the quasi-incompressible nature of formation waters, and increases in areas of incipient deformation (Davis et al., 2004), fluid flow (Solomon et al., 2009), strong ground motion from EQs (Kopf et al., 2011), or degassing (Linde et al., 1994). Variations of permeability in the vicinity of the instrument affect the amount of pore pressure, fabric of sediments/rocks, and the hydrological properties of faults (Rojstaczer et al. 1995). *Temperature (T)* measurements are simple and benefit from the effective heat capacity of water. Surface heat flow data are readily available in many marine settings, so that extrapolation to the ambient T at depth may be meaningful. Dey & Singh (2003) have demonstrated that, with some uncertainty, the amount of heat flow increase prior to a large EQ is proportional to the magnitude.

The detailed instrument design of the MeBo CORKs and MeBo-Plugs will be outlined below.

Flowmeters

Chemical and Aqueous Transport (CAT) meters (Tryon et al., 2001) have been in use for over a decade and have played a major role in quantifying the flux of water from benthic seeps, its impact on geochemical cycles and biological systems, and the nature of the driving forces of seepage in a wide range of settings (e.g. Tryon et al., 1999; 2002; 2004; 2010a; 2010b; Labonte et al., 2007). A description of the instruments can be found in the Facilites section of this proposal. In brief, these instruments are capable of recording a temporal record of fluid flow through the sediment surface in the sub mm to 10s of meters range at a temporal resolution of a few days. They also continuously

collect fluid samples for later analysis, both for temporal changes in chemistry and to collect samples of fluid unaffected by coring and more specifically targeted to active expulsion sites than is often possible with coring.

The primary purpose of the CAT-meter deployments is to look for correlations between flow rates at seeps, regional seismicity (DONET, NanTroSEIZE CORKs and onshore stations), and pore pressure transients at the instrumented boreholes (MeBo as well as NanTroSEIZE). Such correlations have been observed with these instruments at a very large and highly gas-charged submarine mud volcano on the Nile delta (Brückmann et al., 2010) and by other instrumentation in Dashgil MV on land (Kopf et al., 2010). Questions to be directly addressed are: Is this correlation typical of mud volcanism or only for the largest and most gas-rich volcanoes? Alternatively, is it more typical for mud volcanoes and the fluid flow systems within them to respond to their own internal cycles driven by the buildup of gas and/or pore pressure? We will also collect a time series of samples of the fluid being emitted. This will augment the core pore fluid sampling as we will be able to more directly target fluid emissions, however, this is by no means an alternative to coring as we will not be able to analyse the fluids for the more reactive or ephemeral species due to the long storage time in the sample coils.

Objective 2: Study of MV products

Solid phase

Working on the solid phase of mud volcano ejecta offers a wide range of investigations regarding the nature and physical properties of the materials. The first shed light on the types of materials (matrix as well as embedded clasts, if present), their origin from a regional (provenance) as well as tectono-stratigraphic (mobilisation depth) perspective, and geological evolution with time. Measurement of physical properties on discrete samples help explain the mechanism of ascent and emplacement and define crucial geotechnical parameters such as permeability, hydraulic diffusivity, viscosity, or shear strength.

The mud matrix usually originates from deeper levels than the clasts, because the majority of the latter is believed to be collected during ascent along a fault or conduit (Robertson et al., 1996; Kopf, 2002). Since the matrix usually contains large amounts of clay minerals, illite crystallinity or smectite-illite ratios are indicative of a certain degree of thermal maturation. The same is true for matured organic matter so that vitrinite reflectance has been demonstrated to be powerful in reconstructing MV mobilisation depths (e.g. Schulz et al., 1997; Kopf et al., 2000). Physical properties of the matrix unravel the ascent history and fluid content, and may range from stiff, low-porosity mud (often from shear-enhanced dewatering at the outside of a conduit) to gooey mousse with gas pockets (Emeis et al., 1996; Kopf et al, 2012a, b). Polymictic clasts are a powerful hint

towards mobilisation depth as well, in particular if the regional tectono-stratigraphy is known (Robertson & Kopf, 1998). Also, the habitus and size of the clasts and their abundance relative to the matrix do not only define the texture of the individual layers of mud breccia, but also serve to reconstruct the evolution in time (Kopf & Flecker, 1996).

Fluid phase

Geoichemical signatures of the fluid phase help to assess their source depth, the physical, metamorphic, or diagenetic processes that generated the fluids, what processes occur in the pathways of the fluids, and the rate of transport of the fluids. In order to achieve this in the *MEMO* project, we will specifically be looking at:

Chloride: Reduced Cl can be indicative of an input of pure water from dehydration of hydrous minerals (e.g., smectite, opal, serpentine) or from dissociation of gas hydrate. When combined with other tracers (below) the responsible processes can be constrained.

Na, K, Mg, and Ca: Common silicate diagenetic reactions are responsible for characteristic increases/decreases in the concentrations of these elements.

Ca, Mg, Sr: Common carbonate diagenetic reactions are responsible for characteristic increases/decreases in the concentrations of these elements (calcite, dolomite, siderite precipitation/dissolution or reprecipitation).

B, Li: Typically taken up during low temperature clay formation from ash and typically released during the smectite-illite reaction. As sediments reach higher temperatures (200-300°C), Li concentrations in pore fluids increase exponentially while B increases rougly linearly. B is also taken up during low temperature serpentinisation of oceanic lithosphere, particularly at faults and fractures, and is released during alteration from low T to high T serpentine phases.

Na, K, Ca, Mg, and Li are used variously in geothermometry to determine the temperature of the source region and, through the extrapolated regional temperature gradient, the source depth (see [Verma et al., 2008] for a thorough review).

$\delta^{18}OH_2O$ and δDH_2O: δD is the primary tracer for differentiating between dehydration reactions and hydrate dissociation. The former leads to low δD and the latter leads to high δD while both increase $\delta^{18}O$. A number of other processes affect these isotopes in a predictable manner (see [Dählmann et al., 2003], for a good review).

B isotopes are considered powerful tracers in subduction zones and characteristic patterns are known for specific mineralogies, environments, and temperatures (see review by [Deyhle et al., 2005] and also Fig. 4).

Hydrocarbons: The makeup of hydrocarbon gases and their carbon isotopes primarily differentiate between shallow-sourced microbial methane and deep-sourced thermogenic gases and are thus a strong indicator of fluid source depth/temperature.

DIC: Carbon can be derived from a number of potential sources from shallow marine organic matter down to the mantle. Its isotopic composition can potentially be used to distinguish between these possibilities, particularly when combined with other tracers. Typically, isotopically-depleted methane and ^{13}C-enriched DIC produced by deep methanogenesis are carried from depth to the surface by upward flow of fluids derived from sediments of the subducting slab. If this transport is slow, most of the ascending dissolved methane will be oxidized via sulfate reduction, generating DIC with low $\delta^{13}C_{\sum CO2}$ values. However if fluids are passing rapidly (and recently) from depth, there will be a large contribution of DIC originating from deep methanogenesis with high $\delta^{13}C_{DIC}$ values.

The application of the above to the data set resulting from the *MEMO* project will lead to determining the processes involved in the fluid's genesis. For example, the effects of gas hydrate dissociation will likely be seen in the fluids in the form of low chlorinity. Since this is a simple addition of pure water and the O and H isotopic relationship is well known, this process can be easily distinguished from others. If we only see the results of low-T silicate diagenesis (high Cl, Ca, low B, K, Li, Mg, positive δD, negative $\delta^{18}O$) then the source is likely compaction-driven high pore pressures at or just below the base of the basin. Low chlorinities along with high B and Li, low δD, and high $\delta^{18}O$ suggests advancing smectite dehydration, the transition to illite, source depths of 2 km or more, and temperatures of 80-130°C. If illitisation is indicated, then the relationship between B isotope fractionation and temperature (Deyhle et al., 2005) can be further used to constrain the depth of the mud volcano's roots. A very low B/Li ratio can be indicative of higher temperatures (>200°C) and this ratio may be useful in bracketing source temperature based on experimental results (You et al., 2001). As sources become deeper and multiple sources and processes have various effects on the ultimate fluid chemistry, the determination of the fluid genesis and history becomes increasingly complicated. Often responsible processes can only be bracketed or eliminated and thus, some constraints put on them. Also the results of initial analyses may suggest further procedures that may be utilised to achieve the projects goals.

Headspace gas in gravity cores as well as gas analysis from dissociated gas hydrate recovered shed additional light on the depth of fluid origin. Analysis in the MEMO project will include measurements of the C_1/C_{2+} ratio as well as $\delta^{13}C$ to determine the significance of a thermogenic component as well as $\delta^{18}O$ of the gas hydrate water (in comparison to that of the regular interstitial waters). See also detailed descriptions in the "Methods" section (Ch. 5) below.

4. Narrative of the cruise

(A. Kopf)

Cruise SO222 had to be split into two legs given the fact that RV Sonne is too small to host the MeBo seafloor drill rig and the ROV Quest at the same time.

Leg SO222A started on 09 June 2012 in Hong Kong. After a 5-day transit towards Japan, the vessel arrived in the Kumano Basin working area late on 14 June. Station work started with CTD, a roll & pitch calibration, Parasound profiling and Posidonia transducer calibration. Gravity coring as well as heat flow and CPT measurements were taken up on 15 June, and the MeBo seafloor drill was deployed on 16 June for the first time. Work continued until the late night of 18 June, when RV Sonne had to head northwards to escape typhoon *GUCHOL*. After almost 48 hrs somewhere close to Japan, we headed south again and commenced gravity coring, Parasound and heat flow work on 21 June. During the night to 22 June, typhoon *TAMIL* passed the research area and R/V *Sonne* went southwards to wait on weather. Station work continued in the afternoon of 23 June and three more MeBo deployments were performed in addition to the smaller seagoing devices. Late on 29 June, R/V *Sonne* headed northwards for the Nagoya mid-cruise port call.

During the 4-day port call in Nagoya, Japan, MeBo had to get demobilised first. During the first two days, this included heaving of all components to the pier as well as detaching all welded support structures of the LARS (MeBo **L**aunch **a**nd **r**ecovery **s**ystem) from the aft deck. On day 3 and 4, the ROV Quest was mobilised and other components were received. Over the course of the port call, part of the scientific crew was exchanged (see "List of participants" above). On 03 July, a scientific meeting of observatory specialists from Japan, the USA and Germany was held in R/V *Sonne*'s conference room in order to review the acievements during Leg SO222A, plan measures during Leg SO222B, and prepare for a scientific workshop in Houston, USA, in September 2012 as well as a Japanese cruise in the Kumano Basin in Jan/Feb 2013, where more observatory work is envisaged.

On 04 July, 9.00, R/V *Sonne* headed back out towards the Kumano Basin for Leg SO222B research tasks. Station work continued later the same day after a 10 hr-transit back to the mud volcano field. Apart from gravity coring, Parasound, CPT and heat flow deployments, ROV Quest was used twice (05 July and 06 July) to survey and sample mud volcanoes, carry out *in situ* T-measurements, and deploy observatory components. Problems with the vehicle enforced alternate station work including flowmeter deployments for the remainder of the cruise. This included gravity coring, TV grab and heat flow surveys, and multibeam mapping. On 16 July, 7.00 station work was ended and R/V *Sonne* started the transit to Busan, Korea. There, the cruise ended on July 18 in the late afternoon with all scientists evacuating the ship since a typhoon escape was ordered by the port authority for that night.

5. Methods

5.1. CTD, Seafloor and Parasound surveys

(P. Wintersteller, T. Fleischmann, G. Bohrmann)

CTD (Conductivity – Temperature – Depth)

To obtain information about the distribution of the water masses along the Iberian coast a CTDOS (Conductivity, Temperature, Depth, Oxygen, Salinity) profiler combined with a rosette water sampler (24 Niskin bottles, 1 l volume, HydroBios; see Fig. 10) was used at two different sites during SO222. The CTD data were primarily needed for the conversion of the recorded SIMRAD EM120 travel times into depth values.

Figure 10: CTD on main deck of RV *Sonne* prior to deployment.

KONGSBERG EM120 Multibeam system

The hull-mounted KONGSBERG EM120 multibeam echosounder (MBES) allows accurate bathymetric mapping up to depths deeper than 11,000 m. The system is composed of two transducer arrays, sending successive frequencies coded acoustic signals of 11.25 to 12.6 kHz. Data acquisition is

based on successive emission-reception cycles of the signal. The emission beam is max 150° wide across track, and 2° along track direction. The reception is obtained from 191 overlapping beams, with widths of 2° across and 2° along track. Using the 2-way-travel-time and the beam angle known from each beam, and taking into account the ray bending due to refraction in the water column by sound speed variations, depth is estimated from each beam. A combination of phase (lateral beams) and amplitude (center beams) is used to provide a measurement accuracy practically independent of the beam pointing angle.

During cruise SO222, MBES was used continuously in parallel with PARSOUND sub-bottom surveys. In total MBES/PS - surveys of about 1500km has been acquired during SO222 leg A and B. Tab. 1 shows the settings used to acquire the data.

Table 1: Settings used during SO222

Coverage angle	60°/60°	65°/65° for the last survey
Beam spacing	in between	
Pitch stabilization	on	
Yaw stabilization	rel. mean HDG	medium
SSV at Transducer	from sensor	
Pinge Mode	auto	

For reasonable hydro acoustic recording a proper sound velocity profile (SVP) is essential. Thus, two CTD's were taken during the cruise. Two SVP's were calculated based on the SEABIRD CTD measurements (see above and section 6.1). The graph shows a wide variability in sound velocity over the upper most 200m of the water column. The SVP's have been applied to EM120 according to time noticed in the hydro acoustic protocol. There was no chance to get CTD data from the southern Kumano basin since the current was simply too strong (4-5kn) to deploy the equipment.

During leg SO222a a patch-test has been performed. The results of this roll- and pitch-calibration showed no changes in the already given offsets of the system.

ATLAS PARASOUND profiling

The ATLAS Hydrographic PARASOUND sediment echosounder is also a hull-mounted system on R/V Sonne. It determines the water depth and detects variable secondary low frequencies from 1 up to 5.8 kHz thereby providing high-resolution information of the sedimentary layers up to a depth of 200 meters below sea floor. For the sub-bottom profiler task, the system uses the parametric effect, which produces additional frequencies through non-linear acoustic interaction of finite amplitude waves. If two sound waves of similar frequencies (18 kHz, 22 kHz) are emitted simultaneously, a signal of the resulting frequency (e.g. 4 kHz) is generated for sufficiently high primary amplitudes. The new component is travelling within the emission cone of the original high frequency waves, which are

limited to an angle of 4° for the equipment used. The resulting footprint size of 7% of the depth is much smaller than for conventional systems and both vertical and lateral resolutions are significantly improved.

Primary high and secondary low frequencies are recorded as raw-format (*.asd) as well as ps3 and SeGY formats. The survey of both legs SO222a and SO222b is split into subfolders according to the frequencies (PHF, SLF). SeNT, a program made by Dr. Hanno Keil, Univ. of Bremen, has been used for post processing. All specifications and settings applied to the PARASOUND system during SO222 are listed in Table 2. The sound velocity profile measured by the CTD has been applied to the system for accurate raypathing.

Table 2: PARASOUND settings during SO222b

Hydromap Control	Single Pulse	Quasi-Equidistant Transmission
Desired Time Intervall	-	300ms
Manual Pulselength	0.250ms	0.250ms
Periods pro Pulse	1 PpP	1 PpP
Max. Transmission Power	100% (160V)	100% (160V)
Pulse Type	continous wave	continous wave
Pulse Shape	Rectangular	Rectangular
Desired PHF freq.	18.8 kHz	18.8 kHz
Desired SLF	4 kHz	4 kHz
Online Filtering Parastore SLF		
Low Pass	Iteration	1
	High Cut	2kHz
(Auto-)Correlation		On
Amplitude Scale		
Clip	50 - 500mV	depends on sediments & wave angle
Logarithmic Scale	On	
Gain Bottom TVC	0.05-0.2	depends on Clip & it's dependencies

Acquiring data in “Single Pulse” mode was mainly driven by investigations in the water column. The mode allows using the primary high frequency (PHF) to search for gas-flares in the water column. Unfortunately no degassing could be observed in the Kumano basin.

The open-source software MB-System version 5.3.1 (Caress & Chayes, 1996) and GMT version 4.3.1 (Wessel & Smith, 1995) were used for bathymetric data processing, editing and evaluation. ESRI ArcGIS version 10 is inserted to create maps and a sustainable spatial data management.

5.2. *In situ* temperature measurements

(N. Kaul, B. Heesemann, T. Feseker, K. Asshoff)

The ascent of warm fluids and mud at mud volcanoes and along faults creates temperature anomalies at the seabed. Detecting and quantifying these anomalies in turn provides information about the seepage rates and sediment mass movements. Furthermore, in situ sediment temperature measurements are cruicial for determining the extent of the gas hydrate stability zone in the sub-seabed. During this cruise, we conducted heat flow measurements at both local and regional scales in order to assess the activity of faults and mud volcanoes in the Kumano basin and to map the regional background heat flux.

In situ sediment temperature and thermal conductivity measurements were conducted using the 6 m-long Bremen heat flow probe (Fig. 11). The probe has a Lister-type violin bow design. The sensor strings contain 21 thermistors spaced at an interval of 26 cm and a heater wire along the entire length of the string. The electronics are integrated into the head of the probe. Four 8-channels 22-bit A/D converters are used to record temperature readings at a sampling interval of 1 s. The probe can be operated in an autonomous mode or with real-time data transmission when using the ship's coax wire (Fig. 12).

Figure 11: The 6 m-long Bremen heat flow probe on the working deck of R/V *Sonne*.

During this cruise, measurements were conducted with real-time data transmission in so called 'pogo-style', performing several penetrations in a row at small distances. Each penetration consisted of raising the probe some hundred meters above the sea floor from the previous penetration, slowly moving the ship to the next penetration site and letting the wire angle become nearly vertical before dropping the probe into the sediment for the next penetration. Once the probe had penetrated the

seafloor, it was left undisturbed for 8 minutes for the sediment temperature measurement and another 8 minutes, in case a thermal conductivity measurement was conducted. For the spacing of stations used in this survey, the transit between measurements took between 30 and 75 minutes. Transit speed was governed by the trade-off between keeping the wire angle small and minimizing the time between measurements.

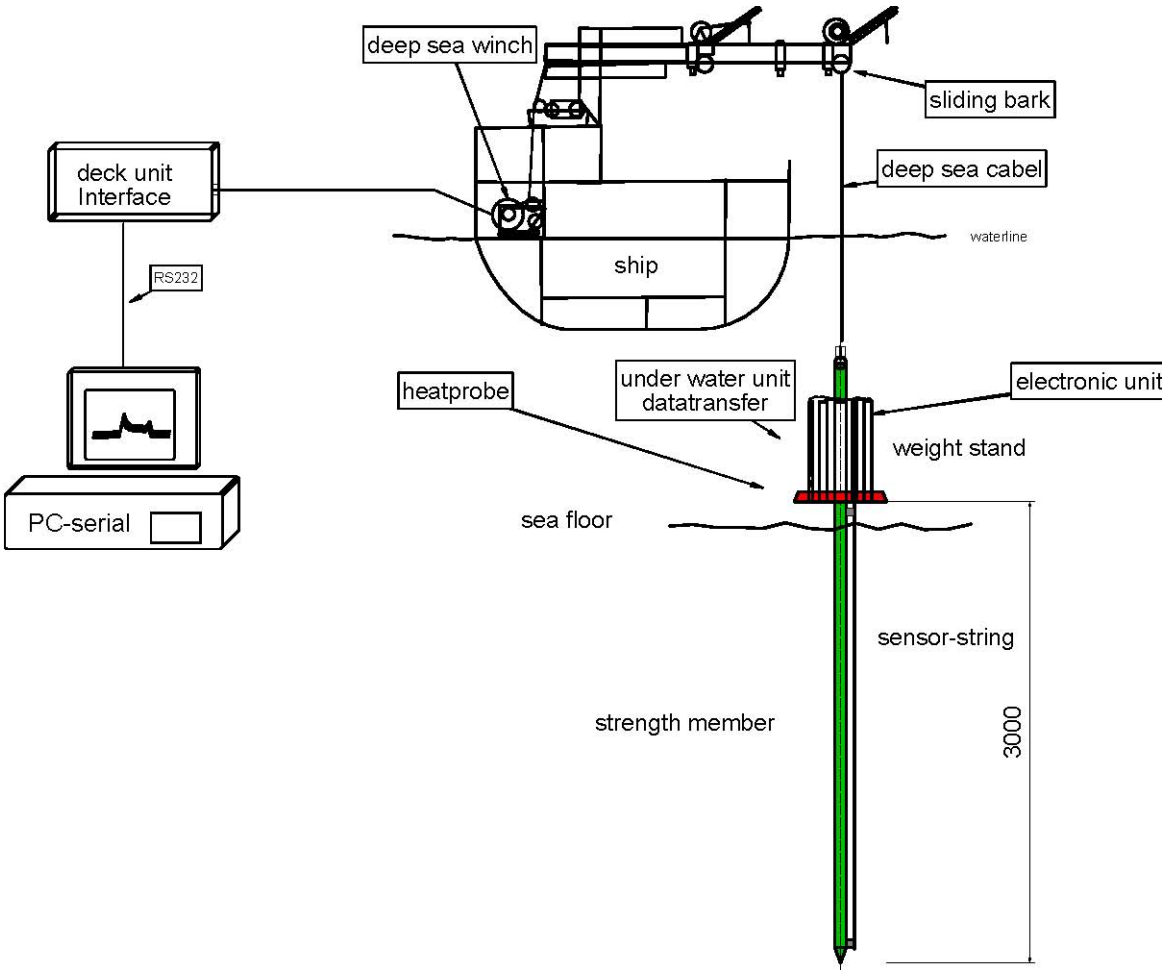

Figure 12: Schematic view of heat flow probe operation with real-time data transmission

Winch speed during payout and retrieval of wire was 1 m/s. Deployment of the instrument was from amid ship on the starboard side, employing a beam crane and assistance crane. This procedure ensured safe operation even during medium sea state and minimum interference due to the ships vertical movement during station work.

For precise positioning of the probe at the seafloor, an IXSEA transponder was mounted on the wire 100 m above the instrument. The IXSEA Oceanos Abyss positioning system was used to track the probe at depth. At mud volcanoes, individual heat flow measurements were condcuted at a spacing of between 100 and 200 m, while a spacing of around 1000 m was used for regional surveys.

Full processing of the measurements included the calibration of thermistor sensors, calculation of sediment temperatures and temperature gradients, correction for probe tilt during penetration, and calculation of thermal conductivities. Prior to each series of measurements, the probe was stopped at 100 to 200 m above the seabed for three to five minutes to inter-calibrate the temperature sensors. The software MHFRED (based on Villinger & Davis, 1987) was used to extrapolate the equilibrium sediment temperatures from the recorded time series at each station and to determine the thermal conductivity of the seabed at selected stations.

5.3. *In situ* CPT testing

(M. Lange, A. Steiner, A. Kopf)

On R/V *Sonne* cruise SO222, we used the MARUM free-fall CPTu probe for deep water. Cone Penetration Testing (CPT) is an effective method for *in situ* measurements of these geotechnical parameters with one instrument (Lunne et al., 1997), namely sedimentary strength (tip resistance, sleeve friction), pore pressure, tilt and acceleration. For these measurements, the CPT system relies on 15 cm^2 cone and pore pressure (u1, u2 and u3 positions depending on instrument and configuration; see below) and a pressure housing containing a all other sensors and the microprocessor at the top. In addition, deceleration and tilt are monitored for vertical profiling of the penetrated sediment column.

The free-fall CPT (FF-CPT) instrument for deep (up to 4000 m water depth) marine use consists of a 15 cm^2 piezocone and a water-proof housing containing a microprocessor, volatile memory, battery, and accelerometer (see Fig. 13a; and Stegmann and Kopf, 2007 for details). Two pore pressure port (u_1 and u_3) are equipped with differential pressure transducers. The stainless steel pressure-tight housing containing a microprocessor, standard secure digital memory card (SD), tiltmeter, accelerometer, power supply (battery packages), absolute and differential pore-water sensors as well as power and data interface module (PDIM). The tiltmeter (dual-axis tilt sensor) monitors the penetration angle at +/- 45° relative to vertical. Five different accelerometers with different ranges (+/- 1.7g, +/- 18g, +/- 35g, +/- 70g and +/- 120g) provide information about the descent de/acceleration behaviour of the DWFF-CPTU instrument upon penetration. These data allow the researcher to calculate penetration velocity and depth during multiple deployments by 1^{st} and 2^{nd} integration.

The reference pore-water pressure port at the pressure-tight housing is equipped with an absolute 40.0 MPa (400 bar) pressure sensors (WIKA ECO-1). The pore-water pressure ports at the tip (u_1) and 0.75 m behind the tip (u_3) are connected to the differential pore-water pressure transducers (VALIDYNE P55D) via stainless steel tubing. Pore-water pressure changes can be monitored over a

range of 85 kPa (12.5 PSI) to 100-140 kPa (15 - 20 PSI) with a resolution between 8 and 15 Pa (Fig. 13b). The sensors are protected with valves if high excess pore-water pressures are met (e.g. owing to blocked hydraulic tubes). They are further used to bleed the tubing in case of gas is trapped inside, especially during the initial phase of deployment when the instrument is lowered through the water column.

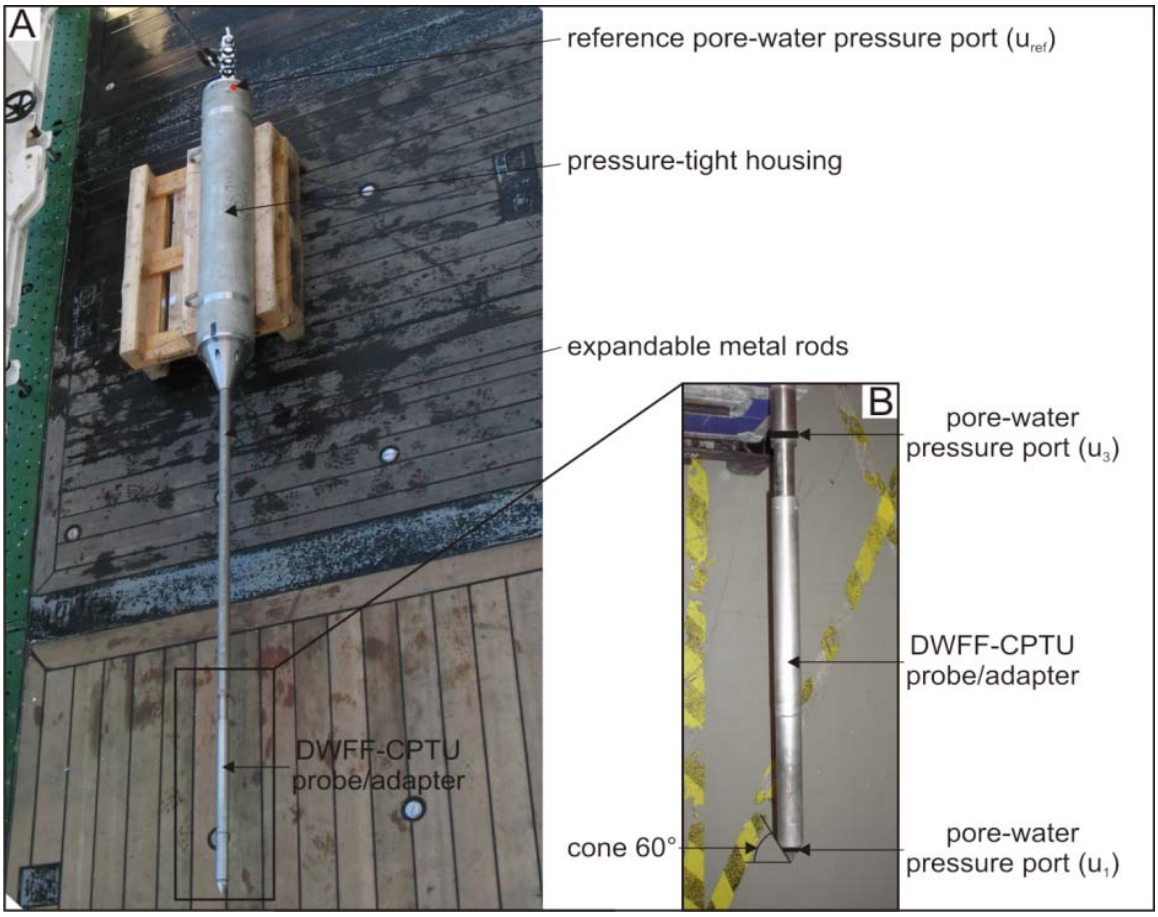

Figure 13: Deep-water FF-CPTu instrument (a). Panel (b) shows blow up of the frontal portion with the pore pressure ports.

The DWFF-CPTu instrument is used in an autonomous mode, at which all sensor and transducer information will be stored on a standard secure digital memory card (SD) with a very high sampling frequency (1 kHz). In addition, a data transmission telemetry system (Seabird Electronics SBE36 CTD) is used to monitor all sensor and transducer parameter on board the research vessel in real-time (lower sampling frequency 1 Hz). The telemetry system consists of a deck unit (SBE36 CTD) and a PDIM. A schematically sketch of the telemetry system is shown in Figure 14. It provides real-time data acquisition and control of the instrument (e.g. operation of the valves) via an attached personal computer (PC) using a self-developed LABVIEW control software.

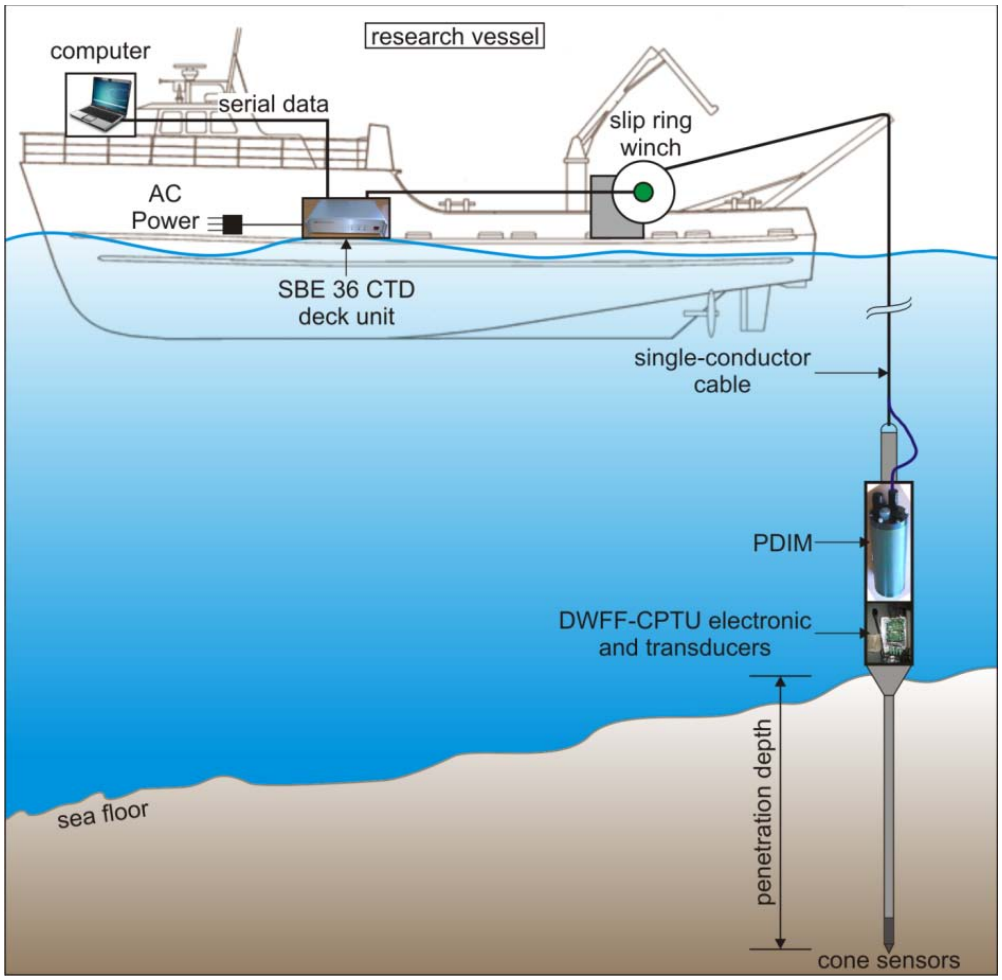

Figure 14: Schematic of SBE36 CTD and PDIM telemetry system.

The frequency of data acquisition is variable and depends on the operation purpose of the DWFF-CPTU instrument (e.g. sub-seafloor profiling or pore-water pressure dissipation). Binary data are temporarily stored on a standard secure digital memory card (SD) and then downloaded via W-LAN to a PC. The two non-volatile battery packs available provide performance times of about eight to twelve hours, respectively. A self-developed deck interface box is used to download the recorded data and to charge the battery packs.

The length of the DWFF-CPTU instrument is variable from 4.1 m to a maximum length of 6.8 m depending on what type of sediment is anticipated. The extension is accomplished by adding 1.4 m long metal rods and internal extension data/power cables as well as steel tubing within them. Hence, the weight of the DWFF-CPTU instrument ranges from approx. 500 kg to max. 550 kg. The DWFF-CPTU instrument is deployed as individual measurement or pogo-style and remains in the sub-seafloor for about 15 minutes.

The DWFF-CPTU instrument was used with a self-developed piezocone probe/adapter (Fig. 13b) equipped with pore-water pressure ports at two locations (at the tip - Δu_1 and 0.75 m behind the tip -

Δu_3). During cruise SO222, the DWFF-CPTU instrument was generally deployed in 4.1 m long mode (CPTU probe/adapter + 1 rod + pressure-tight housing).

A 1 kHz microprocessor data recording unit (AVISARO microcontroller) was utilised during deployments, focusing at the shape of the pore-water pressure dissipation curve (> 20 min deployment time according telemetry real-time data) and aiming at the sub-seafloor profiling of the sedimentary succession. The sub-seafloor profiling takes less than 7.0 sec and at the high sampling rate, provides the user with data of a vertical resolution < 5.0 $x10^{-3}$ m thickness.

The deployment mode aims (i) at a high-resolution vertical record (1 kHz logging frequency) of crucial in-situ sediment physical properties and (ii) at the recording of the excess pore-water pressure evolution once the DWFF-CPTU instrument is stuck in the sediment (dissipation test). Pore-water pressure dissipation is usually recorded for 20 to 30 min. The DWFF-CPTU instrument was veered at 1.2 m/s winch speed to a level 30 – 50 m above the seafloor, then the winch speed was varied between 0.5 - 1.2 m/s until the DWFF-CPTU probe hits the seafloor and dynamically decelerated until its penetration depth of several meters sub-seafloor (a fix winch speed for each location). The instrument is recovered after the dissipation test.

5.4. CAT-meters

(M. Tryon)

The Chemical and Aqueous Transport (CAT) meter (Fig. 15) (Tryon et al., 2001) is designed to quantify both inflow and outflow rates on the order of 0.05 cm/yr to 100 m/yr. At high outflow rates, a time series record of the outflow fluid chemistry may also be obtained. These instruments have been in use since 1998 and have been successful in monitoring long term fluid flow in both seep and non-seep environments (e.g. Tryon et al., 2004, Tryon, 2010). The CAT meter uses the dilution of a chemical tracer to measure flow through the outlet tubing exiting the top of a collection chamber (Fig. 16). The pump contains two osmotic membranes that separate the chambers containing pure water from the saline side that is held at saturation levels by an excess of NaCl. Due to the constant gradient, distilled water is drawn from the fresh water chamber through the osmotic membrane into the saline chamber at a rate that is constant for a given temperature. The saline output side of the pump system is rigged to inject the tracer while the distilled input side of the two pumps are connected to separate sample coils into which they draw fluid from either side of the tracer injection point (Fig. 16). Each sample coil is initially filled with deionized water. Having two sample coils allows both inflow and outflow to be measured. A unique pattern of chemical tracer distribution is recorded in the sample coils allowing a serial record of the flow rates to be determined. Upon recovery of the instruments the sample coils are subsampled at appropriate intervals and analyzed

using a Perkin-Elmer Optima 3000XL ICP-OES. Both tracer concentration and major ion concentration (Na, Ca, Mg, S, K, Sr, B, Li) are determined simultaneously.

Figure 15: CAT meter

As explained in Tryon et al. (2001), diffusion in the sample coils is negligible. Typical sample sizes are 25-75 cm of tubing, many times the characteristic diffusion length for typical seawater ions at ocean bottom temperatures. Our data has shown that we typically achieve resolutions of ~0.5% of the deployment time in the latest portions of the record and ~2% in the oldest portion for deployments of a year.

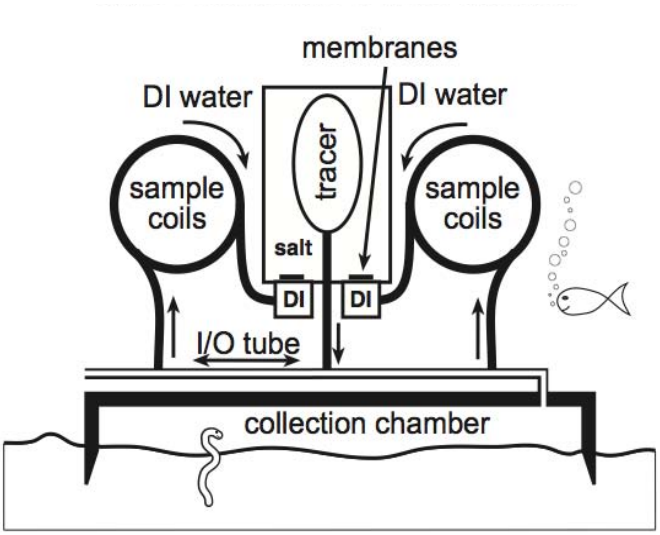

Figure 16: CAT meter schematic (from Tryon et al., 2001).

5.5. MeBo and Gravity coring / sediment description / IR imagery

(M. Vahlenkamp, A. Hüpers, S. Hammerschmidt, M. Belke-Brea, J. Wei, A. Kopf, M. Bergenthal, R. Düßmann, K. Kaszemeik, S. Klar, C. Noorlander, U. Rosiak, U. Spiesecke, A. Stachowski, W. Schmidt, C. Seiter)

Gravity corer

In order to recover sediment cores, a gravity corer with tube length of 6 m and a weight of approximately 1.8 tons was used during cruise SO222 (Fig. 17). Before using the coring tool, the plastic liners were marked lengthwise with a straight line in order to retain the orientation of the core for potential paleomagnetic analyses and then placed inside the steel tube of the gravity corer.

Figure 17: Gravity corer on board R/V *Sonne*.

Once back on deck, the sediment cores were cut into sections of 1 m length, closed with caps on both ends and labelled according to a standard scheme (Fig. 18). By definition, the half core with the marked line was stored as archive half, while description, sampling, etc. were carried out on the remaining half. For the detailed procedures each working half core underwent, see below.

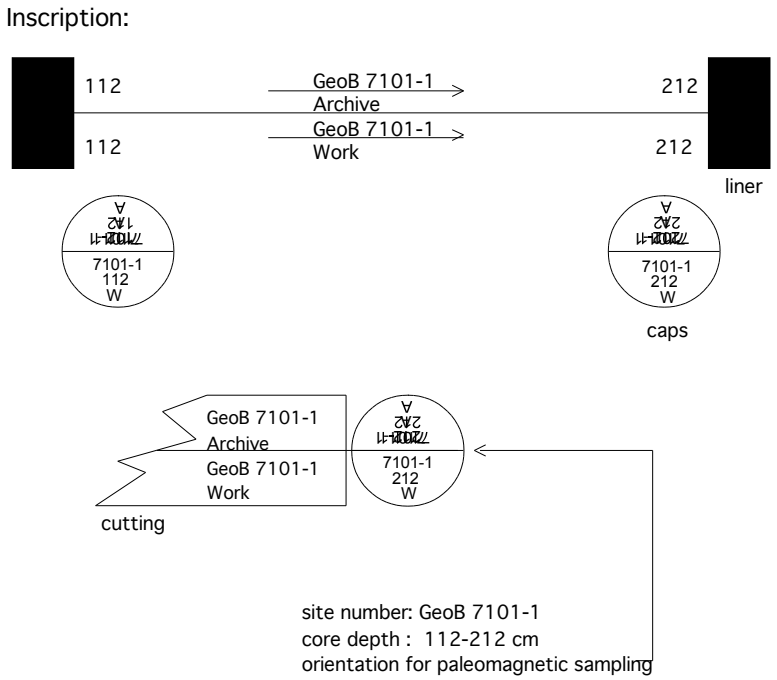

Figure 18: Scheme of the inscription of gravity core segments used during cruise SO222.

MeBo

During RV *Sonne* leg SO222a, the seafloor drilling rig MeBo (Fig. 19) was used for getting long sediment cores and to install borehole corks. MeBo is a robotic drill that is deployed on the sea bed and remotely controlled from the vessel. The complete MeBo-system, including drill, winch, launch and recovery system, control unit, as well as workshop and spare drill tools is shipped within six 20' containers. A steel armoured umbilical with a diameter of 32 mm is used to lower the 10-tons heavy device to the sea bed where four legs are being armed out in order to increase the stability of the rig. Copper wires and fibre optic cables within the umbilical are used for energy supply from the vessel and for communication between the MeBo and the control unit on the deck of the vessel. The maximum deployment depth in the current configuration is ~2000 m.

The mast with the feeding system forms the central part of the drill rig. The drill head provides the required torque and rotary speed for rock drilling and is mounted on a guide carriage that moves up and down the mast with a maximum push force of 4 tons. A water pump provides sea water for flushing the drill string for cooling of the drill bit and for removing the drill cuttings. Core barrels and rods are stored on two magazines on the drill rig. We used wire-line core barrels (HQ) and hard metal drill bit with 55 mm core diameter (push coring). The stroke length was 2.35 m each. With complete loading of the magazines a maximum coring depth of more than 70 m can be reached. Station time can reach more than 24 hrs per deployment.

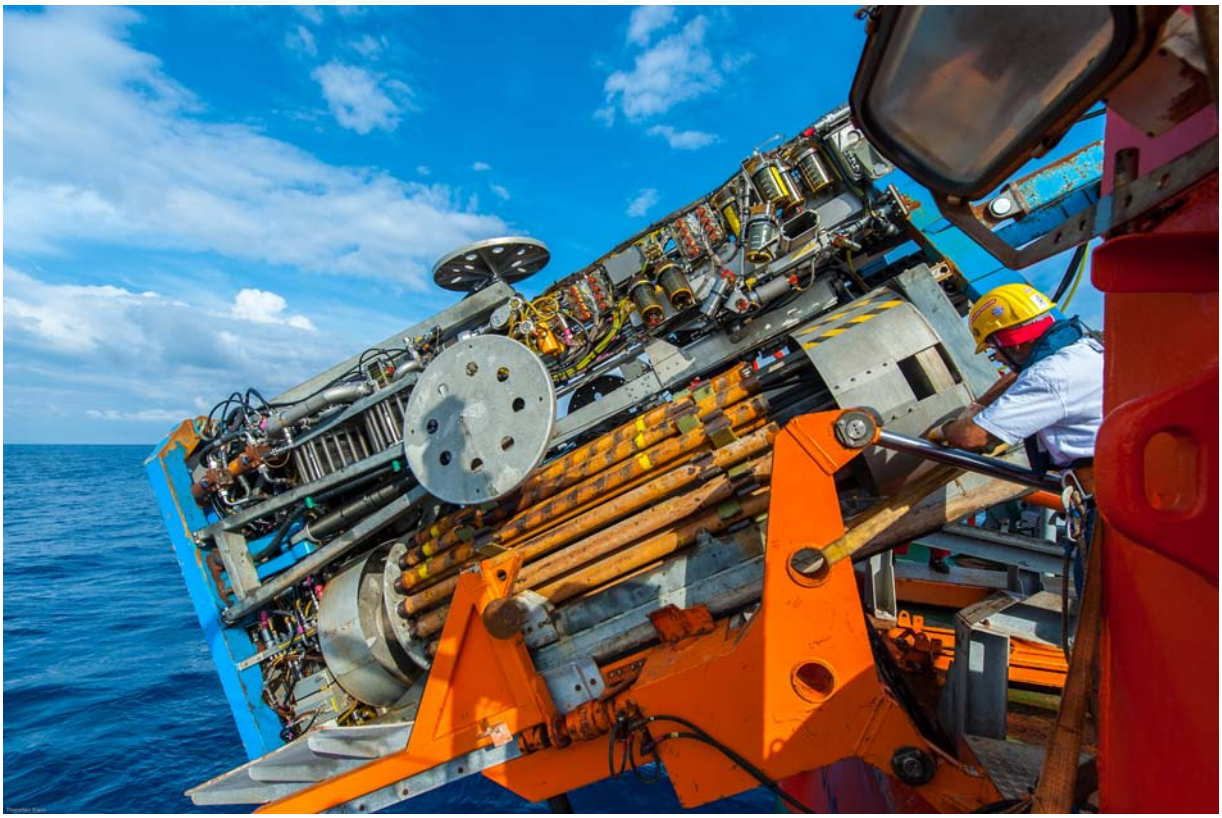

Figure 19: MeBo drill rig during launch on the aft deck of RV *Sonne*.

During this cruise the MeBo was deployed 6 times at 6 stations. The water depth was almost 2000 m and it was the first time for MeBo to drill in 2000 m waterdepth. During the whole cruise no malfunction of the drill rig occurred.

The main objective of this cruise was to install borehole observatories with the MeBo. Therefore the outer drill string were sealed with different kinds of monitoring systems, so called MeBo Plugs (1&2) and MeBo CORKs type A and B (see section 6.8 below).

Gamma Ray logging in MeBo holes

A Spectrum Gamma Ray Memory Probe (SGR-Memory) consisting of a Spectral Gamma Ray Probe (Antares 1460) combined with a Memory Data Logger (Antares 3101) was used for bore hole logging at the MeBo drilling sites. The Spectrum Gamma Ray probe is equipped with a 30 cm long scintillation crystal combined with a photo-multiplier. Light impulses that are generated by gamma ray collisions with the scintillation crystal are counted and analysed concerning the energy spectrum. The three naturally occurring gamma ray emitter - potassium, uranium and thorium - generate different energy spectra. A GeoBase software package is used to calculate a best fit for the spectra. By combining the results of the Spectrum fit with the gammy ray counts the concentrations of K, U, and Th are calculated.

The SGR-Memory is an autonomous tool that is used with the MeBo drilling system. When the maximum coring depth is reached the inner core barrel is replaced by the probe. The gravity point of the sensor is located about 125 cm above the drill bit and measures through the drill pipe. The probe is hooked up the bore hole together with the drill pipe during recovery of the drill string (logging while tripping). Tripping speed was about 1m per minute. In the other cases the measurement was done by hooking up the tool inside the drill string with the MeBo wireline winch.

Figure 20: Antares SGR probe prior to loading into the MeBo carousel on deck of RV *Sonne*.

In situ T-measurements using MeBo

During this cruise a prototype of different kinds of temperature logger probes were tested. Therefore a miniature temperature logger (MTL) build by 'Antares' was adapted to the tip of a pilot tube. The electronic and battery of the MTL is located in a 16mm diameter housing on top of a stainless steel tube (5mm in diameter and ~100mm long). The sensor element is located at the end of this tube. Figure 21 shows a pilot design containing the MTL for soft sediment (left), the MTL (middle) and a pilot for hard grounds where the MTL is sheltered in a steel cone (right). With the feeding system the tip was pushed approx. 20cm into the sediment. The starting points of each curve were aligned. In total, the T-probes were used in three of the six holes drilled with MeBo (Table 3). For results, see section 6.5 below.

Table 3: Station list for the MeBo *in situ* temperature measurements.

Station GeoB No.	Latitude [N]	Longitude [E]	Water depth [m]	Remarks
16709	33° 38’ 01.6’’	136° 40’ 15.4’’	1951	Cone: Hard ground; three temperature measurements in 10m, 20m and 29m bsf.
16728	33° 39' 32.5"	136° 38' 00.9"	2055	Cone: Soft sediment; temperature measurement in 10m bsf
16732	33° 38' 13.3"	136° 40' 30.0"	2035	Cone: Soft sediment; three temperature measurements in 10m, 19m and 29m bsf.

Figure 21: *In situ* temperature probes used during cruise SO222.

Infra-Red imagery of gas hydrate bearing cores

The identification and documentation of gas hydrates in the sediment cores of the Sonne-222 cruise was an important task, which influenced the core handling as well as the sampling strategy of the sediment sequences. Gas hydrates are stable only at lower temperature and higher pressure than atmospheric conditions and are therefore dissociating during the recovery from the seafloor. Decomposition starts as soon as the hydrates moved out of their stability field. Based on the temperature and pressure conditions as well as the chemical compositions gas hydrates of structure I at the research area are stable below a water depth of ca. 500 m. Hydrate dissociation starts slowly in cores during wireline lifting above the stability phase boundary and is probably strongly increasing in

the upper water column where water temperature is around 24°C and on deck of the vessel where air temperature around 25°C occurs. Infrared thermal imaging of the surface of retrieved cores was shown to successfully identify thermal anomalies associated with gas hydrates. The novel method of hydrate identification was first used during ODP Leg 201 in sediments from the Peru margin (Ford et al. 2002). The technique was fully implemented during ODP Leg 204 on southern Hydrate Ridge at Cascadia margin (Tréhu et al. 2004). Although there are other processes related to negative temperature anomalies, distinct strong cold anomalies were shown to be directly associated spatially with gas hydrates due to their dissociation. The dissociation of hydrates is an endothermic process and the sediments containing hydrates are cooled relative to the surrounding deposits, thus creating negative temperature anomalies.

Infrared imaging of cores was used on all the MeBo cores and most of the gravity cores. The major goal was to reach the following benefits during this cruise:

- Rapid knowledge of gas hydrate presence in cores from the temperature anomalies of the core liner on surface for sampling hydrates and pore water above and below hydrate layers.
- To assess and document the approximate distribution of hydrates.
- To understand more about the texture of single hydrate specimen based on the size and shape of cold temperature anomalies and their delta-T values in order to use IR imaging as a proxy.

Infrared radiation (ca. 0.750-350 um) is emitted by the objects as a function of their temperature. Therefore IR cameras which detect various wavelengths within their images can transfer the signals to a temperature pattern on the surface of the objects. We used during this cruise a ThermaCam SC 620 camera (FLIR Systems) to map the thermal structure along the cores. The FLIR system allows using 3 different temperature ranges from which we set to record from -40°C to + 120°C. The precision of the camera is 0.1°C at a temperature of 30°C and has an accuracy of +-2°C. The image presenter mode allows a full IR-image with selected color scale and reference image which is shown together with live IR image.

For the flexible handling on board we decided to use a hand-hold camera, however, to have less influence from external IR radiation we used the same position for most of our IR imaging. Images for MeBo cores and gravity cores were acquired on the catwalk of R/V Sonne immediately after the cores were taken out of the drilling devices. Images were firstly stored in the SD card of the camera and then transferred to a laptop computer after the whole shooting procedure. Due to the limitation of the environment on board, one can only take a photo for about 60 cm of the core each time which means, for each MeBo core barrel (2.46 m), 5 to 6 photos were needed and 10 to 11 are needed for the gravity core (5.75m). In order to have an overview of the temperature distribution, all the images have to be connected (see Results section 6.5).

Sediment description

For sediment description a visual core description (VCD) form was completed for each section of the gravity and MeBo cores. The VCD summarizes in detail the stratigraphy by identifying variations in bedding, lithology, colour and sedimentary structures. The bed thickness is measured with a centimetre scale. We divided bed thickness into five groups: very thick beds (>100 cm), thick beds (30-100 cm), medium thick beds (10-30 cm), thin beds (3-10 cm) and very thin beds (1-3 cm). The contact between two beds is defined based on the transition (sharp, gradational) and the bedding plane (planar, wavy, erosional). Sediment colour of each bed was determined visually onboard using Munsell's colour chart nomenclature giving the hue, value and chroma (e.g. Munsell Color Company, Inc., 1991). The colour was also studied routinely after the cruise with a Multi-Sensor Core Logger (MSCL; see Appendix 9.3). However, onboard colour should be preferred in further studies because storage may alter surfaces of splitted cores. A wide variety of sedimentary structures, bioturbation, soft-sediment deformation, and coring disturbance is indicated by patterns and symbols in the VCD. The full set of patterns and symbols used in the VCD forms is shown in Figure 22. Lithological classification was based on grain size and composition. In the presence of more than 60% of siliciclastic and volcaniclastic grains with a major of siliciclastic minerals and rock fragments the sediment is considered as siliciclastic. The latter was further divided into textural groups after the Udden-Wentwoth grain size scale (Wentworth, 1922). The sediment was named based on the relative abundance between different grain sizes, with the most dominant defining the principal classification (Shepherd, 1954). The suffix "-stone" was added to the principal names sand, silt, and clay when the sediment was consolidated, and the term "breccia" was applied in the present context as principal name for a sediment with (sub-)angular, poorly sorted rock fragments in a finer grained matrix and is produced by mud volcanoes.

If the sediment was dominated by volcaniclastic components, it was subsequently described as volcaniclastic. We followed Mazzullo et al. (1988) who defined for VCD three textural groups of volcaniclastic sediments: a) volcanic breccia with pyroclasts greater 64 mm, b) volcanic lapilli with pyroclasts between 2 and 64 mm and c) volcanic ash with pyroclasts smaller 2 mm. To improve core description and further investigate representative lithologies and intervals of interest, onboard smear slides were prepared and analysed under the microscope with cross-polarized transmitted light. For smear slide preparation a small volume of sample material was mixed into distilled water directly on the petrographic slide. After the sample had dried under room-temperature conditions it was imbedded with Canada Balsam (refractive index =1.54) and covered with a thin glass. A smear slide form was completed that comprises the identification, size and estimation of clastic, authigenic / diagenetic and biogenic components (e.g. Rothwell, 1989). Clastic components were further classified according to their grain size, i.e. clay, silt and sand.

For graphical visualization of the VCD we used the computer program SEDLOG to produce a publication-quality, simplified, and annotated standard graphic report of the cores (Zervas et al. 2009). SEDLOG displays lithologies and sedimentary structures of the core intervals recovered by graphic patterns in the graphic lithology column using the symbols illustrated in Figure 22.

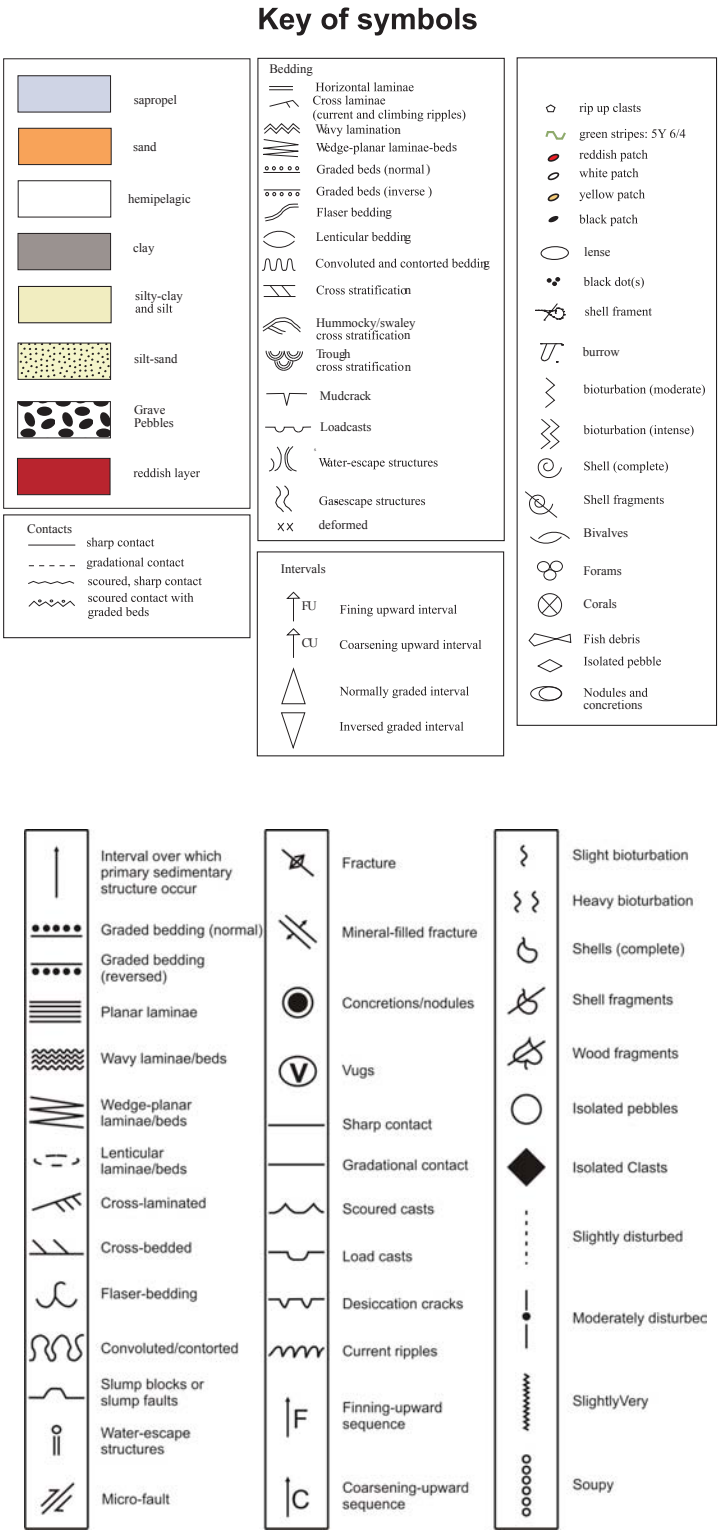

Figure 22: Key of symbols for barrel sheets of gravity core description.

5.6. Physical properties

(M. Ikari, T. Ojima, M. Belke-Brea)

During cruise SO222, shipboard physical properties measurements were restricted to falling cone penetration tests and vane shear tests on the working half of the core.

5.6.1. Cone penetrometer

The geotechnical properties along the sediment cores were determined according to British Standards Institutions (BS1377, 1975). A Wykeham-Farrance cone penetrometer WF 21600 (Fig. 23a) was used for a first-order estimate of the sediment's stiffness. For the measurement, the metal cone was brought to a point exactly on the split core face (Wood 1985). A manual displacement transducer was then used to measure the distance prior to and after release of the cone (i.e. penetration after free fall of the cone). Precision is 0.1 mm of displacement. The distances measured can then be translated into sediment strength (see Hansbo, 1957).

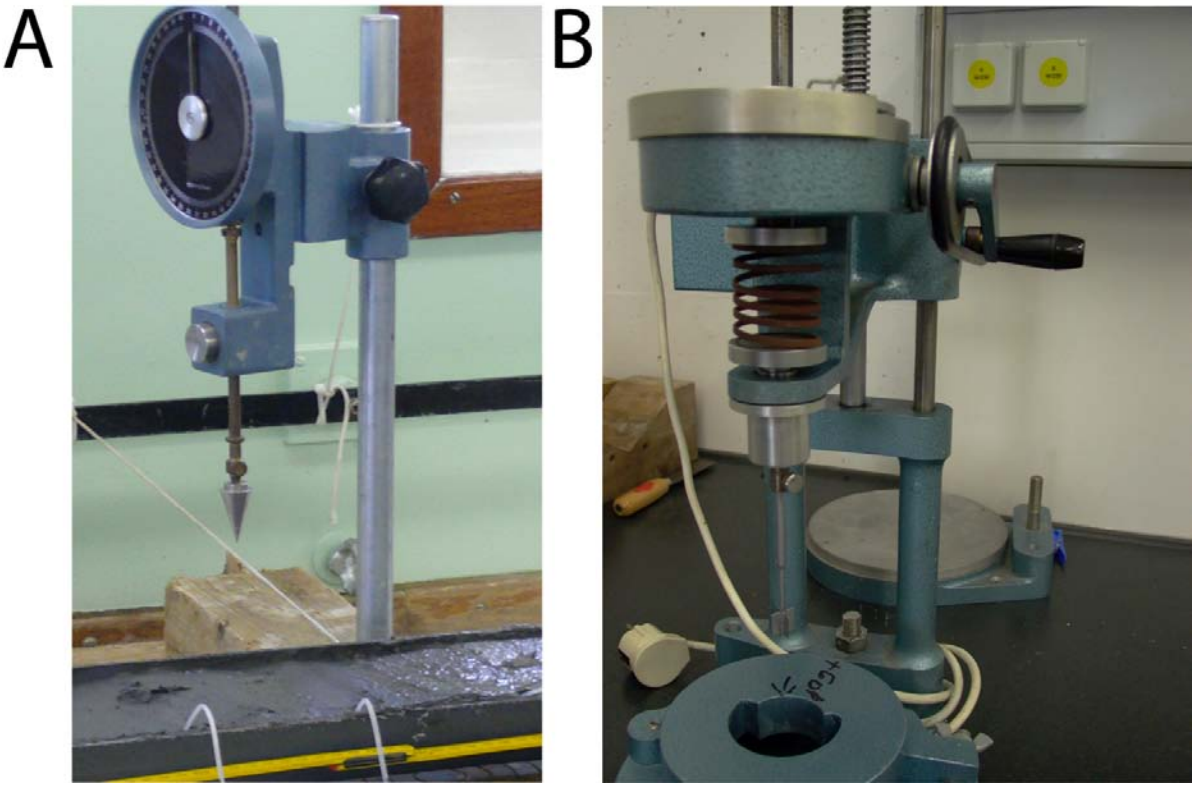

Figure 23: (a) Falling cone penetrometer and (b) vane shear device used on the split core surface.

A falling cone penetrometer with a defined weight (80.51 g) and geometry (30° cone) was used by Hansbo (1957) during a detailed study of the relationship between the cone penetration and soil strength. The undrained shear strength s_u can be calculated from the variables mass and tip angle of the falling cone, gravity g, penetration depth d and the cone factor k via the "cone factor". Wood (1985) calculated from fall-cone and miniature vane tests average values of cone factors (in our case

k=0,85 for a 30° cone). The undrained shear strength can then be calculated using the equation $s_u = (k*m*g)/d^2$.

Shore-based laboratory testing will include ring shear experiments as well as dynamic triaxial shear tests to obtain residual strength and rate-dependent frictional properties as well as the liquefaction potential of the materials recovered.

5.6.2 Vane shear testing

In addition to the Cone Penetrometer a double vane shear apparatus by GSC ATLANTIC was used for more information about sediment stiffness and residual shear strength (Fig. 23b). The distance between the two vanes is 15 cm. For the measurements, four-bladed vanes (L = 12.5 mm, h = 6.25 mm, d = 12.5 mm) were inserted into the split undisturbed core faces and rotated at a constant rate of 90°/min. Data are logged via an interface module (GSC ATLANTIC) using the Testpoint software package.

A spring transmits the rotation at the vane. The torque required shearing the sediment along the vertical and horizontal edges of the vane. The undrained shear strength, s_U depends on the torque T, the vane constant K, the maximum torque angle at failure σ and the spring constant B that relates the deflection angle to the torque (Blum, 1997). The vane constant, K is a function of the vane size and geometry and was used during the measurements with $K=\pi*d^2*(h/2)+\pi*(d^2/6)$ for full dipping vanes. The undrained shear strength can then be calculated using the equation $s_U= T/K$. Shore-based laboratory testing will include ring shear tests to obtain residual strength and rate-dependent frictional properties of the materials recovered.

5.7. Fluid geochemistry

(T. Pape, P. Geprägs, M. Tryon, A. Bräunig, M. Madison)

5.7.1. Gas chemistry

During cruise SO222 gas sampling and analyses was performed in order to evaluate the methane distribution at selected deep-sea mud volcanoes in the Kumano basin and to determine the molecular composition of light hydrocarbons in gas hydrates and vent gas. Whereas special emphasis was laid on MeBo sediment cores during the first leg, works during the second leg concentrated on vent gas collected with the ROV ‘Quest 4000m’. During both legs the sample sets were amended by gravity cores. The objectives of the on-board works were in particular to

- evaluate the source (microbial vs. thermogenic) of light hydrocarbons in the deeper subsurface

- characterise the distribution of light hydrocarbons in the sediments
- evaluate the molecular differentiation of light hydrocarbons during hydrate precipitation
- determine hydrate phase boundaries and hydrate dissociation temperatures considering current field data
- collect gas samples for detailed investigations of the molecular and isotopic composition of light hydrocarbons in the home laboratory.

Gas sampling techniques

Gas from intact hydrate pieces

Pieces of gas hydrates were extracted from gravity cores and MeBo cores. For onboard gas chemical analysis, the hydrate pieces were cleaned in ice-cooled water and placed in plastic syringes for immediate controlled dissociation at ambient temperature. The liberated gas was transferred with a canule into 20 ml glass serum vials prefilled with oversaturated NaCl solution and sealed with butyl stoppers (Fig. 24). A total of 113 subsamples of hydrate-bound gas were prepared from intact hydrate pieces during cruise So222 (Table 4A) for onboard determination of light hydrocarbon composition and for storage and onshore analysis. At the MARUM selected samples will be analyzed for improved molecular composition and for stable carbon and hydrogen isotopic composition of light hydrocarbons and carbon dioxide (see Whiticar, 1999).

Figure 24: Gas hydrate samples from gravity cores were transferred into syringes for dissociation; free gas is ascending into vials for later laboratory analysis..

Sedimentary gas from Gravity cores and MeBo cores

For vertical profiling of methane concentrations using the headspace technique, sediment samples were taken from cores recovered with the gravity corer and the MeBo. 3 ml of sediment were taken using cut-off syringes and transferred into 20 ml glass vials prefilled with 5 ml of 1 M NaOH. For gravity cores, sediments were extracted from the top or the bottom of freshly cut core segments and in most cases through small windows cut into the PVC-liner at defined depths. For MeBo cores, sediments were taken from the top of the pilot chuck immediately after it's dismantling from the core catcher part.

The samples were shaken with an automatized lab bench shaker for 1 h and subsequently stored in the cooling room. All headspace samples will be analyzed for methane concentrations at the MARUM in Bremen. A total of 329 sediment samples were taken for headspace gas analysis during SO222 cruise (Table 4B).

Table 4: Number of samples taken for gas hydrate (part A, above) and headspace (Part B, below) gas analysis.

Tool	**Number of cores**	**Number of gas subsamples**
Gravity corer	10	113
Total		**113**

Tool	**Number of cores**	**Number of samples**
Gravity corer	43	329
MeBo	6	45
Total		**374**

Analytical techniques

Onboard analysis of hydrocarbon compositions in vent gas and hydrate-bound gas

Samples from vent gas and hydrate-bound gas were analysed onboard for concentrations of light hydrocarbons with a Trace GC Ultra (Thermo Scientific) gas chromatograph. Light hydrocarbons (C_1 to C_6) were separated, detected, and quantified with a capillary column (CP-PoraBond Q, 25m, 0.32mm, 5µm, Varian Inc.; He as carrier) connected to a Flame Ionization Detector. Calibrations and performance checks of the analytical system were conducted regularly using commercial pure methane standards and light hydrocarbon mixtures. The coefficient of variation determined for the analytical procedure was less than 2%.

Onshore analysis of stable C and H isotopic composition of light hydrocarbons

For onshore analysis of stable isotope ratios ($^{2}H/^{1}H$, $^{13}C/^{12}C$) of light hydrocarbons and carbon dioxide using the GC-Isotope-Ratio-Mass-Spectrometry system at the MARUM, gas samples were stored in glass vials sealed with NaCl-saturated water or 1 M NaOH as described above.

Hydrate phase boundaries

Gas hydrate phase boundaries were calculated using the HWHYD U.K. software (Masoudi and Tohidi, 2005) loaded with molecular compositions of hydrate-bound volatiles and salinities of interstitial waters.

5.7.2. Pore water chemistry

The composition of pore water in marine sediments is one of the most suitable indicators to characterize the benthic system. Thus, vertical, horizontal and temporal changes in concentrations of dissolved constituents can be used for identification and quantification of specific transfer processes, regardless of whether these are mircobially mediated or caused by abiotic reactions. Furthermore, pore water signatures and profiles can reveal the importance fluid transport mechanisms. In the majority of deep sea-sediments molecular diffusion is by far the dominate process, which controls the transport of dissolved components. When advection becomes important at a specific location (e.g. seep sites), the modeling of pore water profiles allows the calculation of the corresponding flow rates. Last but not least, pore water compositions can also indicate to the history of the waters of even to their primary source.

During this cruise, pore water geochemistry sampling was conducted mainly to find indications for the upward transport of fluids from deeply buried formations, caused by the deformation and subduction of the African plate moving northward below the European plate. In this context salinity, mainly expressed by the concentrations of chloride, sodium, sulfate, magnesium, calcium and potassium, is of particular interest. Inorganic geochemical work, however, was restricted to the extraction of pore water using rhizon samplers (~0.4 μm; Seeberg-Elverfeldt et al., 2005) on the split core (Fig. 25). The vacuum necessary to operate the rhizon samplers was created by pulling up 10 ml plastic syringes. The amounts of pore water retrieved by this method were between 5 and 10 ml. In general, the depth resolution varies approximately between 20 and 30 cm.

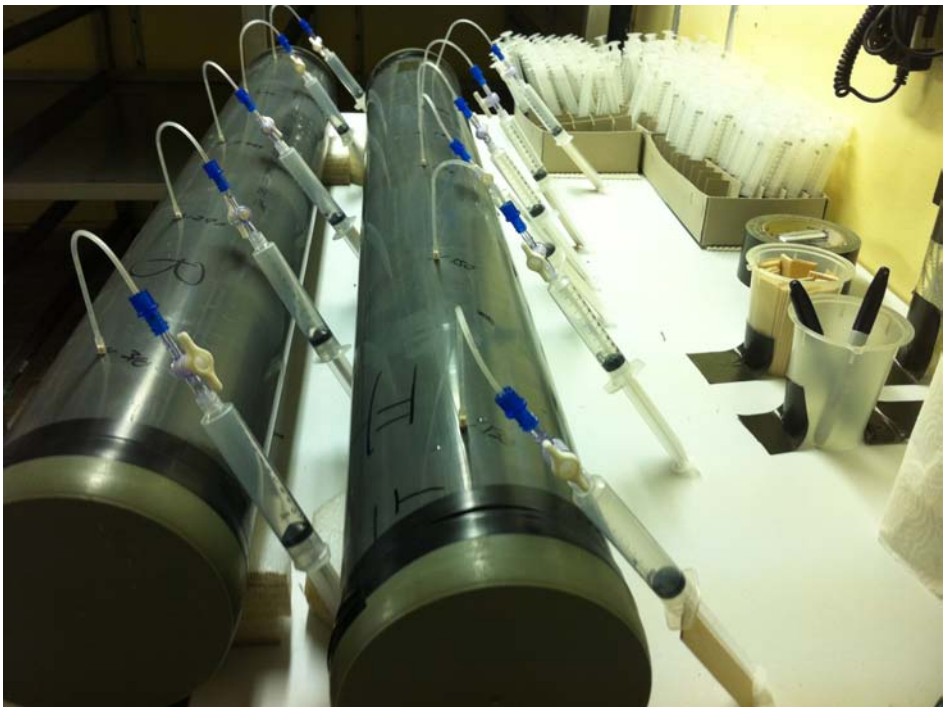

Figure 25: Rhizon pore water extraction in split working half of the gravity core.

5.8. ROV operations

(Christian Seiter, Phillip Franke, Olliver Herschelmann, Hoang Anh Mai, Ralf Rehage, Michael Reuter, Christian Reuter, Marcel Zarrouk)

The deepwater ROV (remotely operated vehicle) "QUEST 4000m" used during SO222B aboard RV *Sonne*, is installed and operated at MARUM, University of Bremen, Germany. "QUEST 4000m" is based on a commercially available 4000 m rated deepwater robotic vehicle designed and built by Schilling Robotics, Davis, USA (Fig. 26). Since installation at Marum in May 2003, it was designed as a truly mobile system specially adapted to the requirements of scientific work aboard marine research vessels for worldwide operation. Today, "QUEST 4000m" has a total record of 321 dives during 28 expeditions, including cruise SO222.

"QUEST 4000m" System description

The total "QUEST 4000m" system weighs about 45 tons including the vehicle, control van, workshop van, electric winch, 5000-m umbilical, and transportation vans and can be transported in four standard ISO 20-foot vans. A MacArtney Cormac electric driven storage winch is used to manage up to 5000m of 17.6 mm NSW umbilical cable.

Figure 26: ROV Quest on the pier of Nagoya port before loading for leg SO222B.

"QUEST 4000m" internal equipment and online tooling

The space inside the "QUEST 4000m" toolskid frame allows installation of mission-specific marine science tools and sensors. The initial vehicle setup includes two manipulators (7-function and 5-function), 7 color video cameras, a digital still camera (Insite SCORPIO, 3.3 Mega-Pixel), a light suite (with various high-intensity discharge lights, HMI lights, lasers, and low-power dimmable incandescent lights), a Sea&Sun online CTD, a tool skid with draw-boxes, and an acoustic beacon finder. Total lighting power is almost 3 kW, total additional auxiliary power capacity is 8 kW. In addition, the permanently installed Kongsberg 675kHz Type 1071 forward looking Scanning Sonar head provided acoustic information of bottom morphology and can be also used for detection of gas emissions.

Video Setup, HDTV and vertical imaging

Continuous PAL video footage was continuously hard disc recorded with two color-zoom cameras (InsitePacific PEGASUS dome port and PEGASUS planar port). In order to gain a fast overview of the dive without the need of watching hours of video, video is frame-grabbed and digitized at 5sec intervals, covering both PAL and HD video material.

For extremely detailed video close up filming, a near-bottom mounted broadcast quality (>1000 TVL) 3CCD HDTV 14 x Zoom video camera was used (InsitePacific Zeus). Spatial Resolution of this

camera is 2.2 Mega-Pixel at 59.94 Hz interlaced. Recording was performed on demand onto tapes in broadcast-standard digital Sony HDCAM format, using uncompressed 1.5 Gbit HD-SDI transmission over a dedicated fibre-optic connection. Image display takes place on two 26" HD TFT display screens inside the control van, one each for pilots and scientists, providing excellent close-up view and covering the full dynamic range of the camera. Distribution of the cameras HDTV video signal was performed through dedicated cabling into the science lab, allowing real-time display on a 26" HD TFT screen at full resolution.

As a standard still image camera, an Insite Scorpio Digital Still camera was used, providing 3.3. Mega-Pixel spatial image resolution and highly corrected underwater optics.

For the task of video mosaicking and vertical downward viewing, a broadcast quality downward looking camera with dedicated corrected underwater optics (InsitePacific ATLAS) was installed on the toolskid in conjunction with one high power HID wide angle flood light. Orientation of light and camera was adjusted in order to gain a large angle between optical axes. Thus, reduced backscatter allowed clear imagery from up to 7 meters above seafloor. In addition to downward looking ATLAS, a digital still camera with 14 Mpix resolution was installed.

Video distribution was provided by dedicated CAT-5 based VGA transmission hardware, als well as by streaming the main tiled video image over the vessel's network.

During SO222B, the following scientific equipment was handled with "QUEST 4000m":

ROV based tools, installed on vehicle:

- ROV interchangeable draw-box for technical tools and devices and scientific samples
- Sea and Sun CTD real-time probe with turbidity sensor
- nets for clusts sampling
- acoustic beacon markers
- simple knife for rope operation

In addition the following scientific sensors and devices were deployed, handled and/or recovered at depth during SO222:

- MeBoCORK B bottom unit
- sediment push cores (Fig. 27A)
- autonomous temperature loggers on frame (so-called MTL stick)
- T-lance (Fig. 27B).

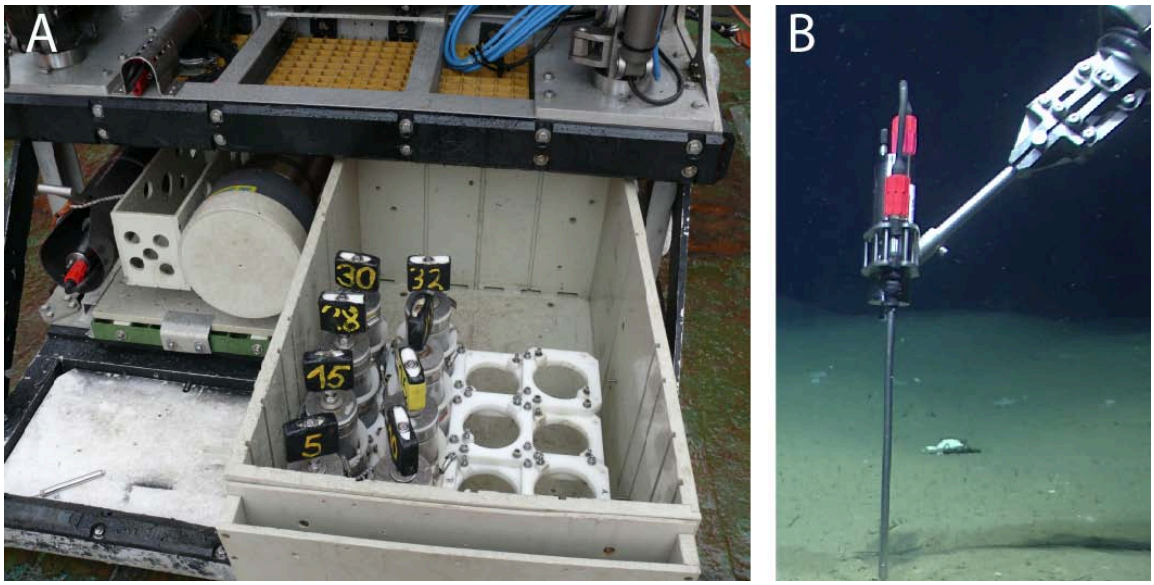

Figure 27: (A) Sediment push coring devices in ROV *Quest* drawer; (B) T probe for *in situ* measurement using the manipulator arm of ROV *Quest*.

5.9. Observatories

(A. Kopf, S. Hammerschmidt, K. Kitada, T. Kimura, T. Fleischmann)

MeBo CORKs

The general principle of a CORK (see above) has to be minimised in case of MeBo where conical threads and a diameter of only 98-110 mm have to be sealed. Space is hence most seriously governing the design of the CORK, which has to seal the inner borehole from the overlying ocean body, and which also has to host the connection of the borehole tubings to the actual observatory unit. Also, this "adapter" has to be most versatile given that shiptime is precious and that cruises with large-scale devices such as MeBo and ROV are costly. The "MeBoCORK concept" thus aims at a smart approach where an observatory can either be set by MeBo alone, or in combination of MeBo and ROV. The first represents a compromise scientifically since very few parameters will be monitored (P and T) over a limited time span, whereas the second has an increased payload and encompasses geochemical sampling as well. However, both approaches appear extremely valuable at this stage and the future will likely provide opportunities for payload being added onto either observatory unit.

The two versions of the MeBo CORK, as sketched in Figure 6B and as detailed in the Appendix (see quotation by *develogic*, where both versions are drawn in detail [Figs. 1 and 2]), are both self-contained with power, data logging, data transmission and transducers. They are recoverable at all times and hence minimize the risk of loosing the investment. In the following paragraphs, the deployment mechanism is explained in some detail. First, the MeBo hole has to be prepared for long-term instrumentation after coring is completed. This is achieved by leaving several pieces of MeBo

outer drilling rods in the ground after wireline core retrieval. These rods, appx. 30-40 m in total length, act as a casing and stabilize the upper subseafloor portion where the deposits are poorly consolidated and otherwise may close in. Only the lowermost part of the hole is free of "casing" and provides direct access to the formation. The first prerequisite to keep the MeBo CORK simple follows the first hydrological observatory in ODP: only hydraulic tubing is lowered into the hole to access fluid pressure (or fluids) at depth [*Wheat et al*., 2011], and all electronics remain at the wellhead. For MeBo, a string of 2 armored PTFE tubes is coiled up in the lower part of the MeBo-set observatory unit (termed MeBoCORK A, where A stands for "autonomous", i.e. MeBo by itself is capable of placing a stand-alone observatory), namely in the lower portion of the "adapter" hosting the receptacle for the hotstab. Once the drilling device has set this piece, the coil of tubing is unlocked and a dead weight favours the tubing's descent towards terminal depth where the hole is open. The upper end of the individual tubings connects to borings of the hotstab receptacle. The lower unit also hosts battery packs.

The upper portion of the MeBoCORK A hosts the data transmission unit, data logger and transducers, the latter of which are connected to the borings of the male hotstab end (Fig. 28). The hotstab is mated with its female counterpart, and the two halves of CORK A are further secured by a bayonet connector that allows coupling of the MeBo top drive and hence torque being transmitted (in clockwise direction only!). During installation MeBo fully srews in the entire CORK instrument, which in total is the exact length of a regular MeBo drill rod and which sits on the magazine with the other rods. Once this piece is properly set, MeBo pushes the unit to a depth so that only the titanium part (ca 70 cm long) sticks out of the seafloor and then takes off. In the initial design, this simple, MeBo-set CORK monitors pressure and temperature, which are both indicators for deep-seated fluid flow; pore pressure is additionally valuable as strain proxy (see above). Depending on the sampling rate, the batteries will allow monitoring for many months to a few years (in case of the system deployed during leg SO222A = 7 months).

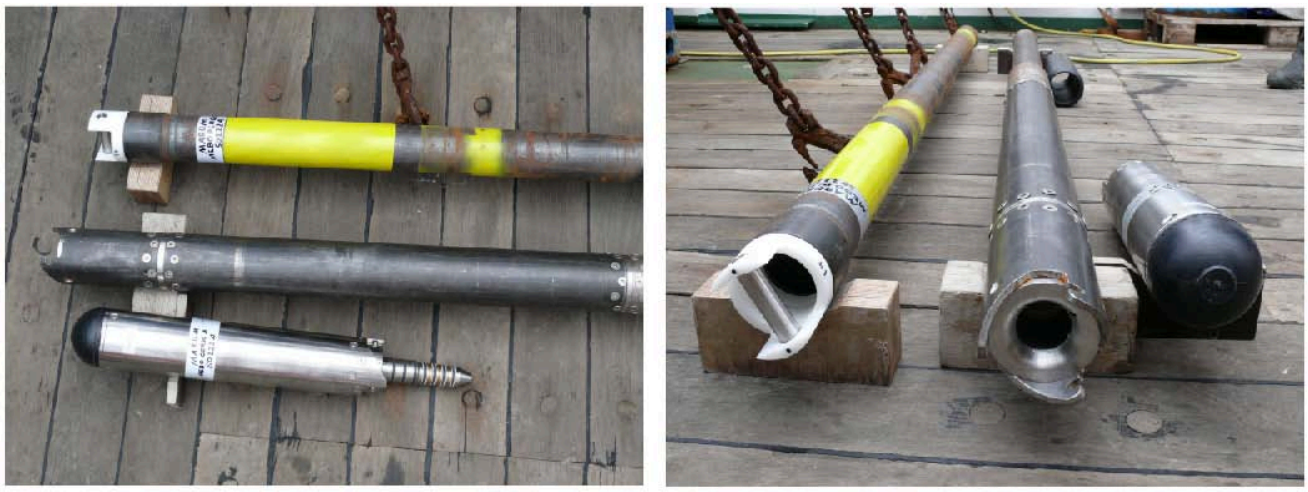

Figure 28: MeBoCORK A (=autonomous) as well as MeBoPlug for comparison. See text.

If monitoring or parameters other than pressure and temperature is desired, the instrumented MeBo rod (CORK A) is too small and an ROV dive is required to recover the CORK A and deploy an external, more sophisticated observatory unit (Fig. 29). Since the ROV dives to the seafloor and connects a seafloor (0sea bottom) unit to the MeBo rod with Hotstab recepticle, this system was termed MeBoCORK B (=bottom). The ROV is able to unlatch the bayonet connector in counter-clockwise direction and can transport the MeBo-set CORK back to the ship, because its weight is low and the diameter is suitable for the manipulator claw. Before this, a seafloor unit will be placed next to the MeBo drillsite (Fig. 29; see also section 6.8 below). This system contains of a pressure housing with an attached hood in which a male hotstab adapter plus the umbilical of armored tubing strings is coiled up. The ROV takes the hotstab and places it into the lower portion of the MeBo-CORK, which is remaining connected to the outer drillstring at all times. This operation is straightforward and has been done in a similar way when pressure units from ODP or IODP CORKs got replaced. The pressure housing at the seafloor can be equipped to the mission's/scientists' specifications, and in the case of this proposal will host the P and T transducers (same as in the instrumented rod) plus an osmo-sampler (Fig. 30; see also *Jannasch et al.,* 2003).

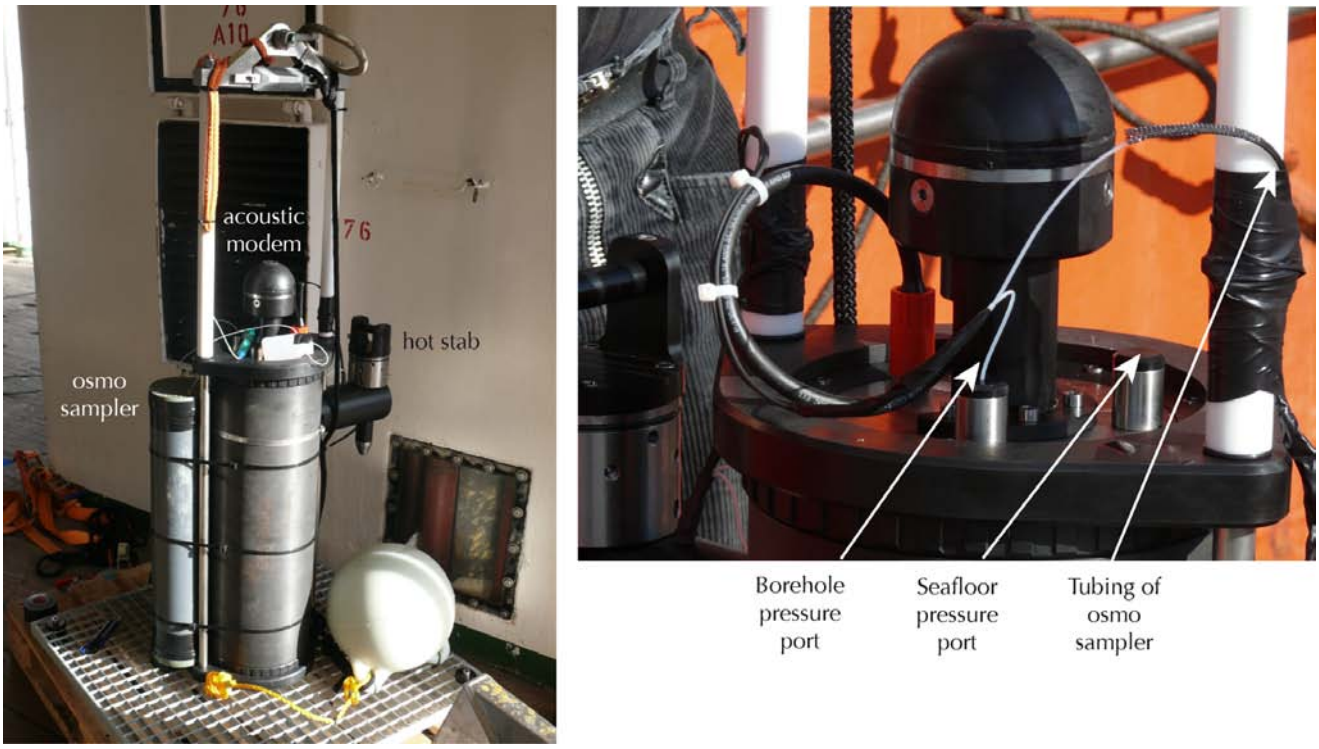

Figure 29: MeBoCORK B (=bottom) unit containing a pressure housing, acosutic modem, attached osmo-sampler, and the hot stab connector to couple to the drill pipe. Left photo shows overall unit, right photo contains detail with layout of tubings. See text.

Both MeBoCORK instruments are programmed to measure the pressure for a period of 30 s and then record the average P value. Seafloor reference and borehole P are offset by 15 s, so that the data are written to the disk alternately.

Figure 30: Osmo-sampler (tubing coil [top] and pumps [below]) that are hosted in a PVC tube attached to MeBoCORK B.

One MeBoCORK A and one MeBoCORK B were deployed during cruise SO222 in addition to simpler, already proven technologies such as the electronics from the MeBoPlugs or the SmartPlug borehole sensors. These latter systems are described below.

MeBo Plugs (and MTL-sticks)

In addition to the MeBoCORKs, which were co-developed with develogic (Hamburg), we used standard RBR data loggers with Keller differenmtial pressure transucers for monitoring strain in the boreholes. For this, plugs from POM were manufactured to seal the conical threads of the uppermost MeBo drill pipes (Fig. 31). At the top, a handle designed to specification of the ROV *Quest* manipulator were added. In the borehole-facing section, a thermistor as well as the downward-looking P port are situated (Fig. 31, inset). Given that only one thermistor was fitted into the so-called MeBoPlugs (named in analogy to the so-salled SmartPlug terminology in IODP), we are lacking a temperature record from the seafloor (i.e. upward-looking. In order to overcome this shortcoming, a simple self-contained device for seabottom T monitoring was designed and deployed by ROV (see next section). The sampling rate of the MeBoPlugs was set to 10 s on the RBR data loggers, which is providing them with an estimated lifespan of a few years (anticipated end of recording is Feb. 2016).

Figure 31: MeBoPlug prior to being screwed into a MeBo drill pipe (left); right photograph shows bottom view into the borehole with ports for P [hole at left] and T [little pin at right] monitoring. See text.

Two MTL sticks, named after the Antares mini-temperature logger (MTL) being their key component, were fabricated to be placed next to the MeBo sites containing MeBoPlugs. This was realised during leg SO222B with ROV *Quest*.

The MTL stick is only 70 cm long and comprises a stainless steel rod that has a fin in the lower portion (stuck into the sediment to prevent toppling over, even in strong currents), and a second fin with a pipe welded to it in its upper portion (Fig. 32). In the pipe, an MTL can be placed securely. At the top of the MTL stick, a small handle to ROV *Quest*'s specifications was mounted. The systems were programmed at a rate of 1 Hz and will monitor transient changes for 2.5 – 3 years.

Figure 32: MTL stick to be deployed by ROV; those systems complement the MeBoPlugs at two sites to get high-resolution seafloor temperature variations as reference for the MeBoPlug data. ROV handle is seen left, MTL is hosted in a metal tube; lower portion is stuck into the sediment (with metal shield for stabilisation in case of bottom currents).

SmartPlug piezometer

The SmartPlug borehole observatory belongs, together with the MeBo-CORKs, to a series of recently developed Mini-CORK systems. In contrary to the original borehole observatories (Becker and Davis, 2005; Wheat et al. 2010), Mini-CORKs are relative simple, self-containing instruments which can be easily deployed from any ship of opportunity. The SmartPlug instrument package includes a data logger/pressure period counter, a temperature sensor inside the data logger housing, a battery package, and two pressure transducers which are connected to pressure gauges via hydraulic tubing. One pressure gauge is "upward looking", the other is "downward looking", monitoring the hydrostatic reference (i.e. seafloor) and formation fluid pressure and temperature, respectively. The formation pressure gauge is isolated from the overlying water column by the bottom seal located at the lower part of the SmartPlug structural outer shell (the "bullnose") and usually by a mechanically released packer, to which the SmartPlug is attached before being installed in a borehole (for a more comprehensive outline of the technical details, please see Kopf et al., 2011a, b). Originally, the instrument was designed to be deployed in standard-sized boreholes drilled by ships operated by the Integrated Ocean Drilling Program (IODP), namely D/V *Joides Resolution* and D/V *Chikyu*. The SmartPlug got already installed during IODP Exp. 319 within the Nankai Trough accretionary prism, where the borehole penetrated one of the shallow branches of the Megasplay fault (Site C0010, see Saffer et al., 2010). After 15 months, the instrument got recovered and proved to be reliable in constant monitoring of distinct changes in pressure and temperature (Kopf et al., 2011a, b; Hammerschmidt et al., submitted).

Here, however, due to the unavailability of a drill ship, the SmartPlug was modified to be installed without the need for a drill string, a packer, or even a borehole. The bullnose was extended by a c. 1m long steel pipe, which serves not only as stabiliser once the SmartPlug is pushed into the seafloor but also acts as casing protecting the lower pressure gauge inlet and simulating a borehole-like environment (see Fig. 33). In addition to that, slots were cut into the steel pipe to allow water and sediment to escape during the installation. This is important to allow displacement of water during impact on the seafloor, to prevent overpressurisation within the steel pipe during penetration, and to allow re-equilibration of fluid pressure and temperature with the surrounding formation. The observatory was set to monitor with a sampling frequency of 10 s, which constrains the monitoring period to around 2.5 years (i.e. similar to those of the MeBoPlugs). For deployment procedure, see section 6.9 below.

Figure 33: SmartPlug converted into a piezometer before being mounted to the TV-grab for deployment.

5.10. TV grab and USBL Posidonia

(T. Pape, A. Hüpers, J. Wei, G. Bohrmann, P. Wintersteller, P. Geprägs, M. Belke-Brea)

TV grab

The TV-guided grab sampler (Fig. 34) is a tool located permanently onboard R/V *Sonne*. Providing either colour or black and white video signals from the seafloor, it allows to select a well-defined position for its deployment. The video signal is transmitted via a LWL cable and is displayed online onboard the ship. The grab function is also controlled through a deck unit located in the laboratory, but the power for the hydraulics and the underwater lights is provided by two deep sea batteries, which limits the operation time of the TV-grab. The digital videos are available as well as the USBL position by POSIDONIA.

When the desired sampling spot has been found with the video system, the tool can be deployed on the seafloor by the winch and the 'close' button has to be pressed. Depending on the material sampled, the maximum volume to be recovered is approximately 0.8 m^3.

Figure 34: TV grab on board R/V *Sonne*.

USBL Posidonia

IXSEA's POSIDONIA 6000 is an ultra-short baseline underwater navigation (USBL) that is used during ROV dives and for one of the box corer stations. The moon-pool mounted antennas require a calibration and a proper sound velocity profile. Most recent calibration for the system was done during SO222a by the *Scientific Technical Service* from RV Sonne. POSIDONIA 6000 receives motion sensor data from Simrad MRU5, located in the ideal ships center. SVP has been updated according to the measurement of CTD-1. Specifications and offsets of POSIDONIA 6000 were measured and corrected for whenever the device was used (e.g. when placing observatories and CAT meters, run the CPTu lance or TV grab, drill with MeBo, etc.). Although well calibrated, the positions calculated by the system jump by the time the vessels heading changes more then 45-90°. This has been observed during other cruises on other research vessels as well. IXSEA is informed about the problem.

6. Preliminary Results

6.1. CTD, Seafloor and Parasound surveys

(P. Wintersteller, T. Fleischmann, G. Bohrmann)

CTD (Conductivity – Temperature – Depth)

The shipside hydro-cask-rosette with an integrated SBE9plus CTD-probe from Sea-Bird Electronics, Inc. was used to collect data from the water column with focus on appropriate sound velocity profiles. The measured temperatures and conductivities, the later recalculated in salinity, shown in Figure 35, are evidence for a highly dynamic area. Within days there are big changes in the uppermost 200m of the water column. A reason for that are for sure the strong W-E-ward currents especially in the southern part of the Kumano basin. The very homogenous looking surface layer in CTD-1 can be explained by water masses mixed thoroughly due to stormy weather conditions.

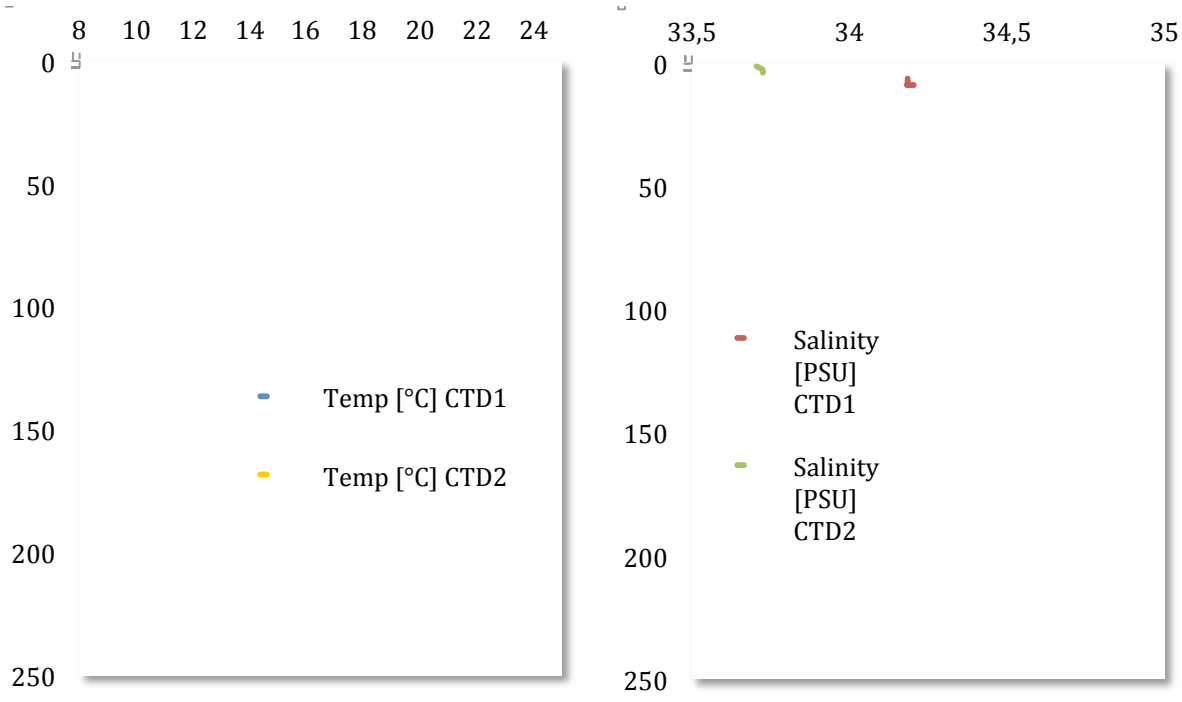

Figure 35: CTD data from cruise SO222.

KONGSBERG EM120 Multibeam system

During cruise SO222, we mapped an estimated area of 15951 km^2, which resulted in a fairly complete spatial coverage of the Kumano Basin with its mud volcanoes (Fig. 36). Since the latter were the main focus of our research effort, it was exciting to see that the multibeam data revealed additional features (i.e. small domes previously not known / discovered). These encompass MVs #9 - #13, plus a number of features which appear to be a result of mud diaprisim and ascent, but where the mud apparently has not quite reached the seafloor (see also next section on Parasound profiling).

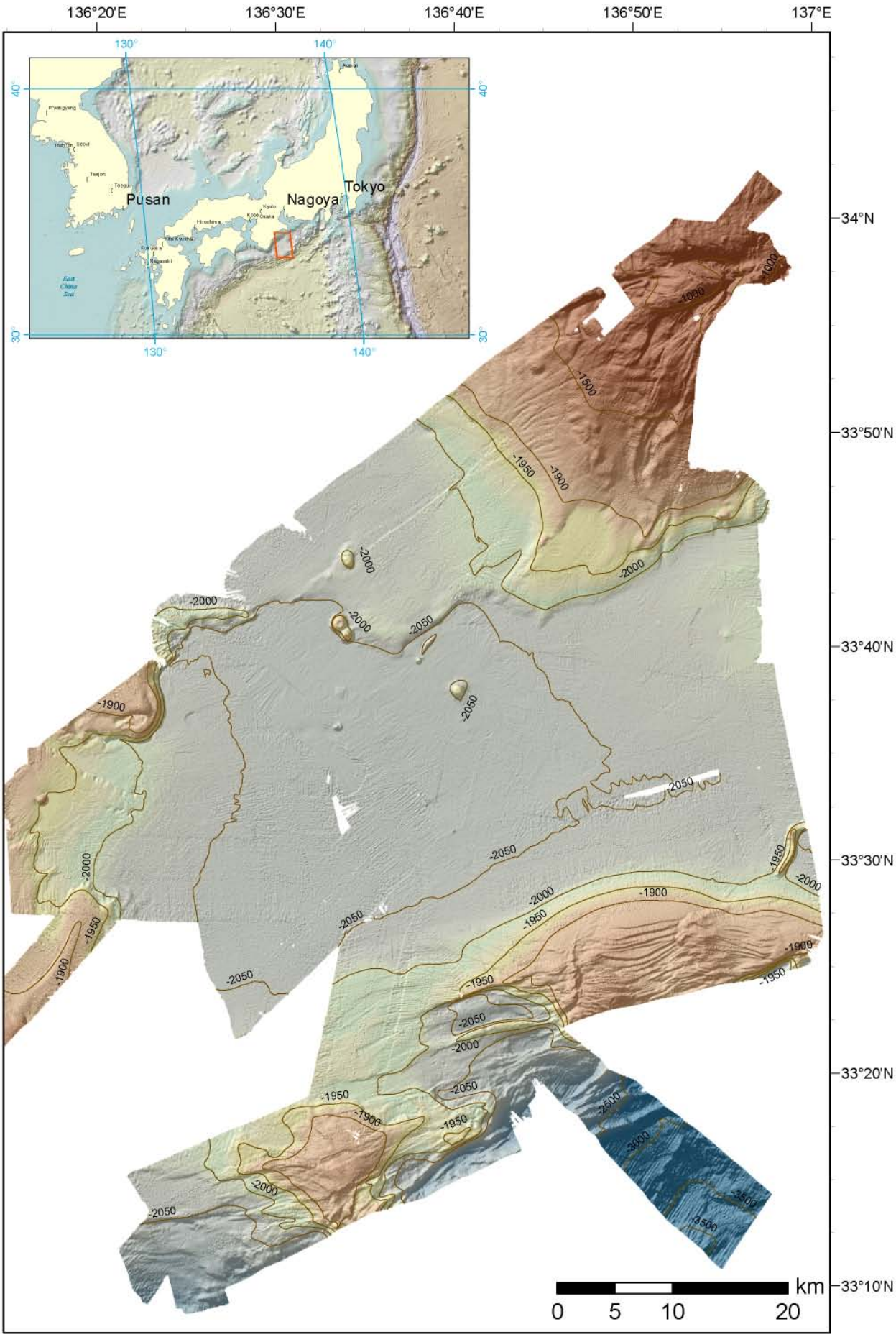

Figure 36: Bathymetric map acquired during cruise SO222.

The full information on the metadata to the Multibeam grid is:

FILENAME=G:\SO222\EM120\SO222_EM120_MBproc\SO222_Kumano_A2C3F5E50proc.grd
DESCRIPTION=SO222_Kumano_A2C3F5E50proc.grd
UPPER LEFT X=135.6051000000
UPPER LEFT Y=34.0375581538
LOWER RIGHT X=137.0109170776
LOWER RIGHT Y=32.9385000000
WEST LONGITUDE=135° 36.30600' E
NORTH LATITUDE=34° 2.25349' N
EAST LONGITUDE=137° 0.65502' E
SOUTH LATITUDE=32° 56.31000' N
PROJ_DESC=Geographic (Latitude/Longitude) / WGS84 / arc degrees
PROJ_DATUM=WGS84
PROJ_UNITS=arc degrees
EPSG_CODE=4326
COVERED AREA=15951 sq km
NUM COLUMNS=2614
NUM ROWS=2439
PIXEL WIDTH=0.000538 arc degrees
PIXEL HEIGHT=0.0004508 arc degrees
MIN ELEVATION=-3623.029 meters
MAX ELEVATION=-732.934 meters
ELEVATION UNITS=meters
BIT_DEPTH=24

ATLAS PARASOUND profiling

When acquiring geophysical information in the Kumano Basin, we covered a length of 543 km during leg SO222A and 1104 km length during leg SO222B. The tracks of where RV *Sonne* was going are shown in Figure 37.

The majority of the profiles recorded with Parasound are of good quality and reveal subseafloor stratification and other geological features. Signal penetration was generally poor in the mud volcanoes, in particular along the steep flanks. This is partly explained by topography, and may have partly resulted from their incoherent geological evolution with absent stratification, large amounts of free gas, and substantial quantities of indurated clasts in the mud breccias (see section 6.5. below).

One good example of active mud volcano KK #2 is given in Figure 38A where the collapsed, inward facing strata beneath the crest region is seen. A second example shows the imbriicated thrust slices in a long paradsound line which is underlain by the regional bathymetric chart (Fig. 38B).

Post-cruise work will include processing of those data for publications.

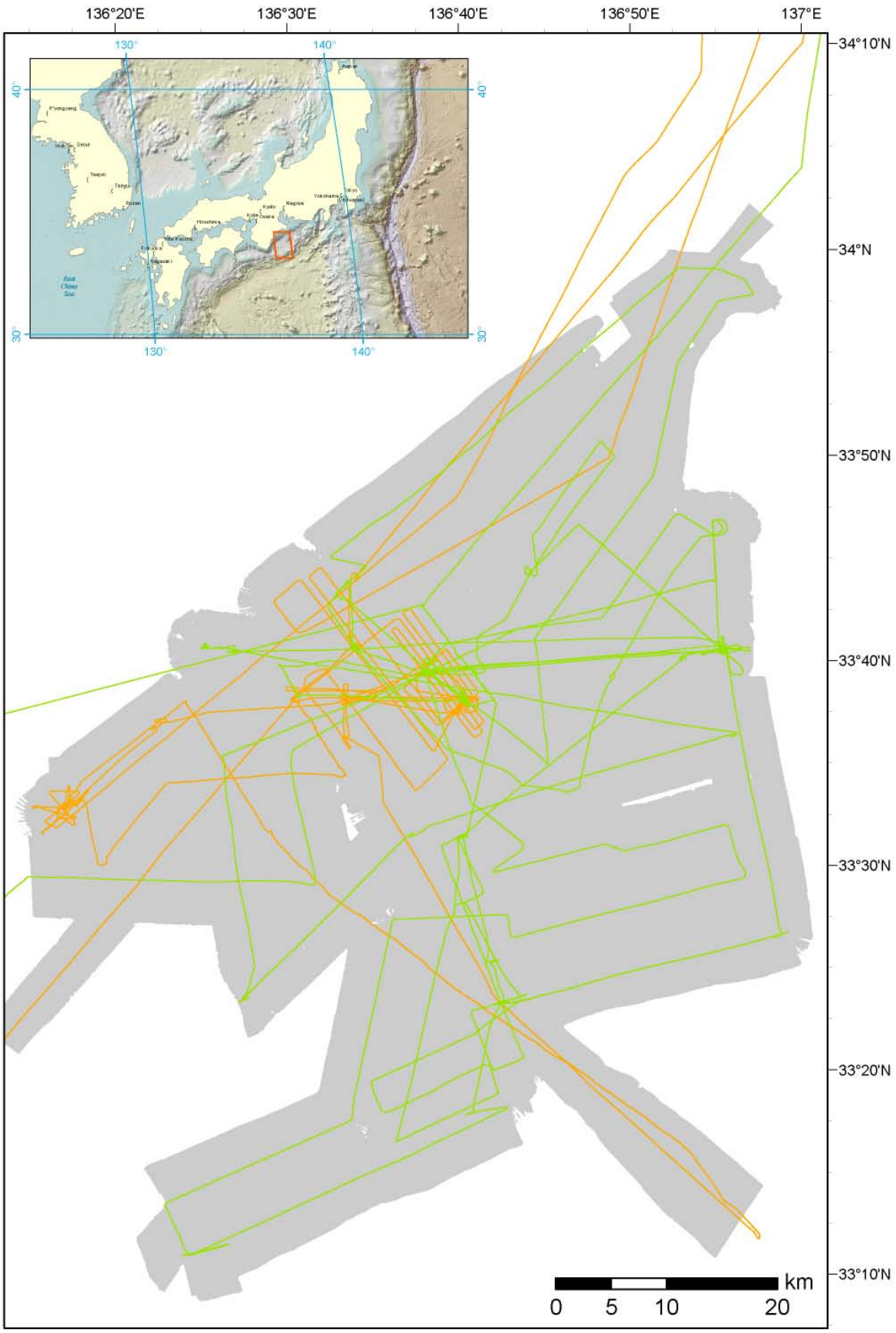

Figure 37: Tracks from cruise SO222, with leg A in orange and leg B in green.

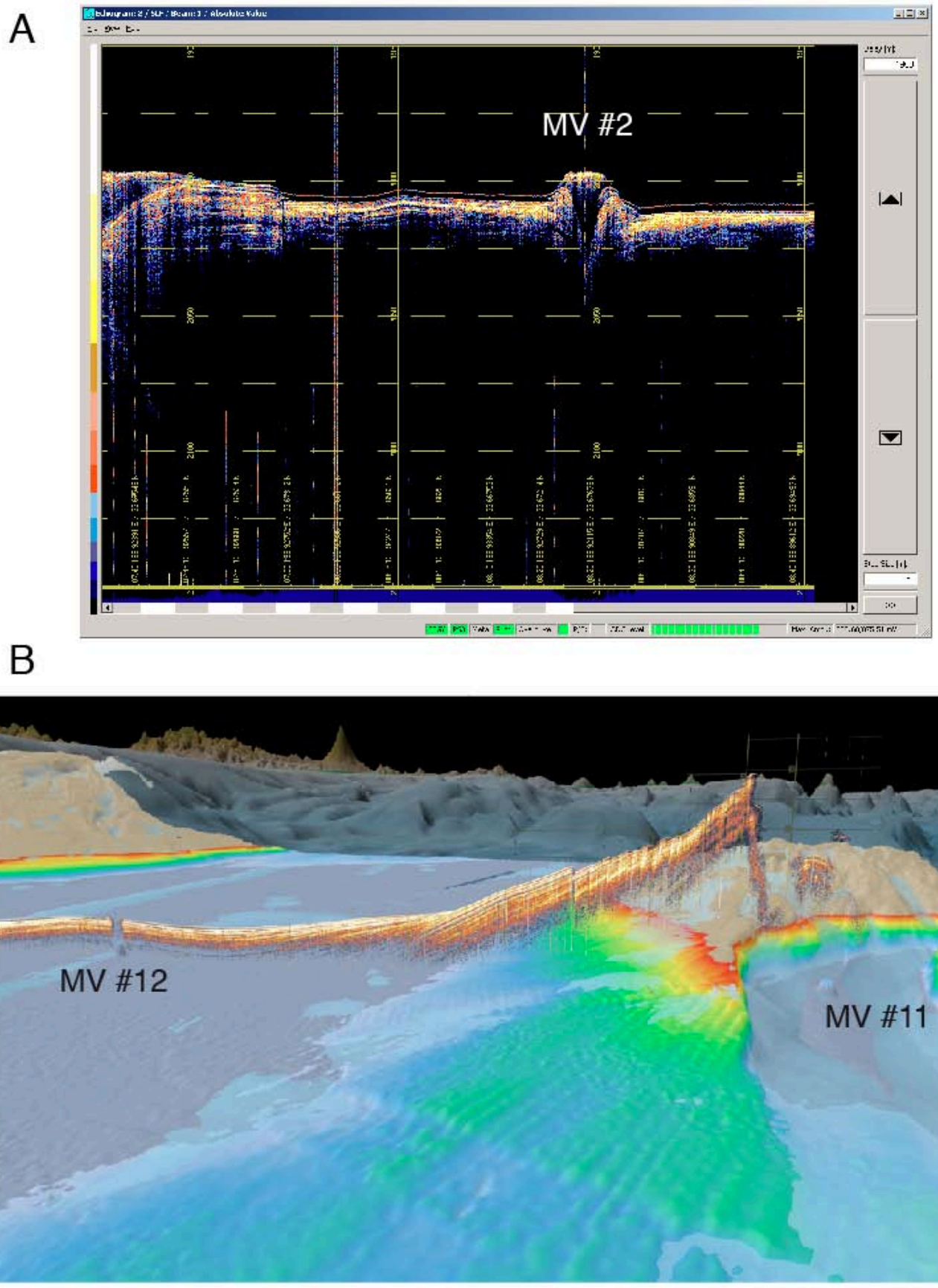

Figure 38: Parasound examples from cruise cruise SO222. (A) Short profile across active mud dome KK #2; (B) long profile from the outer forearc high across MV #12 into the Kumano basin, projected over a bathymetric "flying carpet" diagram of the frontal portion of the SO222 study area.

6.2. *In situ* temperature measurements

(N. Kaul, B. Heesemann, T. Feseker, K. Asshoff)

During both legs of this cruise, we conducted 110 *in situ* sediment temperature measurements in total. 58 measurements were aimed at investigating the thermal structure of mud volcanoes in detail, while the remainder of the measurements served to map the regional background heat flow in the Kumano basin and the activity of faults. Compared to mud volcanoes in the Eastern Mediterranean or the Håkon Mosby mud volcano on the Barents Sea slope, the mud volcanoes in the Kumano basin are associated with very small thermal anomalies at the seabed, which points to a low level of activity. Only MV #2 and MV #3 showed geothermal gradients that were raised significantly above the background level of between 0.03 and 0.06 °C/m (Tab. 5). As illustrated in Figure 39, the geothermal gradient at MV #2 mirrors the bathymetry, suggesting that seepage is focused at the highest point of the mud volcano.

One of the heat flow transects crossed a fault in the central Kumano basin, which had been observed in seismic lines. Figure 39 shows that the fault seems to be associated with a local increase in geothermal gradient. Another transect east of MV #4 and MV #5 crossed a morphological step in the bathymetry. Here, the relationship between water depth and geothermal gradient illustrates the effect of the topography on heat flow.

Table 5. Temperature gradients in the different mud volcanoes visited with the *in situ* HF probe.

	MV #2	MV #3	MV #4	MV #5	MV #9	MV #10	MV #13
Max. geothermal gradient [°C/m]	0.290	0.122	0.064	n/a	0.062	0.044	0.055

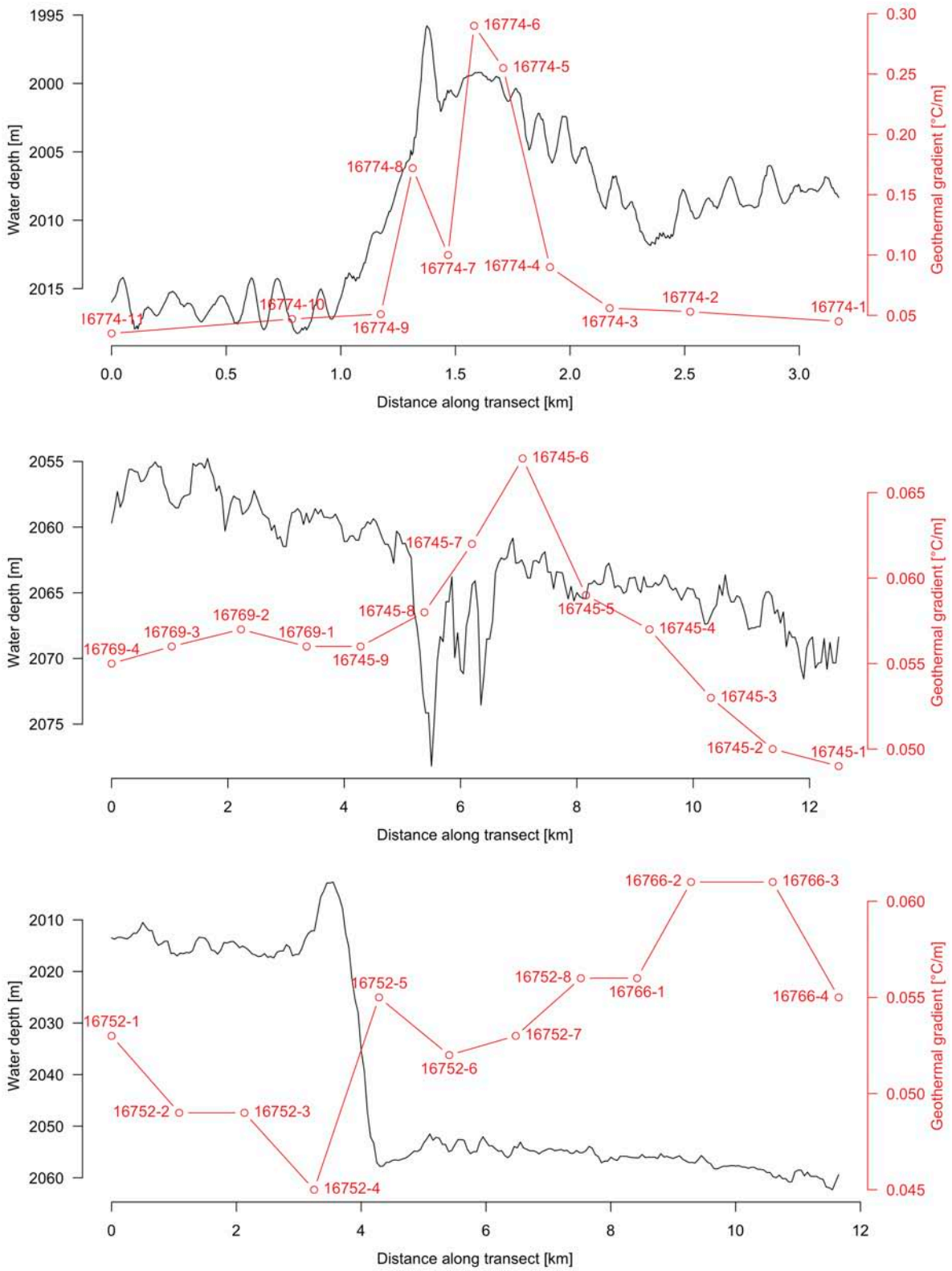

Figure 39: Bathymetry and geothermal gradient along a transect lines across MV #2 (top), across a fault in the central Kumano basin (middle), and across a morphological step in the bathymetry east of MV #4 and MV #5 (bottom). The numbers indicate the GeoB-numbers of the stations.

6.3. *In situ* CPT testing

(M. Lange, A. Steiner, A. Kopf)

During SO222 cruise, a total of 10 DWFF-CPTU measurements were conducted at three different mud volcanoes (MV #2, 3 and 4). The measurements are located on top and down-slope of these MVs (Table 6).

Table 6: Selected protocols from DWFF-CPTU deployments.

GeoB 167x x-yy	pos. Lat	pos. Lon	date	WD [m]	v_0 [m/s]	penetr. depth [m]	probe	MV No.
10-01	33° 37.97' N	136° 40.20' E	17.06.12	1954	1.27	1.1	length 4.1 m; tip pp; u2 and u3	3
10-02	33° 37.95' N	136° 40.15' E	17.06.12	1953	1.24	2.4	length 4.1 m; tip pp; u2 and u3	3
10-03	33° 37.93' N	136° 40.10' E	17.06.12	1980	**failed**		length 4.1 m; tip pp; u2 and u3	3
10-04	33° 37.90' N	136° 40.00' E	17.06.12	1971	1.26	2.2	length 4.1 m; tip pp; u2 and u3	3
30-01	33° 39.38' N	136° 38.01' E	24.06.12	1974	0.93	2.1	length 4.1 m; tip pp; u2 and u3	4
30-02	33° 39.44' N	136° 38.03' E	24.06.12	1986	1.46	1.5	length 4.1 m; tip pp; u2 and u3	4
30-03	33° 39.49' N	136° 38.04' E	24.06.12	2040	1.29	2.9	length 4.1 m; tip pp; u2 and u3	4
73-01	33° 40.65' N	136° 55.20' E	09.07.12	2004	**unprocessed**		length 4.1 m; tip pp; u2 and u3	2
73-02	33° 40.60' N	136° 55.25' E	09.07.12	2003	**unprocessed**		length 4.1 m; tip pp; u2 and u3	2
77-01	33° 40.64' N	136° 55.19' E	10.07.12	2014	**unprocessed**		length 4.1 m; tip pp; u2 and u3	2

The water depth varies between 1950 and 2050 mbsl (meter below sea-level). The penetration rate ranges between 0.9 and 1.5 m/s resulting in penetration depths of 1.1 to 2.9 m.
The DWFF-CPTU tests address following strategies:

- Comparison between DWFF-CPTU measurements and gravity core data (fall-cone experiments [f-c]) with respect to the strain-rate correction of the in-situ data.
- *In situ* characterisation of the MV shallow sediment succession in order to evaluate the fluid/gas conditions, consolidation settings and strength properties.

Mud volcano #3

The first 4 DWFF-CPTU deployments were undertaken on top of the MV #3. One of the dynamic-CPTU tests (16710-03) fails due to technical problems of the equipment (logging failure). All other tests present probable results displayed in Figure 40, which comprises three CPTU measurements represented by the excess pore-water pressure (pp) evolution during failure measured at two different pp ports (Δu_2 and Δu_3). Based on these data sets, the undrained shear-strength (s_u) are derived using the empirical excess pp factor ($N_{\Delta u1\text{-}3}$). In addition, the lithological core description including core photo and f-c shear-strength of two adjacent gravity cores are illustrated (GeoB16712 and -16735). The lithology is subjected by homogeneous to slightly heterogeneous clay to silty clay with irregular distributed clasts (sandstone to siltstone). Single sharp stratigraphical features are detected in these two cores. The excess pp varies between 5 and 20 kPa exclude the first meter of the CPTU measurements. In this first section, positive peaks up to 60 kPa are encountered. These peaks are probably caused by gas/fluid escape structures or gas hydrate. The s_u distribution shows values up to 20 kPa. A very good agreements between the f-c and in-situ data can be seen. Slightly discrepancies can be described by the occurrence of gas/fluid structures and gas hydrate as well as by the fact that core and *in situ* test location are not exact equal (vessel movements).

The consolidation state can be described as normally- to slightly over-consolidated with undrained shear-strength ratios (s_u/σ'_{v0}) of 0.2 to 0.6. More data will be acquired during post-cruise geological/geotechnical laboratory measurements (standard- and advanced experiments).

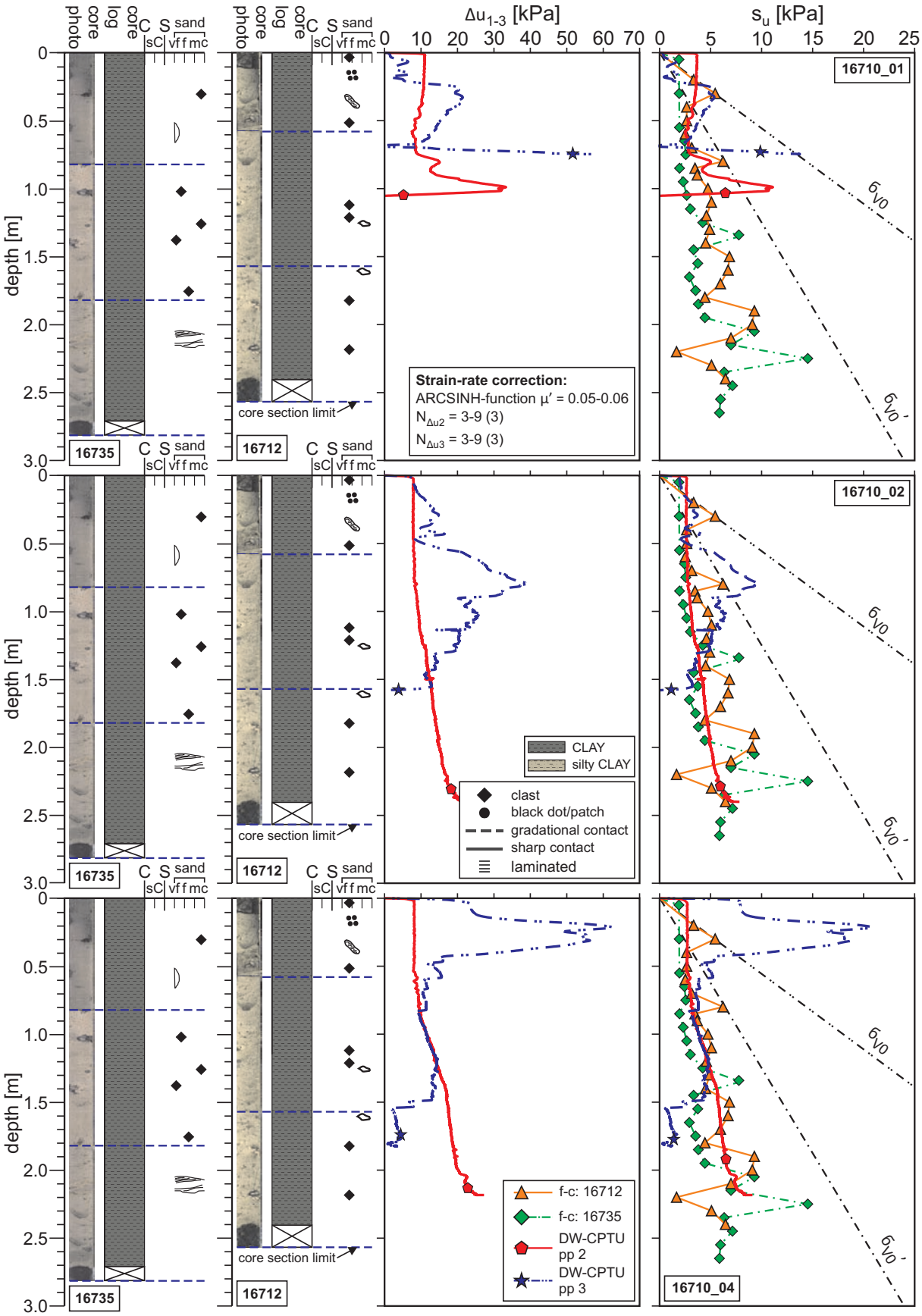

Figure 40: Results from CPTu deployment at MV #3. Corrected excess pore-water pressure behind the tip (Δu_2) and 0.35 m behind the tip (Δu_3) for the MV #3 (GeoB16710-01, -02 and -04). Additionally, the derived undrained shear-strength (s_u) of the DWFF-CPTU measurements compared with the f-c data (GeoB16712 and 35) are illustrated. All dynamic-CPTU data sets are strain-rate corrected using the state-of-the-art ARCSINH-function described in Mitchell & Soga (1976). See also Table 6.

Mud volcano #4

In total, 3 DWFF-CPTU tests were carried out on top and down-slope of the MV #4 (Fig. 41), which illustrates CPTU measurements represented by the excess pore-water pressure (pp) evolution during failure measured at two different pp ports (Δu_2 and Δu_3). Based on these data sets, the undrained shear-strength (s_u) are derived using the empirical excess pp factor ($N_{\Delta u1\text{-}3}$). In addition, the lithological core description including core photo and f-c shear-strength of two adjacent gravity cores are illustrated (GeoB16725 and -16736). The stratigraphical sequence is characterized by homogeneous to slightly heterogeneous clay to silty clay including irregular scattered clasts of sandstone and siltstone. The in-situ measurements (GeoB16730-01 and -02) show a sharp step between soft and stiff sediments at penetration depth of 0.6 m. This step are also detected in the f-c experiments. The excess pore-water pressure of the sediments varies between 5 and 20 kPa for the first 0.6 m and increase up to 60 kPa in the deeper sections. In test GeoB16730-03, this sharp increase are not encountered due to the fact that the location of this tests is at the shoulder area of the MV #4. Hence, only homogeneous slope sediments were characterized. The derived in-situ undrained shear strength varies from 5.0 to 10 kPa with an increase to approx. 15 kPa at >0.6 mbsf for GeoB16730_01 and _02. The dominated sediments are normally-consolidated to slightly over-consolidated due to a undrained shear-strength ratio (s_u/σ_{v0}') of 0.2 to 0.5. The consolidation state of the increases section is describes by s_u/σ'_{v0} values up to 1.3 characteristic for highly over-consolidated sediments.

In all tests, fluid/gas structures, coarser sediments and angular to well rounded clasts are scattered along the sediment succession. More data will be acquired during post-cruise geological/geotechnical laboratory measurements (standard- and advanced tests).

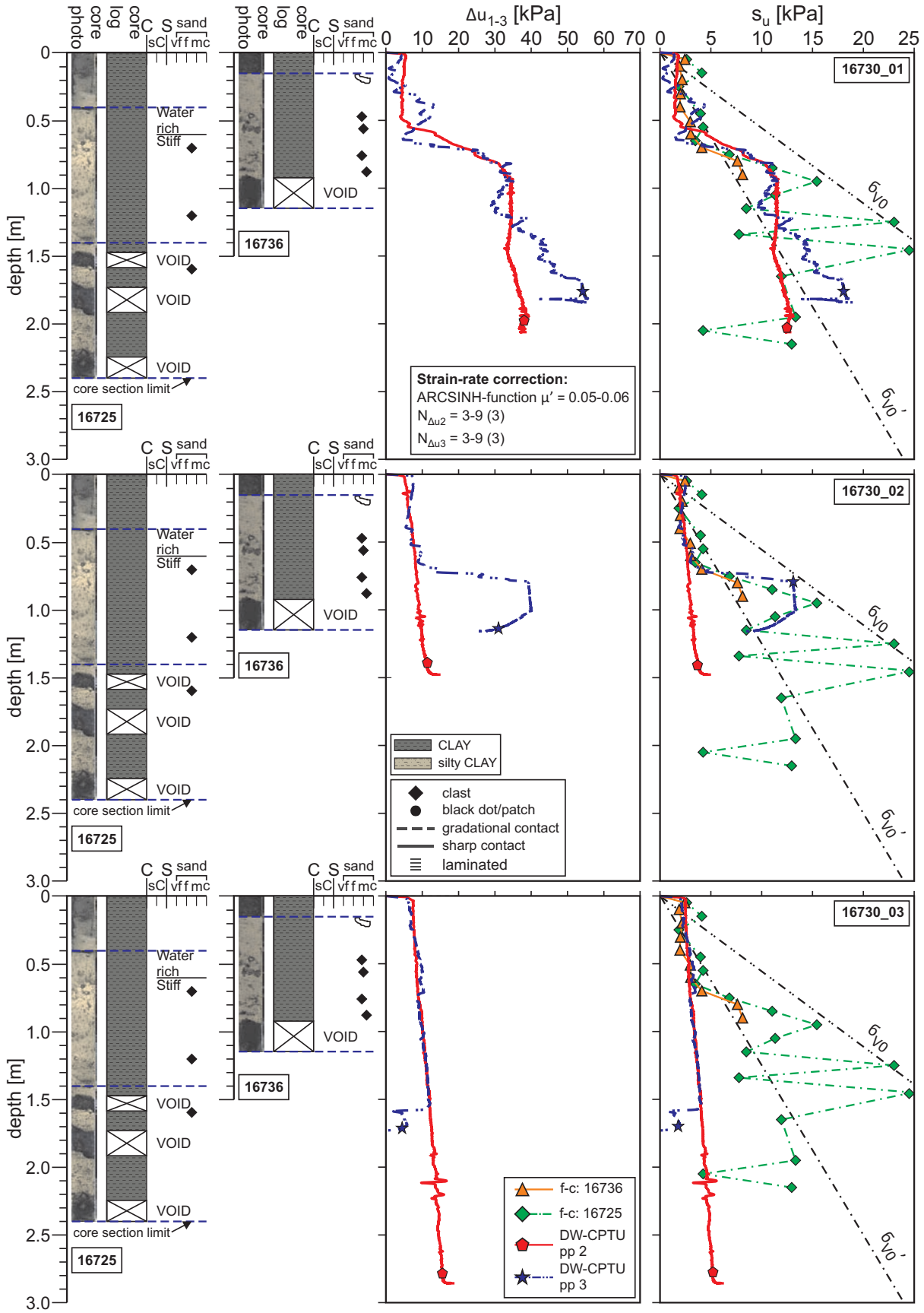

Figure 41: Results from CPTu deployment at MV #4. Corrected excess pore-water pressure behind the tip (Δu_2) and 0.35 m behind the tip (Δu_3) for the MV #4 (GeoB16730_01 to _03). Additionally, the derived undrained shear-strength (s_u) of the DWFF-CPTU measurements compared with the f-c data (GeoB16725 and -36) are illustrated. All dynamic-CPTU data sets are strain-rate corrected using the state-of-the-art ARCSINH-function described in Mitchell & Soga (1976). See also Table 6.

Two additional dynamic-CPTU tests were carried out at MV #2, however, those data have not been processed yet.

6.4. CAT-meters
(M. Tryon)

During SO222B, 2 CAT meters each were deployed on mud volcanoes #2, 3, and 4 (Fig. 42). These site were determined to be our best strategy for detecting and sampling fluid flow and fluid chemistry, based on the cores retrieved at each. The locations and times of deployments are tabulated at the end of this section (Table 7). Deployment was accomplished by lowering them to the sea floor via wire and releasing. Subsequently some of them were revisited by the ROV to inspect whether the sampling chamber has sealed against the seafloor (see also section 6.8 below).

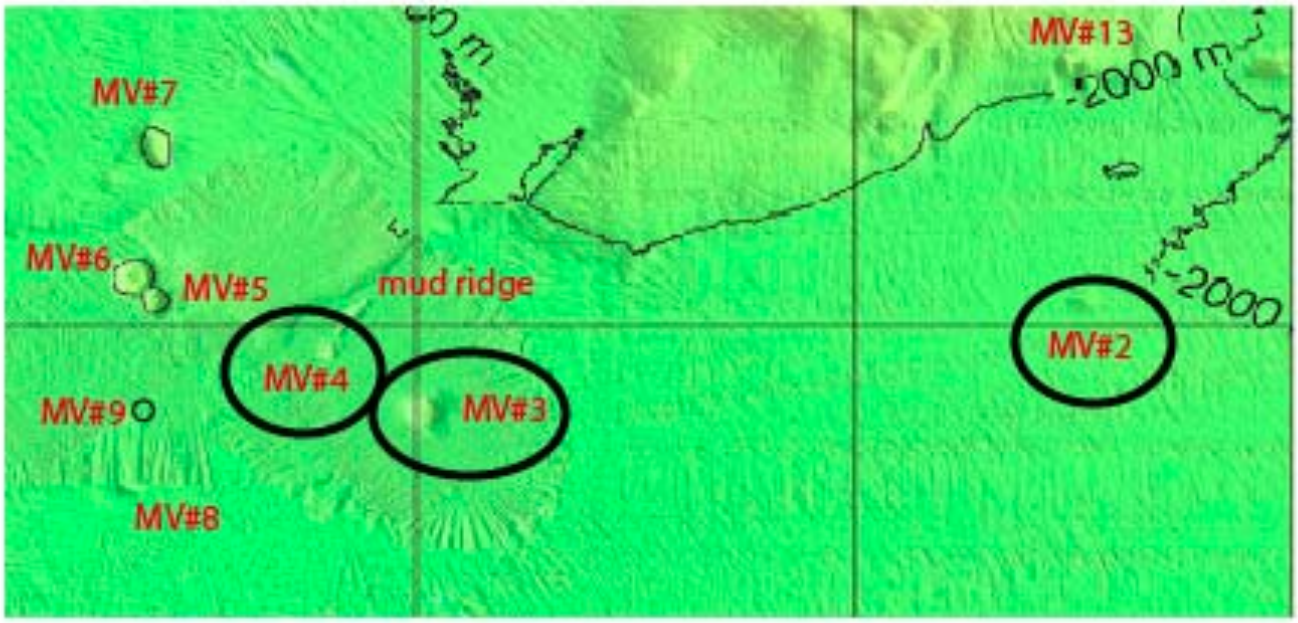

Figure 42: Map showing the locations of the CAT meter deployments.

Table 7: Positions of CAT meters deployed during cruise SO222.

Station	Date	UTC	PositionLat	PositionLon	Feature	Depth [m]	Remarks
GeoB16753-1	04.07.12	23:46	33° 39,36' N	136° 38,05' E	MV#4	1977	CAT Flowmeter #0
GeoB16753-2	04.07.12	23:48	33° 39,37' N	136° 38,05' E	MV#4	1978	CAT Flowmeter #5
GeoB16767	07.07.12	23:30	33° 38,02' N	136° 40,25' E	MV#3	1952	CAT Flowmeter #8
GeoB16776-1	10.07.12	03:50	33° 40,54' N	136° 55,28' E	MV#2	1955	CAT Flowmeter #7
GeoB16776-2	10.07.12	03:58	33° 40,53' N	136° 55,28' E	MV#2	1950	CAT Flowmeter #9
GeoB16785-1	12.07.12	04:57	33° 38,06' N	136° 40,26' E	MV#3	1945	CAT Flowmeter #6

6.5. MeBo- and Gravity coring / sediment description / IR imagery

(M. Vahlenkamp, A. Hüpers, S. Hammerschmidt, M. Belke-Brea, J. Wei, A. Kopf, M. Bergenthal, R. Düßmann, K. Kaszemeik, S. Klar, C. Noorlander, U. Rosiak, U. Spiesecke, A. Stachowski, W. Schmidt, C. Seiter)

Core description

A total of 51 gravity cores were taken during cruise SO222, of which 44 had at least some recovery. A 6m long core barrel was used to obtain sediment cores from the Kumano basin. The majority of the cores were taken on the tops or flanks of the several mud volcanos within the basin which were compared to reference cores showing background sedimentation. Additionally six MeBo cores of up to 35.6 m length were drilled at selected mud volcanoes (also known as Kumano Knolls, or KK). Three of the MeBo cores were taken at Kumano Knoll (KK) #3, two cores at KK #4 and another one on top of MV #10. The MeBo cores taken in the center of the mud volcanos revealed the presence of mud breccia to >15m depth with no other lithologies recovered from below. GeoB 16728 was taken on the N-flank of MV #4 and showed strongly varying lithologies. Recovery of MeBo cores was generally fairly low averaging between 40-50%.

A list of all gravity- and MeBo cores, also including TV grabs (see section 6.10. below) during cruise SO222, sorted by the topographic features where they were taken, is listed in Table 8.

Table 8: List of TV grabs, gravity- and MEBO core stations during SO222. Legend: MB, MS = mud breccia, mud stone; BS = background sediment; ~BS, ~MB = intersections; AL = ash layer; AP, AC = ash patch, clast; T = turbidite; SS = black sandstone; G = graphite; GH = gas hydrates; FES = fluid escape structures/dykes/conduits; WF = wood fragments; H2S = hydrogen sulfide. For further abbreviations used, see Figure 22.

	Site	recovery	Water depth	remarks	Lith. (Top --> Bottom)	features
KK #2						
	16764	269	1988	top	MB	GH, H2S
	16770	0	2000	no recovery		
	16771	259	2000		MS, MB	GH, H2S
	16772	322	2000		MS, MB	GH, H2S
	16788-1	plastic hose	1992	top	MB	GH,H2S
	16788-2	plastic hose	1993	top	MB	GH,H2S
	16793	0		no recovery		
KK #3						
	16703-1	320	1945	top	MB	-
	16704	270	2017	MV#3 NE-flank	MB	-
	16709	1102	1950	MeBo N' flank	MB	-

	16711	353	1950	MeBo top	MB	-
	16712	256	1942	top	MB	H2S
	16713	-	1940	TV Grab	MB	-
	16731	25	2028	NE-flank	MB	-
	16732	1182	2032	MeBo NE-flank	MB, BS, MB (~BS), AL	AP, AC
	16735	400	2030	NE-flank	MB, MB (~BS)	-
	16785-2	200	1945	top	MB	H2S
KK #4						
	16722-1	0	1980	no recovery	-	-
	16722-2	306	1980	Top	MB	GH,H2S
	16723	365	2050	NE-flank	MB	H2S, AC
	16725	240	1970	top	MB	GH,H2S
	16726	338	2052	N-flank	BS	T
	16727	338	2007	MV #4 Mud ridge	BS	-
	16728	457	2043	MeBo N-flank	BS, MB, BS, SS, AL, SS, G, SS (~BS), G, SS	AC
	16729	400	2016	Mud ridge	BS, AL, BS	AP
	16736	115	1980	Top	MB	GH,H2S, AC
	16737	165	1981	MeBo top	MB	-
	16754	254	2030	N-flank	MB	H2S
KK #5						
	16746	200	1900	top	MB	GH,H2S, AP
	16747	21	1906	top	MB	-
	16748	166	1934	SW-flank	MB	-
KK #6						
	16749	300	1924	top	BS	AP
	16750	320	1926	top	BS, MB	AP
KK #7						
	16751	20	1935	top	BS, AL, BS	T
KK #8						
	16707	360	2025	N-flank	BS (~MB)	H2S
	16720	573	2020	Top	BS	H2S, AC
KK #9						
	16708	284	2044	NW-flank	BS	H2S
	16721	576	2050	top	BS	T
	16734	226	2057	N-flank	BS	H2S, AP
KK #10						
	16716-1	0	1825	no recovery	-	-

	16716-2	137	1825	top	MB	GH,H2S
	16717	0	1816	no recovery	-	-
	16740	65	1824	top	MB	-
	16741	156	1823	MeBo top	MB	-
	16743	100	1825	top	MB	-
NE of KK #10						
	16738	475	1828	mud wedge	BS, AL	H2S
	16739	575	1900	mud wedge	BS, AL, BS	H2S, AC
KK #11						
	16756	425	2010	NE top	MS, AL, MS	H2S
	16757	469	2000	top	MS	H2S
KK #12						
	16759	558	2050		BS	H2S, AP, T
	16762	74	2010	top	MB	H2S
KK #13						
	16780	0	1870	no recovery		
	16781	370	1880		BS, MB	WF, H2S
	16782-1	0	1891	no recovery		
	16782-2	300	1890	top	MB	AC
KK #14						
	16791-2	479	2000		BS	H2S, FES
Background						
	16758	400	2040		BS	T, WF
	16763	370	2012		BS	AP, T

Two main lithologies were recovered by gravity coring within the upper 6m during SO222:

1. Stiff to soupy or moussy dark grey claystone with clasts of various sizes (mm-cm) (Fig. 43). The clasts found within the mud breccia are claystones of various degree of consolidation, but also lithified sedimentary rocks (mudstones, fine to coarse grained ashes and sandstones). Degassing structures were abundant in several cores where small gas hydrate chips, a few centimeters in size, disintegrated. This lithology was interpreted as mud breccia. Clasts are thought to be transported upwards from the lower Kumano Basin or the accretionary prism. Post-cruise analyses will hopefully clarify this aspect.

2. Dark grey to very dark greenish grey silty claystone (Fig. 44). Silty to sandy lenses and turbidite layers of very dark grey colour occur in an apparent regular spacing of almost every 10 – 40 cm. Foraminifera and shell fragments are rare, dewatering structures are present in several sections. This lithology was interpreted as Kumano Basin background sediment.

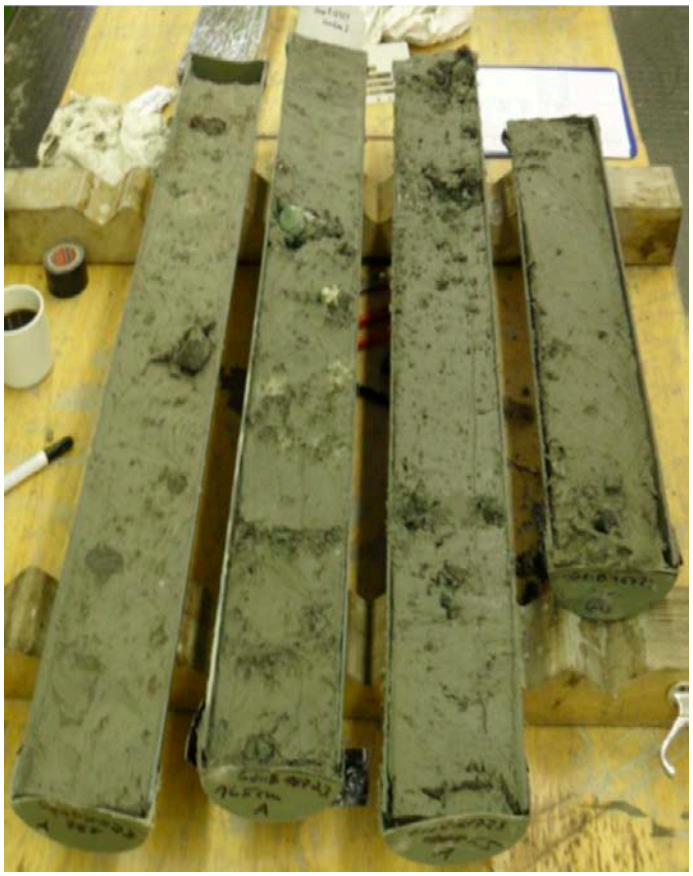

Figure 43: Consolidated, dark grey mud breccia from the northern flank of KK #4 (GeoB 16723). Note the clasts of a few cm size.

Figure 44: Consolidated, dark greenish grey claystone from a reference location in the Kumano basin (GeoB16758). Note the black silty turbidites.

Figure 45: Mousse-like, dark grey mud breccia from the top of KK #2 (GeoB16764).

Cores were taken at 13 different mud volcanos (Kumano Knolls #2-14). Table 8 specifies in detail how many cores were taken on which feature and gives a short summary of the lithological observations plus the length of the recovered sections.

In general, the group of features sampled can be broadly divided into active and currently inactive ones, with the recovery of grey mud or mud breccia and the presence of gas hydrates having been the main criterion.

Most cores were taken on KKs #2, 3, 4 and 10 where dark grey mud breccia or mudstone was found in the center of the mud volcano, accompanied by a strong smell of H_2S. Gas hydrates were found at KKs #2, 4 and 10. Together with data from pore water and gas chemistry our observations suggest that these features are among the most active ones in the Kumano basin, especially KK #2. The presence of free gas as well as gas hydrate causes the texture to appear mousse-like (Fig. 45), similar to what has been described in the Mediterranean Sea, e.g. for Napoli MV (Emeis et al., 1996).

From the eight cores taken at KK #4, a fairly comprehensive picture can be gained, as shown in Figure 46. Gravity cores GeoB16725, -16736, -16722-2, -16754 and -16723 indicate that the top and

the northern flank of the feature are build up by mud breccia, which is also suggested by the steep angle of the flanks. MeBo core GeoB16737 covers depths of 14-19 mbsf at the top of KK #4 and shows that the mud breccia extends to greater depth. At the location of gravity core GeoB16726 at the northern base of the feature Kumano basin background sediment is recovered which overlies the mud breccia. An exception from the previously described succession can be found in MeBo Core GeoB16728 further north, which shows unusual sedimentary structures at the base. Here, background sediment is underlain by mud breccia and black sands and graphite-like clays, partly with slumping structures in depth intervals of 7 to 16 mbsf. Those layering at the base of the northern flank of the feature is tentatively interpreted as products of earlier phases of mud volcanism; post-cruise work will include dating of those event layers and XRD analysis to identify the main minerals.

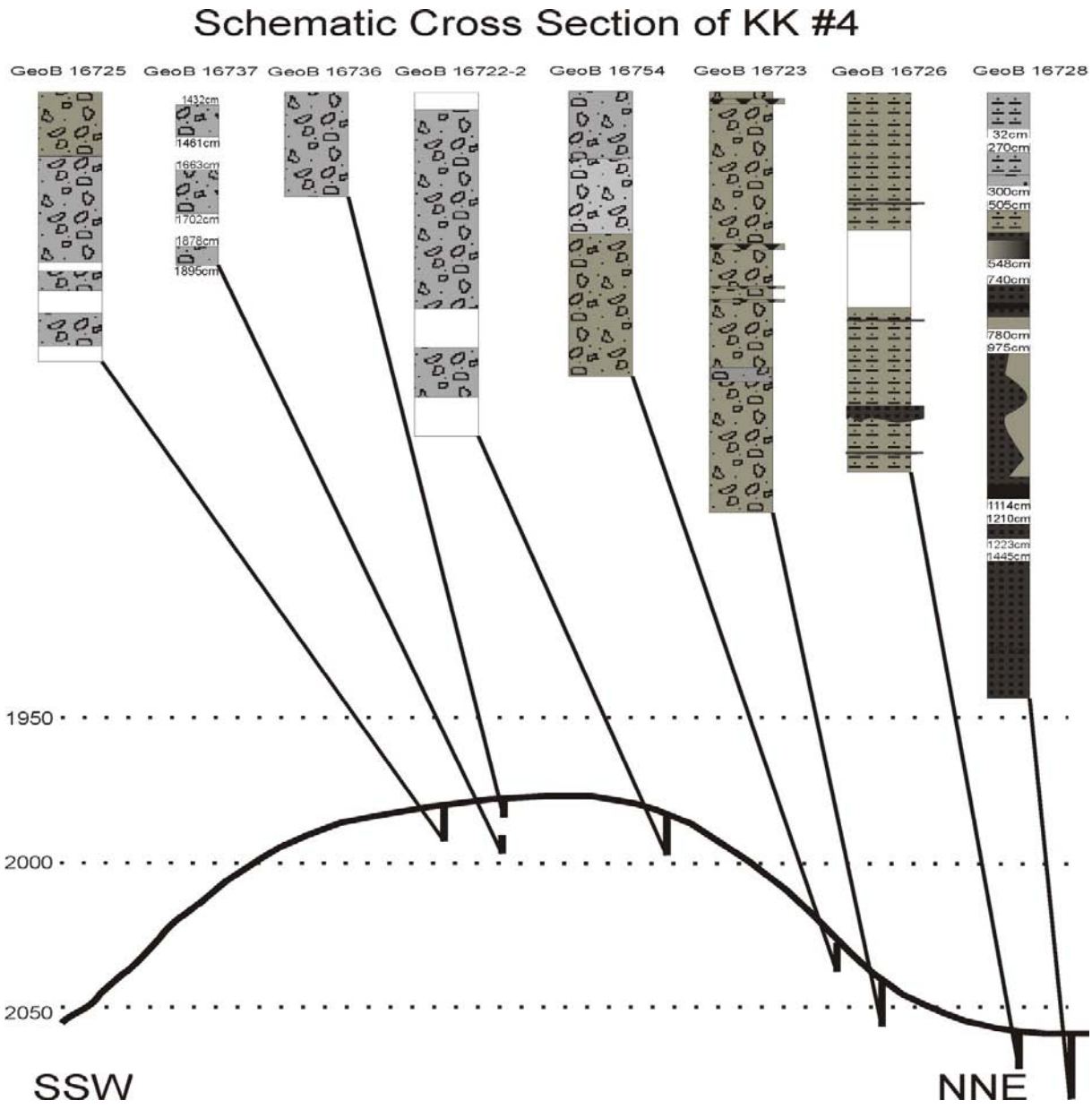

Figure 46: Schematic cross section of Kumano Knoll 4 including lithologs of gravity and MeBo cores.

Cores taken on KK #2 look similar, but contain extremely mousse-like, grey mud breccia with clasts of mm-cm size (Fig. 45). Elongated gas hydrate chips of up to 5 cm in length were sampled from all cores on this feature. KK #2 is the mud volcano with the highest presence of gas hydrates investigated during cruise SO222. KKs #3 and 10 show very much the same lithologies and structure as the ones mentioned before.

At Kumano Knolls #5, 12 and 13 two to three coring attempts with recovery each have been carried out. Mud breccia was found on top of all three mud domes, too, and was overlain by background sediment at the flanks of KKs #12 and 13.
Cores from mud volcano #11 contain no mud breccia but grey mud, which is also interpreted as a product of mud volcanism in the Kumano Basin. Based on observations in the sediment we suggest that all these mud volcanoes were recently active. However, no active fluid seepage could be observed on either of those KKs (see also in situ temperature data, section 6.2 above).
On the remaining features, including KKs #6, 7, 8, 9, 14 and the mud ridge near KK #10, no mud breccia has been recovered or the mud breccia is overlain by Kumano Basin background sediment. We suggest that these features were recently dormant. Background sedimentation on the mud volcanoes and in the basin is to a large extend interrupted by very dark grey to black, silty turbidites with an erosional contact at the base and a gradual contact (Fig. 44). Usually these layers are only ca. 1-3 cm thick, but in some cores, especially GeoB16758, a large fraction of wood fragments is present within the turbidite layers (reaching up to 15 cm in thickness). These turbidites seem to occur regularly between every 15 – 30 cm in parts of the succession recovered. The regular spacing of the turbidites might reflect the seismic cycle of the Nankai Subduction Zone which nowadays generates earthquakes of magnitude 8 and higher every 100-200 years (*Ando* 1975). Dating of the event layers will be carried out and allow a better understanding of those processes. Distinct layers of fine white ash and thickness of a few cm have been discovered in cores GeoB16728, -16729, -16732, -16738, -16739, -16751 and -16756 and will be helpful with the development of an age model. In many cores the background sediment shows water filled vugs of ~ 1cm diameter. We interpret these structures as channels through which fluids can migrate upwards.

MeBo deployments

Apart from the standard coring routines, MeBo's main task during expedition SO222 was the deployment of long-term monitoring systems. In total, four observatories were successfully installed

during the cruise (see Table 9, which also contains some drilling statistics). MeBo was deployed for a total of ca. 126 hours; detailed information on deployment of MeBo and recovery of sediments is summarised in Table 9 and the station list (Appendix 9.1).

Table 9: Station list for MeBo deployments.

Station GeoB No.	Deployment duration [hrs:min]	Latitude [N]	Longitude [E]	Water depth [m]	Drill depth [cm]	Coring interval [cm]	Recovery [cm] [%]	Remarks
16709	27:09	33° 38' 01.6''	136° 40' 15.4''	1951	2855	0-2855	1102 cm 39%	Drill string length 30.9m; sealed with MeBo Plug 1
16711	24:40	33° 38' 00.8''	136° 40' 16.3''	1951	3325	2620 – 3325	354 cm 50%	Drill string length 33.3m sealed with MeBo Cork B
16728	17:45	33° 39' 32.5"	136° 38' 00.9"	2055	1710	0-1710	419 cm 25%	Drill string length 17.5m sealed with MeBo Plug 2
16732	10:30	33° 38' 13.3"	136° 40' 30.0"	2035	3560	0-3560	1182 cm 33%	
16737	12:15	33° 39' 21.3"	136° 38' 02.2"	1980	1895	1445-1895	72 cm 16 %	Drill string length m sealed with MeBo Cork A
16741	11:15	33° 32' 51.9"	136° 16' 56.5"	1830	1445	0-1445		Core recovery is not reported
Total	**126:34**				**14790**	**10725**	**3129 cm 33 %**	16741 not included

In situ T-measurements using MeBo

Figure 47 shows temperature measurements with the soft sediment cone in three different depth (9.8m, 19m and 28m). With the feeding system the tip was pushed approx. 20cm into the sediment. The start of each curve were aligned. The graphs shows the typical increase of temperature due to the friction after pushing the tip into the sediment. An increasing temperature with depth is also observed, which is in good agreement with the *in situ* heat flow data at the same site (see section 6.2 above). Furthermore the curve at 28m shows a little increase of temperature with time, which can be interpreted as a cause of gas hydrates forming.

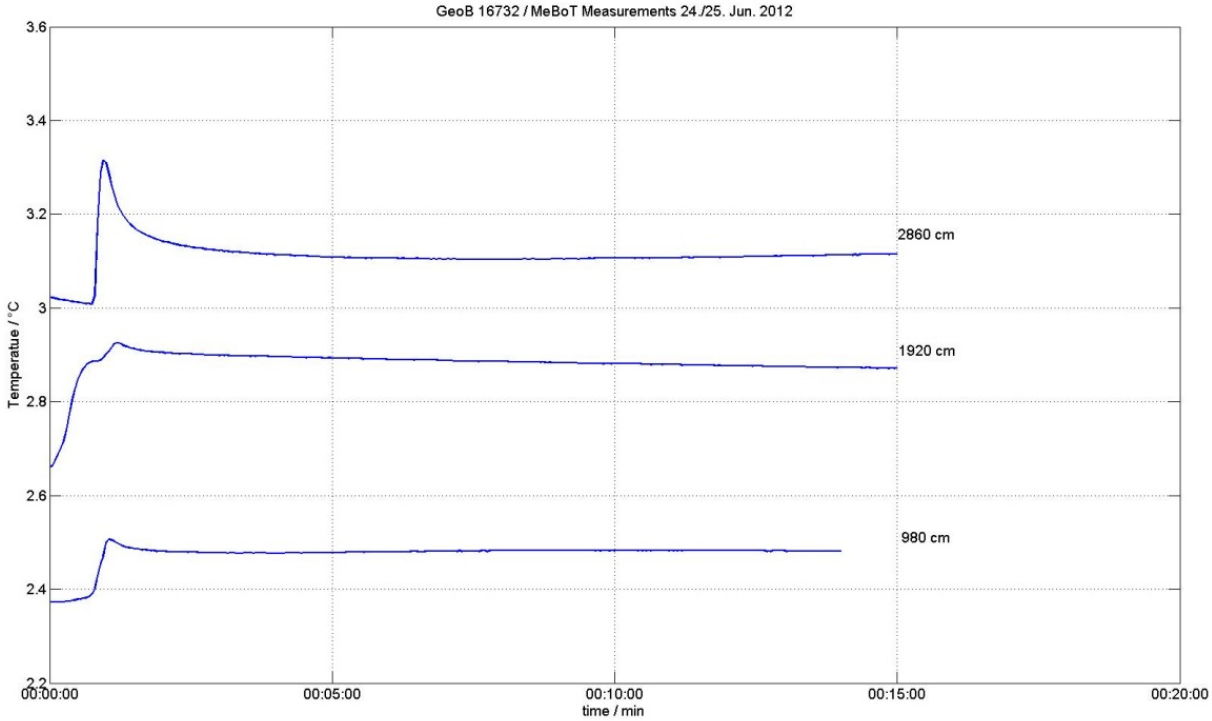

Figure 47: MeBo Temperature measurements at station GeoB 16732.

IR imagery

In order to get coherent IR images of the core, all raw data were imported into the ThermaCAM™ Researcher Professional software. Based on the observation and test, the color scales of most gravity cores were set to be 12-30°C which shows the best performance of the three major constituents: gas hydrate, normal sediment and voids. Then all the raw data were output as bitmap files for further processing on the PC. During this procedure all the images were rotated and scaled in order to make all the core sections horizontal and the same diameter. Finally, using the obvious hot or cold reference points, the images were connected. All the measurements performed are listed in Table 10.

Table 10: all IR measurements from SO222 and basic information

GeoB No.	Image number	Remarks
16703	52-64	disseminated GH in CC
16709	66-120	Poor recovery without gas hydrate(GH), no image process
16711	122-146	Poor recovery without GH, no image process
16716	157-159	round rock in the core catcher disseminated GH in CC
16720	160-172	two images for one core section (1m), core_5 is 74cm long,GH observed at 4.4m from bottom
16721	173-185	Poor recovery without GH, no image process
16722-2	186-197	disseminated GH in CC and in the bottom 1m (sampled)
16723	198-209	1.4mbsf soupy(4cm)
16725	217-228	disseminated GH in CC
16726	229-240	
16727	241-252	
16728	254-290	Poor recovery without GH, no image process
16729	291-302	

16732	303-368	Poor recovery without GH, no image process
16734	369-379	
16735	380-391	
16736	392-403	GH in CC
16737	404-411	Poor recovery without GH, no image process
16738	412-422	
16739	423-434	
16741	435-439	Poor recovery without GH, no image process
16742	440-443	
16746	444-455	GH in CC
16747	456	Empty core
16748	457-467	
16749	468-479	
16750	480-491	
16751	492-504	

Downcore thermal imaging was performed on the cores and results are presented in the appendix. In general, temperatures measured on the surface of the liner can be divided into four categories which represent gas hydrate, normal sediment, voids and artefacts as show in Figure 48 varying between 12 and 30°C. Those temperatures are clearly not representing in-situ temperatures of the seafloor sediments which are around 2° C depending on the depth below seafloor. The thermal structure of the cores developed during the ascent trough the water column and within the air temperature plus additional influence by frictional heating during the core handling. Background temperatures of gravity core liners which have been filled by muddy sediments were calculated between 16-20°C depending on how long the cores have been retrieved before the IR imaging was performed. In general the cores were imaged immediately when on deck. Anomalies from the background temperature occur in both directions (Fig. 48). Negative thermal anomalies are generally associated with gas hydrates, whereas gaps in the liners are represented by positive anomalies. The gaps were dominantly developed due to gas expansion and/or dissociation of disseminated gas hydrates during the decompression and heating process during the ascent of cores. In general gaps show up with warm anomalies because of the low heat capacity of gas in comparison with sediment. Some higher temperature values are also related to further artificial heating when liners were taken by hands during transportation on deck. Cold spots or patches are clearly related to gas hydrates. This was well observed when the core is on deck. Only a few gravity cores show gas hydrate occurrence and no gas hydrate in the MeBo cores within IR thermal scanning.

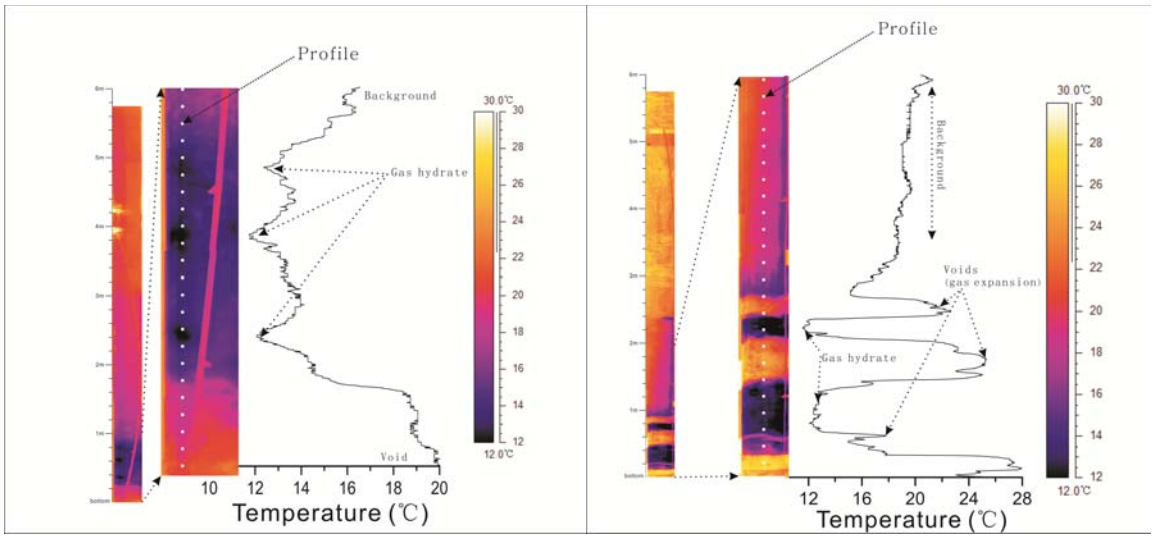

Figure 48: Infrared record of gravity cores GeoB16722-2 (left) and GeoB16725 (right).

6.6. Physical properties

(M. Ikari, T. Ojima, M. Belke-Brea)

Shear strength was measured aboard RV *Sonne* on all cores recovered that had sufficient core recovery (i.e. a coherent internal structure and intact core in the PVC liner). Both devices, the fall cone penetrometer and the vane shear apparatus were used in parallel, however, the spacing with fall cone was much narrower (every 5 cm) than for the more destructive vane shear method where we did 1-2 measurements per core segment.

Figures 49 – 51 show three exemplary examples of the results obtained in different lithologies. All other data will be published as part of a printed cruise report in "Berichte aus dem Fachbereich Geowissenschaften der Universität Bremen" shortly, both electronically as well as in the Appendix (together with lithologs of sediment description).

Figures 49 and 50 represent examples from mud breccia sediments from two active features, MV# 3 and MV#8 show weak to moderately strong shear strength of sediment, usually well below 10 kPa within the uppermost meters below seafloor. For MV#8, vane shear and fall cone data show a good agreement, while for MV#3, vane shear is higher than the dynamic fall cone values. This is unexpected, but was observed in other MV cores as well. A tentative explanation is the high abundance of small mudclasts within the matrix of the mud breccia, which may not affect the tip of fall cone during penetration. Thoise mudclasts may, however, get in the way of the rotating blöades of the vain, this way pushing those readings to higher values. Figure 51 provides an example from inactive mud volcanao KK #7 in the north of the research area (Fig. 8). Here, hemipelagic background sediment with occasional turbidite and ash layers is found. The ash layer in particular shows unusually high strength, which is in agreement with similar horizons elsewhere.

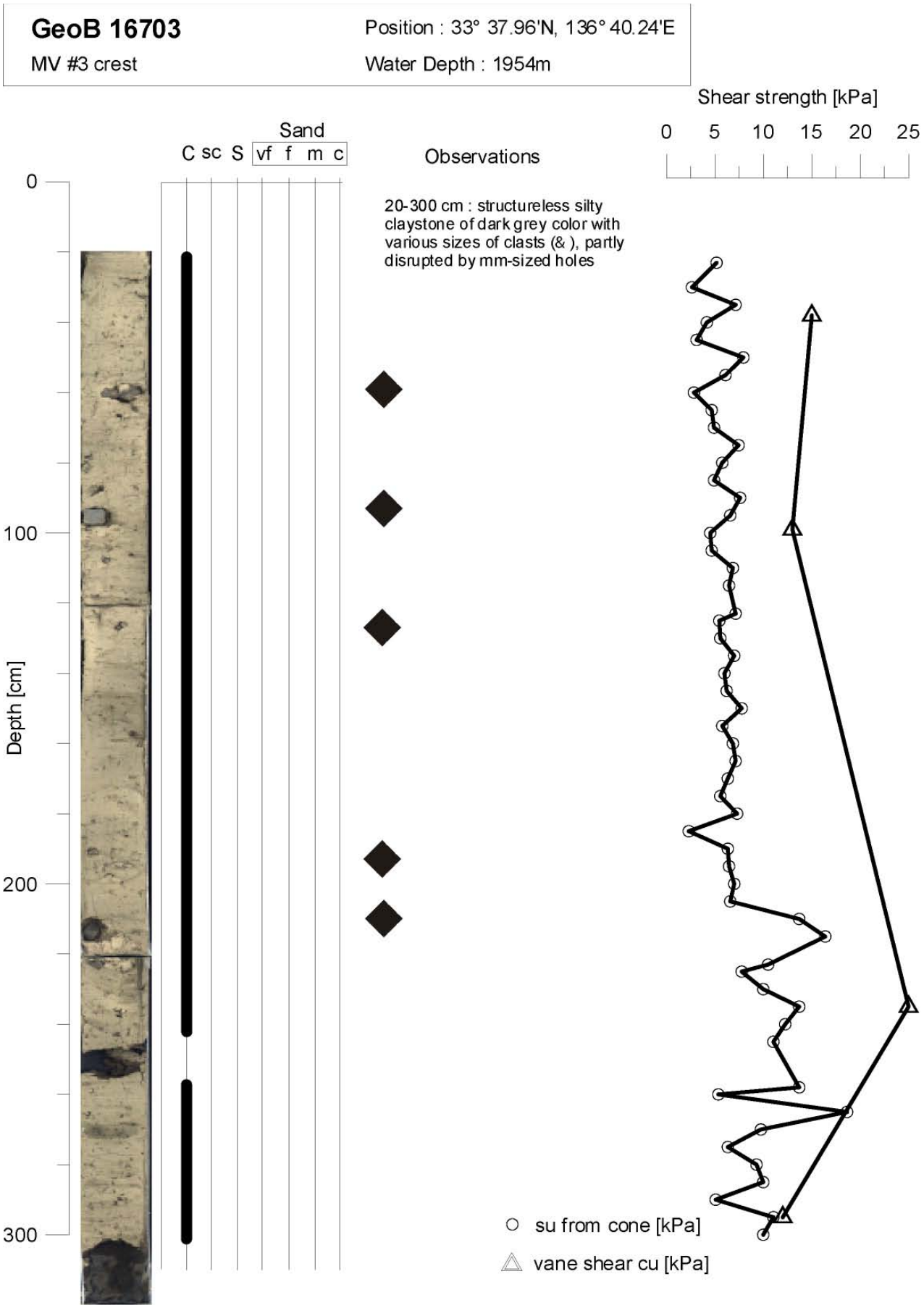

Figure 49: Shear strength from vane shear and fall cone devices compared to lithologs and core observations from station GeoB16703 where mud breccia was recovered from MV #3.

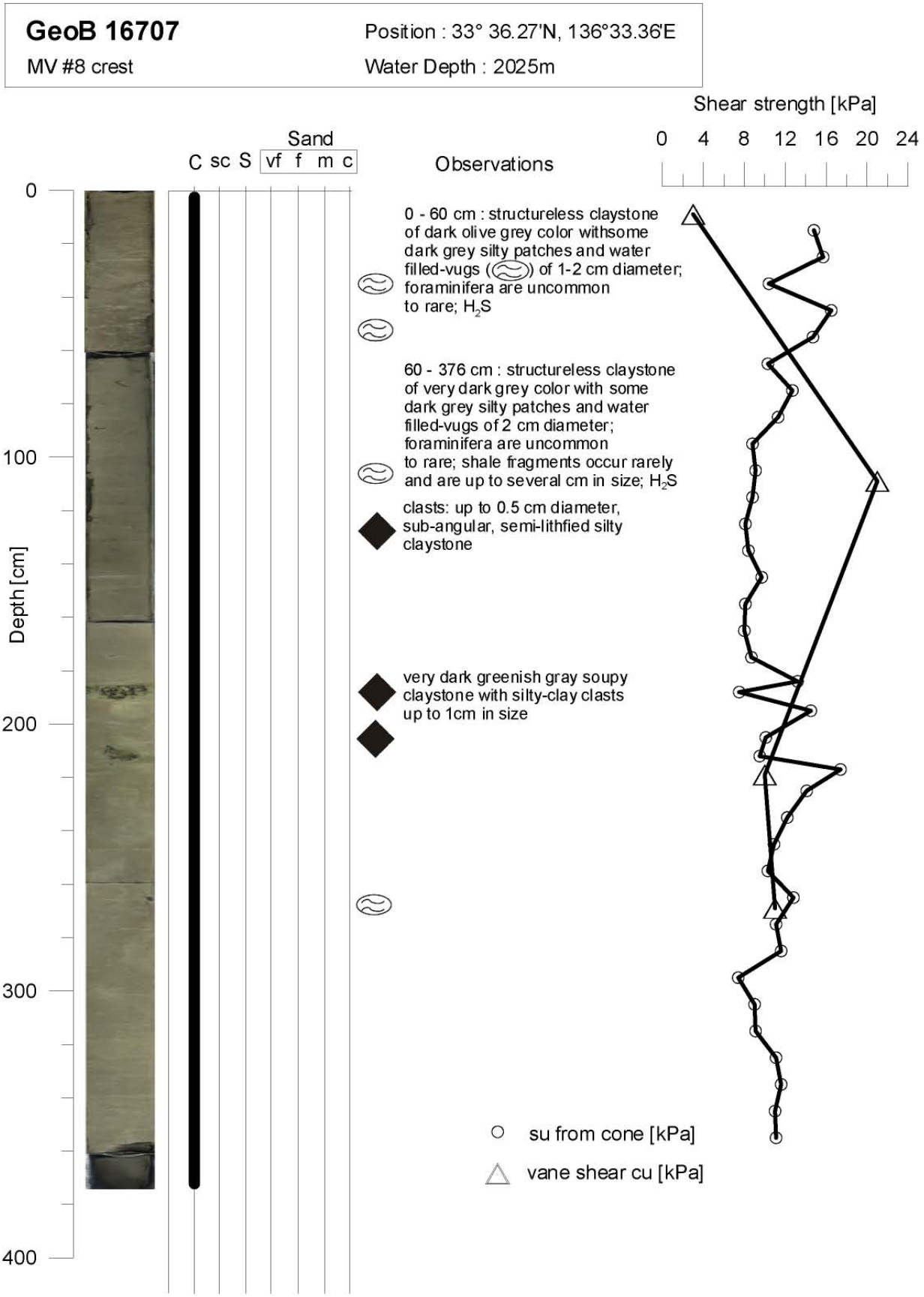

Figure 50: Shear strength from vane shear and fall cone devices compared to lithologs and core observations from station GeoB16707 on mud volcano KK #7.

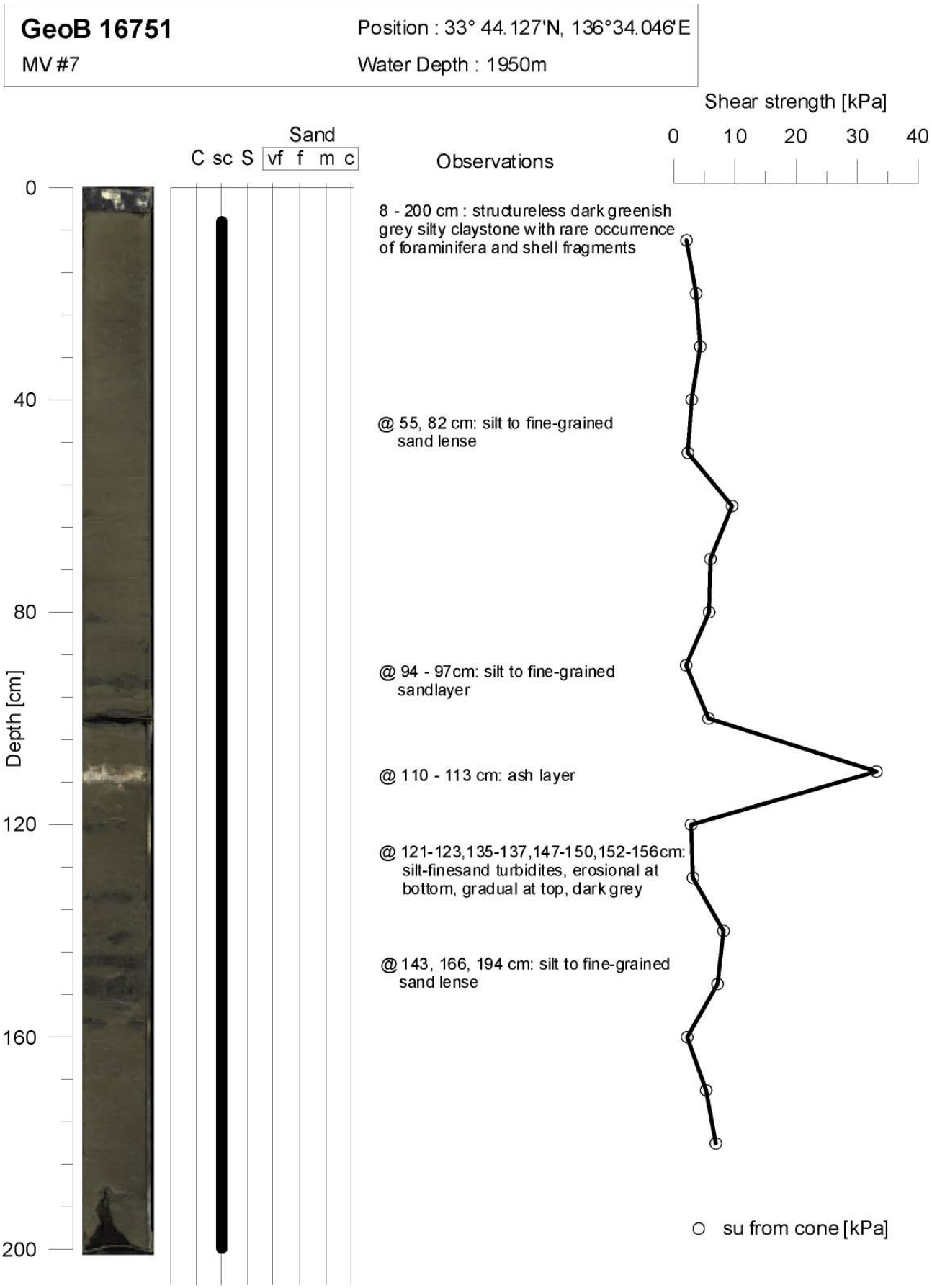

Figure 51: Shear strength from vane shear and fall cone devices compared to lithologs and core observations from station GeoB16751.

6.7. Fluid geochemistry

(T. Pape, P. Geprägs, M. Tryon, A. Bräunig, M. Madison)

6.7.1. Gas chemistry

Regarding the molecular composition of gas hydrate-bound gas, light hydrocarbons were recovered from MVs #2, #4 and #10 with the gravity corer were strongly dominated by methane (CH_4 ≥96.865 mol% ΣC_1 to *n*-C_4), followed by C_2H_6 (1.035 – 3.105 mol%) and C_3H_8 (≤ 0.373 mol%; Table 11). Higher homologues, such as butane and pentane isomers, occurred in much smaller portions or were even below detection limit. The data of KK #5 are different. The C_1/C_2 ratio with a value of 1,512 is very high compared to the other mud volcanos so the impact of microbial gas is much higher at this site (Fig. 52). The respective C_1/C_2 ratios of all samples with thermogenic signature ranged between 31 and 256, suggesting that light hydrocarbons in shallow sediments of both mud volcanic structures predominantly originate from thermocatalytic processes (Bernard, 1976) most likely taking place at greater depths.

In addition, the virtual absence of hydrocarbons ≥C_3 suggests that the crystallographic structure I is the dominant hydrate phase at all sites.

Table 11: Molecular composition of hydrate-bound gas (in mol-% ∑[C_1 to *n*-C_4]) prepared from hydrate pieces at mud volcanoes KK #2, 4, 5, and 10.

GeoB	Mud Volcano #	C_1/C_2	C_1	C_2	C_3	*i*-C_4	*n*-C_4	*n*
			[mol%]	[mol%]	[mol%]	[mol%]	[mol%]	
16722-2	4	31	96.865	3.105	tr.	tr.	tr.	1
16725-1	4	55	98.163	1.807	tr.	tr.	tr.	1
16736-1	4	59	98.226	1.771	tr.	tr.	tr.	2
16716-2	10	65	98.486	1.035	0.373	0.095	0.012	3
16746-1	5	1.512	99.929	0.079	tr.	tr.	tr.	2
16764-1	2	256	99.611	0.406	tr.	tr.	tr.	1
16771-1	2	264	99.623	0.394	tr.	tr.	tr.	1
16772-1	2	178	99.440	0.574	tr.	tr.	tr.	1
16788-1	2	214	99.535	0.479	tr.	tr.	tr.	1
16788-2	2	213	99.555	0.480	tr.	tr.	tr.	1

n = number of samples analysed (mean value)
tr. = trace (≤ 0.01 mol%)

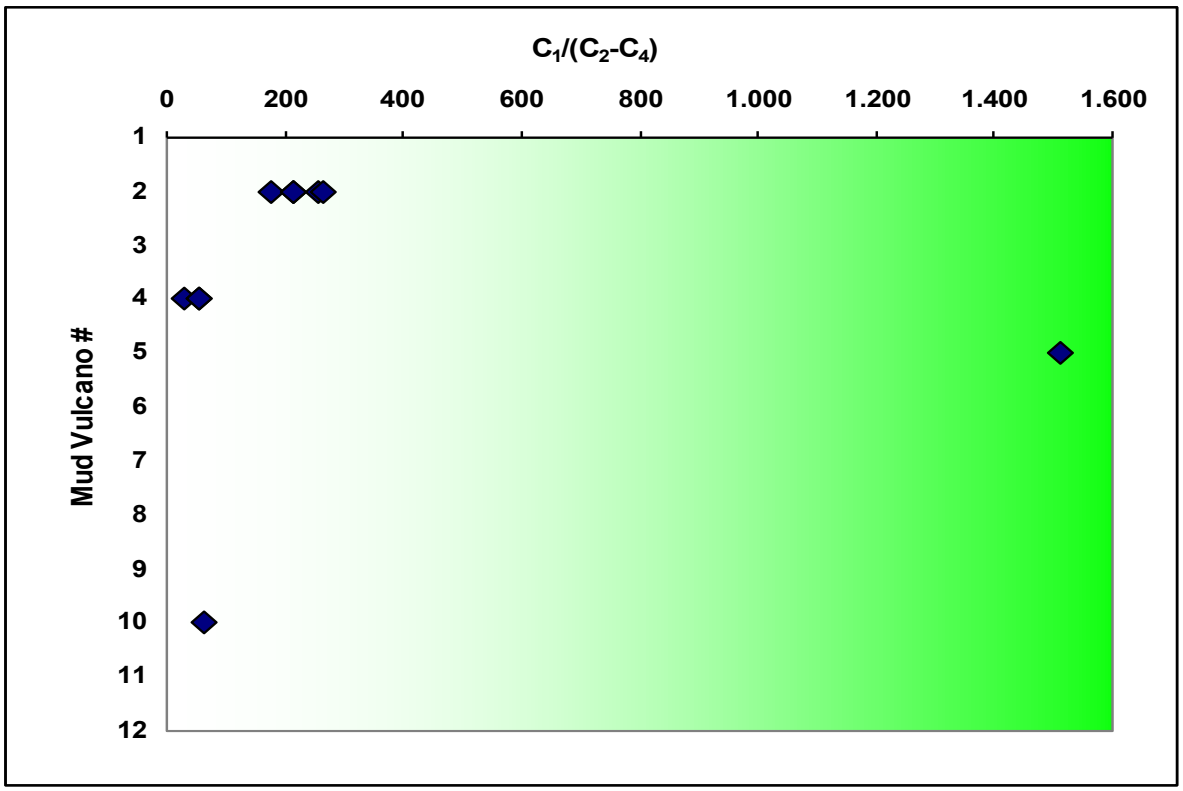

Figure 52: Graphic representation of the C_1/C_2-C_4 values for the mud domes sampled for gas hydrates. See text.

6.7.2. Pore water chemistry

During expedition SO222 we collected 651 samples for pore water analysis, 101 from the six MeBo cores and 550 from a total of 39 gravity cores.

The only measurement of composition made on board was salinity. This was done with a handheld refractometer with a resolution of 1 unit. This simple and rapid measurement is useful for checking for pore water freshening due to gas hydrate dissociation or deep-sourced fluids freshened by mineral dehydration. Figure 53 shows the wealth of results of these measurements. With few exceptions, the cores from mud volcanoes indicate two trends of freshening with depth. Our initial thoughts on this is that the large amount of shallow freshening in the gravity cores are due to gas hydrate dissociation during core recovery and processing (see example from KK #2, Fig. 54A), and the deeper freshening trend may be due to advection of fluids influence by mineral dehydration at great depth.

In all plots, we provide reference cirves for simple advection models with rates of 1mm/yr, 2 mm/yr and 10 mm/yr. Figures 54B and 54C show examples from gravity cores at MV #11 and #13, respectively; those data fit well the assumed trends of 2mm/yr and 1 mm/yr. The best depth profiles were gained from the MeBo drilling, and despite the smaller diameter of the core and potential contamination with seawater while the core is sitting in the magazine (while the MeBo is drilling deeper), the downhole trends seem to be reliable. For instance, the “reference” drill hole at the

northern slope break of MV #3 (GeoB16732; blue curve on right in Fig. 53 that extends to ca. 35 mbsf) shows compositions close to seawater with very little freshening, if at al. By contrast, MeBo core GeoB16709 at the crest of MV #3 shows a 25m-long downhole record towards 5-10 g/l (or appx. 15-20 % SW concentration), aligning well with a 2mm/yr advection rate.

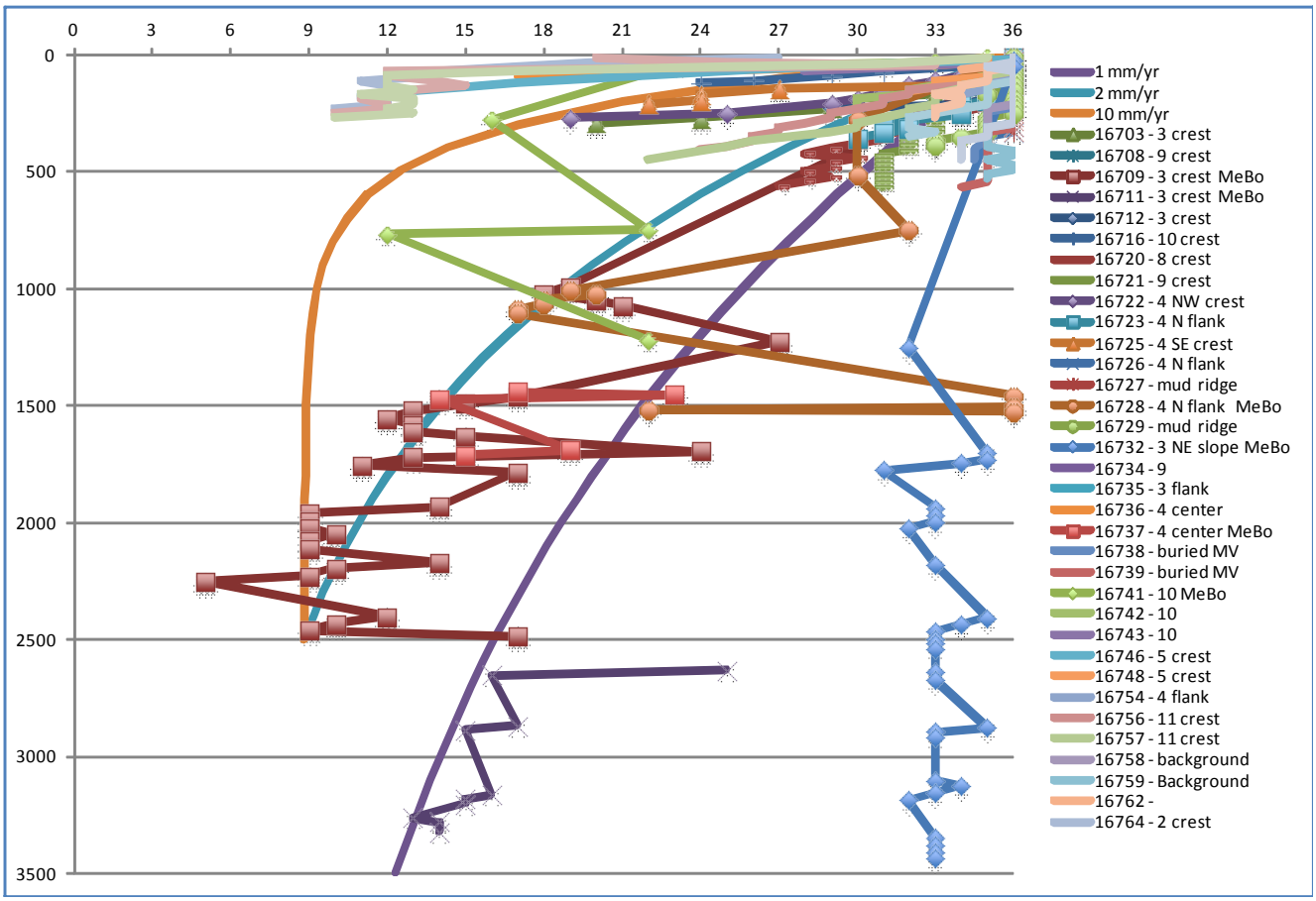

Figure 53: Plot of salinity vs. depth (cm) for the cores collected during cruise SO222.

Shore-based analyses will shed additional light on other element concentrations that may or may not be enriched or depleted based on the abovementioned processes. Preliminary results from ICP-OES on some of the fluids suggest unusually high B contents in some cores, and both Li enrichment and Li depletion in other cores. Additional stable isotope studies, in particular on those two elements, are envisaged.

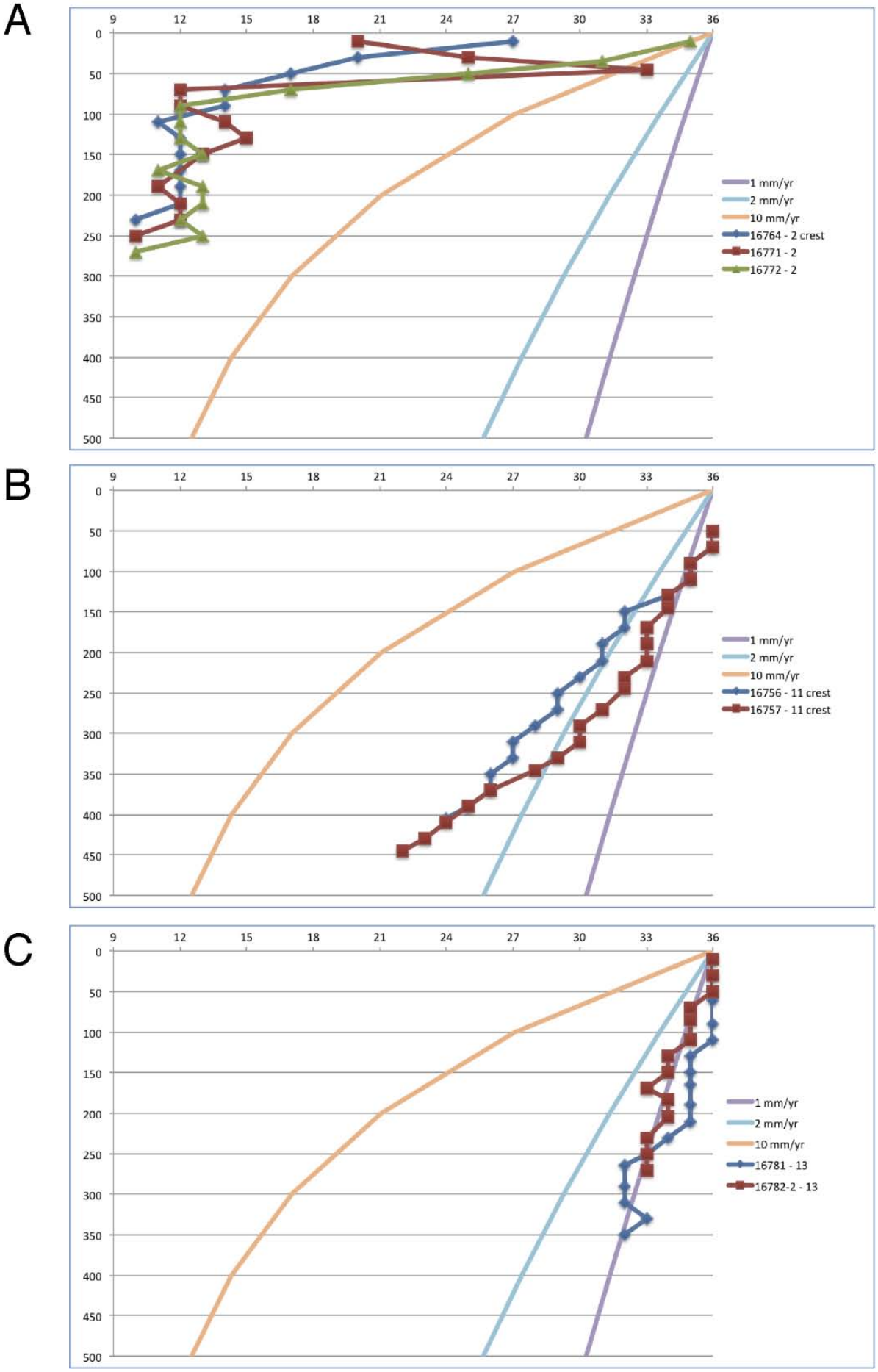

Figure 54: Plot of salinity vs. depth (cm) for the cores collected at MV # 2 (A), #11 (B) and #13 (C) during SO222B.

6.8. ROV operations

(C. Seiter, G. Bohrmann, etc.)

Operated by a team of 8 pilots and technicians, "QUEST 4000m" performed 2 dives ("QUEST 4000m" dive #320 and dive # 321) to 1950 m and 2055 m of water depth with a mean bottom time of 10.5 hours and an overall total dive time of 27.7 hours (see Table 12 for details).

Due to electric shorts affecting the hydraulic power unit and leading to intensive and time consuming maintenance operations, QUEST's technical conditions did not allow to perform further dives.

Table 12: Dive summary ROV "QUEST 4000m" during SO222B "MEMO" (all times UTC).

No.	Dive No.	Date	Site		Depth (m)	Time Launch	Time Start (Bottom)	Time End (Bottom)	Time Recovery	Bottom Time	Total Dive Time	Bottom hours	Total Dive hours
1	320	05.07.2012	33°39,512 N	136°37,9 E	2055	01:02	03:00	12:45	14:29	09:45	13:27	**9.75**	**13.45**
2	321	08.01.1900	33°37,985 N	136°40,272 E	1950	00:39	02:12	13:27	14:56	11:15	14:17	**11.25**	**14.28**
				Max. Dive depth (m):	**2055**				Mean bottom time per dive (hrs):	**10.50**	Total hours:	**21.00**	**27.73**

Dive operations included bottom unit installation on leg SO222A Marum sea bed drill rig "Mebo" deployed MeBoCORK B, sensor recovery with ship's wire support, sediment sampling, *in situ* temperature measurements in the surface sediment, and video/still photo surveys.

Close cooperation between ROV team and ships crew on deck and bridge allowed a smooth and professional handling during all "QUEST 4000m" launch and recovery situations. During diving, this cooperation also allowed precise positioning and navigation of both ship and ROV, which was essential for accurate scientific and technical installation operation tasks aswell as for "QUEST 4000m" umbilical management with an additional umbilical beacon at depth. The ROV team is very grateful for this kind of steady support from the entire ship's crew during the cruise.

6.8.1 Dive 320 (GeoB 16753-1) on Mud Volcano #4

Protocol: Gerhard Bohrmann
Scientists: A. Kopf, T. Feseker, M. Madison, P. Geprägs, M. Vahlenkamp, S. Hammerschmidt
Date: Thursday, 5 July 2012
Start at the bottom: 03:13 UTC 33°39.571'E 136°38.071'N 2056 m water depth
Start ascend: 12:39 UTC 33°39.385'E 136°38.035'N 1978 m water depth
Total bottom time: 8 hours and 26 minutes

Table 12: Instruments/tools during Dive 320 (GeoB 16753-1).

GeoB Number	Tool/instrument	Start (UTC)	Latitude (°N)	Longitude (°E)	Water depth (m)

16753-2	MTL-stick deployed	07:40	33°39.536	136°38.031	2060
16753-3	T-stick-1	08:14	33°39.481	136°38.057	2021
16753-4	Push core 31	08:18	33°39.479	136°38.058	2021
16753-5	Push core 22	08:21	33°39.477	136°38.057	2021
16753-6	T-stick-2	08:45	33°39.428	136°38.051	1990
16753-7	Push core 10	08:48	33°39.429	136°38.022	1989
16753-8	Push core 5	08:50	33°39.430	136°38.054	1989
16753-9	T-stick-3	09:17	33°39.391	136°38.057	1977
16753-10	Push core 29	09:23	33°39.391	136°38.057	1977
16753-11	Push core 16	09:27	33°39.395	136°38.061	1977
16753-12	CAT-0, beacon recovered	10:38	33°39.365	136°38.060	1976

Way points:
MeBoPlug #2 (GeoB16728): 33°39.5409'N 136°38.0153'E, seen at 33°39.535'N 136°38.027'E
MeBoCORK A (GeoB16737): 33°39.3550'N 136°38.0371'E
CAT meter #0: 33°39.361'N 136°38.048'E
CAT meter #5: 33°39.378'N 136°38.056'E

Description of the dive

Mud volcano KK #4 was explored by several gravity cores during the first part of SONNE cruise 222. In addition, two MeBo holes were drilled and installed with a plug (Site GeoB16728, MeBoPlug 2 at the northern rim of the mud volcano) or a CORK (Site GeoB16711, CORK B on top of the mud volcano). During *QUEST* Dive 320 it was planned to survey the MeBo drill sites as well as two CAT meters, which were deployed by the ship's wire and acoustic releaser systems on top of the mud volcano, just before the ROV dive started. In addition, push core sampling accompanied by T-stick measurements along a profile from the flank to the top of the mud volcano should become performed.

The dive started at the sea floor close to MeBoPlug #2, north of the mud volcano in 2050 m water depth, where we first searched for MeBoPlug #2. For several reasons we had problems to find the MeBo position in the forward looking sonar and it took quite a while before we found the Mebo Plug 2. The MSL-stick was deployed close to the borehole instrumentation, which is sticking out of the sea floor around 1,5-2 m. It contains a temperature sensor logging the seawater temperature close to the sea floor for the next two to three years (see section 5.9 above).

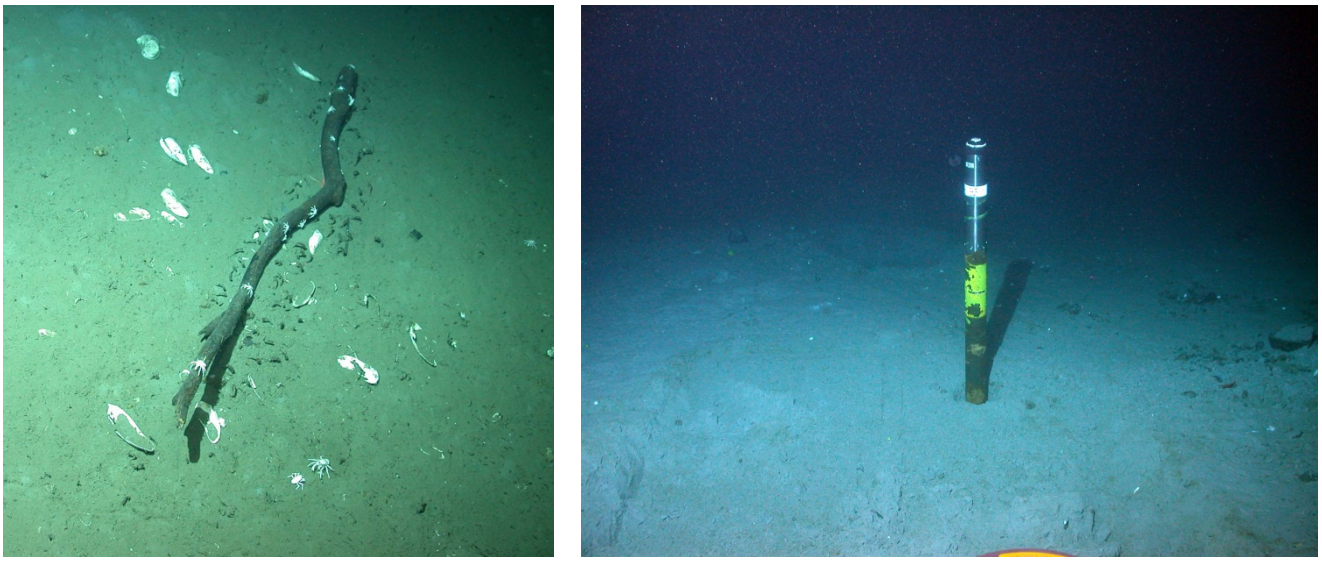

Figure 55: Wood fall on the flank of MV #4 associated with chemosynthetic clams and crabs (left). MeBo CORK A sticking out of the sea floor several decimeters. The imprint of the square-shaped basis of the Mebo drilling system can be seen on the sea floor as well as the round-shaped cast from one of the MeBo's leg (just behind the CORK).

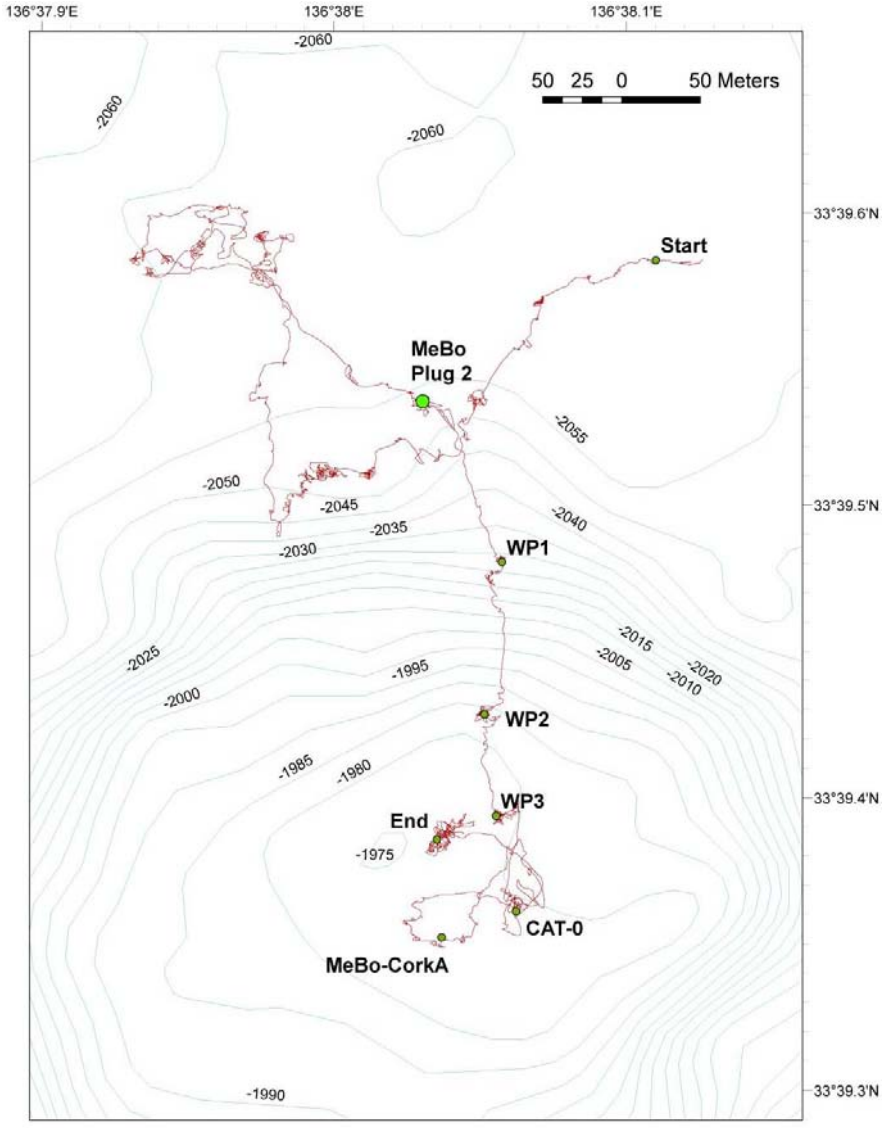

Figure 56: Track line of ROV Dive 320 on mud volcano #4 of the Kumano Basin. WP1 – WP3 mark T-stick measurements with two push core operations.

WP1: T-stick-1 (GeoB 16753-3), push core 31 (GeoB 16753-4), and push core 22 (GeoB 16753-5).

WP2: T-stick-2 (GeoB 16753-6), push core 10 (GeoB 16753-7), and push core 5 (GeoB 16753-8).

WP3: T-stick-3 (GeoB 16753-9), push core 29 (GeoB 16753-10), and push core 16 (GeoB 16753-11).

Afterwards, ROV *QUEST* dove approximately 100 m to the southwest to way point 1 (Fig. 56). Many clasts of different colours and sizes have been observed on the sea floor, which seem to have been accumulated specifically in the foot region of the mud volcano. Disseminated white shells possible from Calytogena-type clams were found in some areas. The open shells are remnants form dead clams and are well to see on the darker sea floor. Live clams are very difficult to see because most part of the shell is sitting in the sediment. Few clams together with crabs were observed close to wood fall deposits (Fig. 55). At way point 1 a T-stick measurement was performed and two push cores (no. 31 und 22) have been taken (Tab. 12).

After flying 100 m further to the south the ROV ascent additional 30 m in height and performed the same sampling (push cores 10 and 5) and T-stick (T-stick-3) measurement program at way point 2 (Fig. 56). At way point 3 (Fig. xx), further 60 m to the south, close to the top of the mud volcano, a third sequence of push coring (push cores 29 and 16) was performed during a T-stick measurement (T-stick-3). After that, ROV QUEST started to search for the different ship-based deployments in the topmost region of the elevated feature. 18 minutes later at 09:58 MeBo CORK A (GeoB16737) was found and documented by several ROV cameras (Fig. 55). After searching 20 minutes to the east and northeast flow meter CAT-0 was found and the beacon was recovered which was mounted on top of the flow meter. Signals from both beacons could not be received on the ROV and it was therefore more difficult to find the tools on the mud volcano. A strong signal in the sonar guided us to move the ROV to the northwest, because we hoped to find flow meter CAT #5. Instead a large bag of tissue with unknown content was found. Interestingly living Calyptogena clams are settled close-by and several large grabs inhabit the bag itself. It was decided to do another T-stick measurement, which failed, because of weather-dependent difficulties of the ROV maneuvering. The T-stick was recovered and the ROV had to dive up after weather conditions take a turn for the worse. At 12:40 the ROV started to ascend from the seafloor and Dive 320 terminated.

6.8.2 Dive 321 (GeoB 16767-1) on Mud volcano #3

Protocol: Gerhard Bohrmann
Scientists: A. Kopf, T. Fleischmann, T. Feseker, T. Kimura, K. Kitada, K. Asshoff
Date: Sunday, 8 July 2012
Start at the bottom: 02:20 UTC 33°38.109'N 136°40.353'E 1959 m water depth
Start ascend: 13:28 UTC 33°37.954'N 136°40.261'E 1944 m water depth
Total bottom time: 11 hours and 2 minutes

Table 13: Instruments/tools during Dive 321 (GeoB 16766-1).

GeoB Number	Tool/instrument	Start (UTC)	Latitude (N)	Longitude (E)	Water depth (m)
16767-2	CAT-8 observed	03:08	33°38.053’	136°40.268’	1949
16767-3	CORK-B + OBE connected	06:18	33°38.023’	136°40.259’	1950
16767-4	MTL-stick deployed	07:39	33°38.034’	136°40.266’	1950
16767-5	T-stick-1	07:52	33°38.033’	136°40.265’	1951
16767-6	T-stick-2	08:57	33°38.006’	136°40.225’	1952
16767-7	Push core 2	09:00	33°38.005’	135°40.224’	1952
16767-8	Push core 15	09:04	33°38.005’	136°40.226’	1952
16767-9	T-stick-3	09:50	33°37.960’	136°40.185’	1954
16767-10	Push core 18	09:54	33°37.961’	136°40.184’	1954
16767-11	Push core 30	09:59	33°37.960’	136°40.185’	1954
16767-12	OBE disconnected	10:30	33°38.008’	136°40.278’	1952
16767-13	OBE recovered	12:16	33°38.004’	136°40.293’	1950

Way points:
MeBoPlug #1 (GeoB16709): 33°38.0277’N 136°40.2569’E (Posidonia position from Leg A)
MeBoCORK B (GeoB16711): 33°38.0140’N 136°40.2719’E (Posidonia position from Leg A)
CAT meter #8 : 33°38.0350’N 136°40.2866’E (drop position; ship wire)
OBE: 33°38.0350’N 136°40.2866’E (drop position; ship wire)

Description of the dive

Mud volcano KK #3 was already surveyed in 2000 by Shinkai Dive 588 during cruise YK01-04 (*Kuramoto et al*., 2001) because of its prominent back-scatter signal but by a weak morphological expression in multibeam data. During this surface observation scattered chemosynthetic clams have been found which clearly indicate fluid flow from below. The mud volcano is roughly 60 m higher than the surrounding sea floor and has a flat top area of approximately 500 m in diameter. During leg SO222A, three MeBo drill sites were performed on this feature, one at the northern rim of the volcano (GeoB16732) and two on top of the dome. Both latter drill holes were supplied with long-term seafloor installations, one with a plug (MeBoPlug #1; GeoB16709) and the second with a MeBoCORK (CORK B; GeoB16711). The purpose for diving with ROV QUEST was to install additional instruments and to understand more about the regional fluid flow activities of the mud volcano. Therefore a Chemical and Aquaeous Transport (CAT) meter (CAT-8) and the bottom unit were deployed on the seafloor by the ship’s wire before the dive started (Fig. 57).

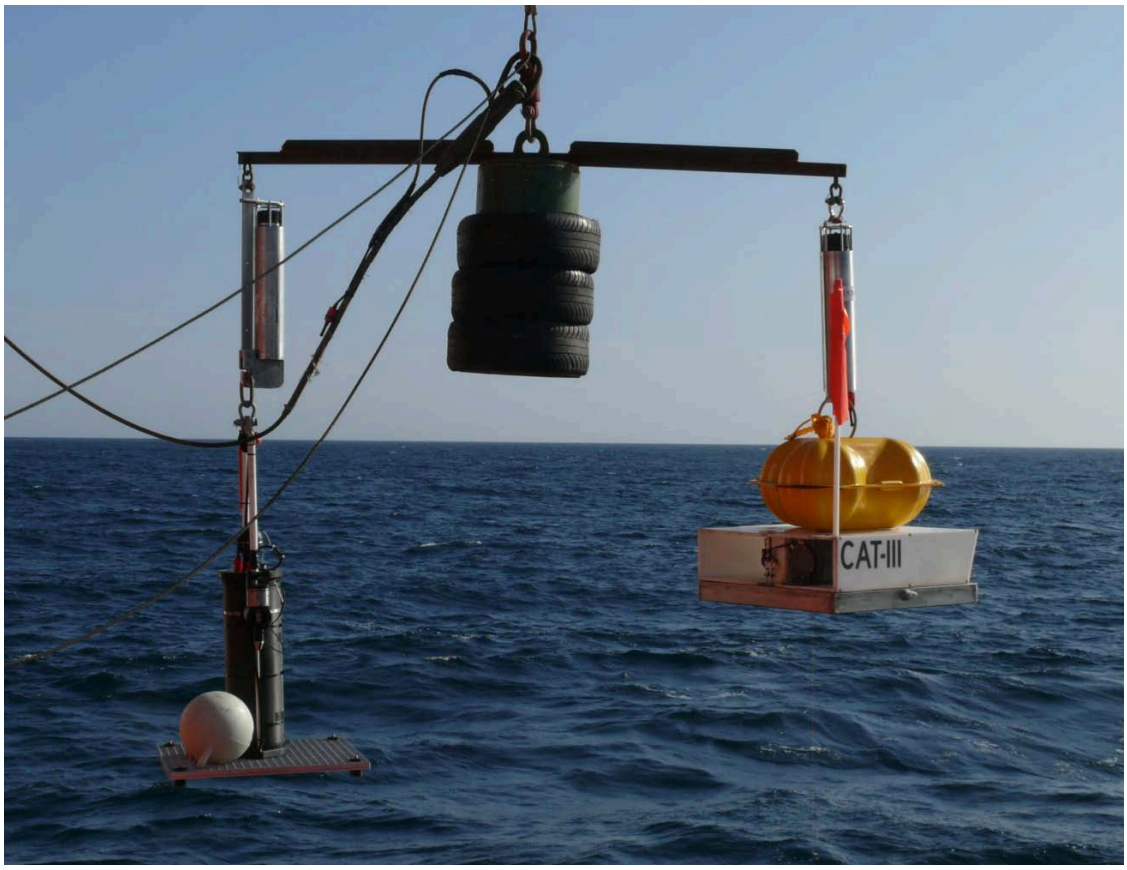

Figure 57: CAT meter #8 and the MeBoCORK B bottom unit (left) on the ship's wire and dummy weight before being lowered to the seafloor. The assembly got veered to appx. 50 m above seafloor, and the individual components were released close to each other by acoustic release.

ROV *QUEST* reached the sea floor at the northeastern upper flank of the mud volcano where the dive started at 02:20 UTC. Due to an offset in the dive map it took a while before the ROV arrived at the dropping location of CAT-meter #8. The sealing of the basic platform from CAT-8 was surveyed by turning around the total instrument. Images from all four sides document a good sealing of the instrument, so that all fluids below the flow meter will be registered by the system (Fig. 58, upper left).

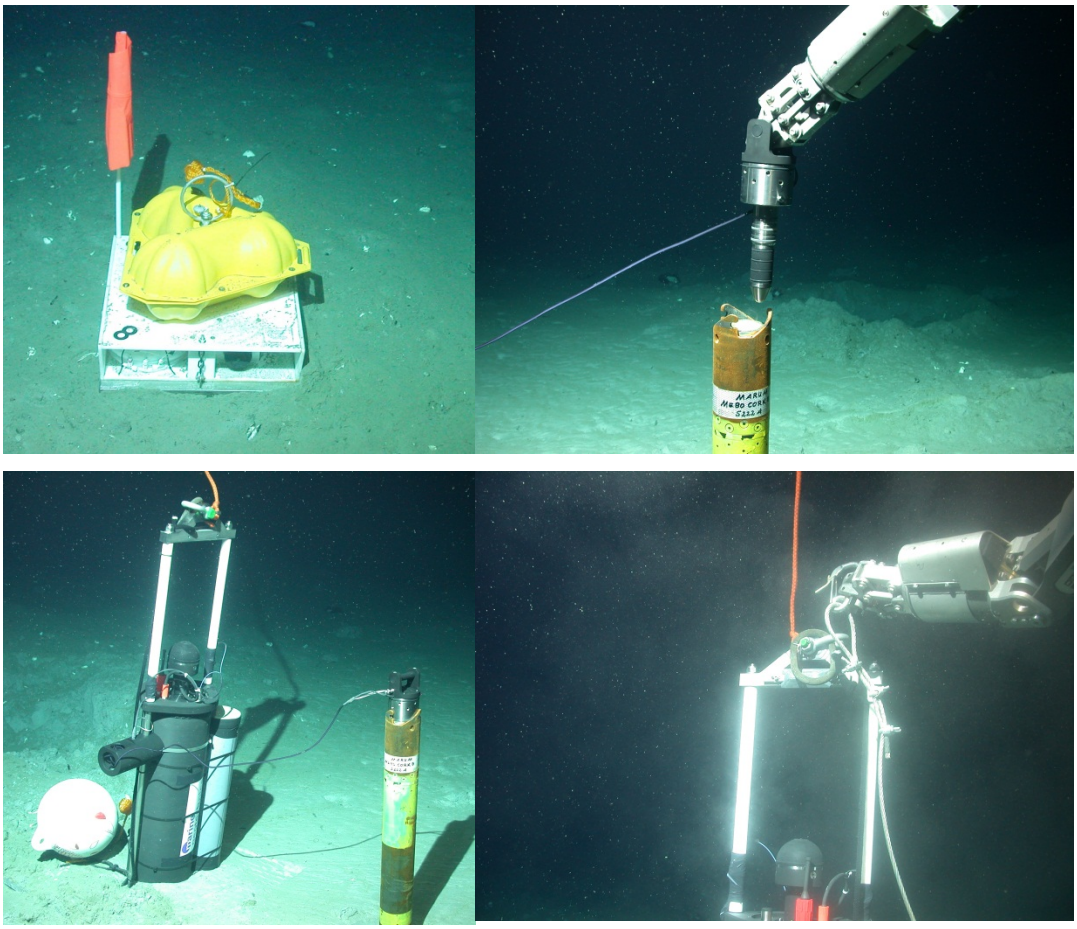

Figure 58: CAT meter #8 on mud volcano observed by ROV QUEST after the deployment by the ship's wire (above left). Connecting procedure of the hotstab to the MeBo CORK-B rod by the manipulator arm (above right). View of the connected bottom unit to the MeBo CORK-B (below left). Attachment of the lowered wire of the ship by a hook to the bottom unit for recovery from the seafloor (below right).

On its way to MeBoCORK B site, ROV *QUEST* could document mostly dead clams of genus *Calyptogena* and *Acharax*, which occurred as scattered open shells lying on the surface or as shell accumulations in some areas. In some cases living *Calyptogena* clams sticking out of the sea floor have been also seen. Further indications of sea floor seepage was indicated by dark gray patches which we interpreted as reduced sediments lifted to the surface by bioirrigation of the clams, by grabs eating the chemosynthetic clams or by other biological activities. Close to MeBoCORK B site a mega-clast was observed on the seafloor and the dropped bottom unit was found nearby. The following transportation of the bottom unit by ROV *QUEST* was hampered by mud suspension, which was released from the base plate of the MeBoCORK B unit. Because of the limited visibility this procedure took more than 1,5 hours before the OBE could be placed nearby the MeBo hole. After the water became clear ROV *QUEST* removed the cap from CORK-B and the hotstab connecting the CORK-B with the bottom unit was placed in its recepticle in the upper drill rod (Fig. 58, upper right). The connecting procedure was finished after the plug was rotated in the locking mechanism.

Documentation of the connected tools was performed by video footage and still images (Fig. 58, lower left).

During the further dive we searched for the second MeBo drill hole (MeBoPlug #1), which was reached just ca. 50 m northwest of former MeBo position. Close to the drill rod the MTL-stick (GeoB16767-4) was deployed into the sediment, so that the temperature sensor was placed some cm above the seafloor (Figs. 59 and 60).

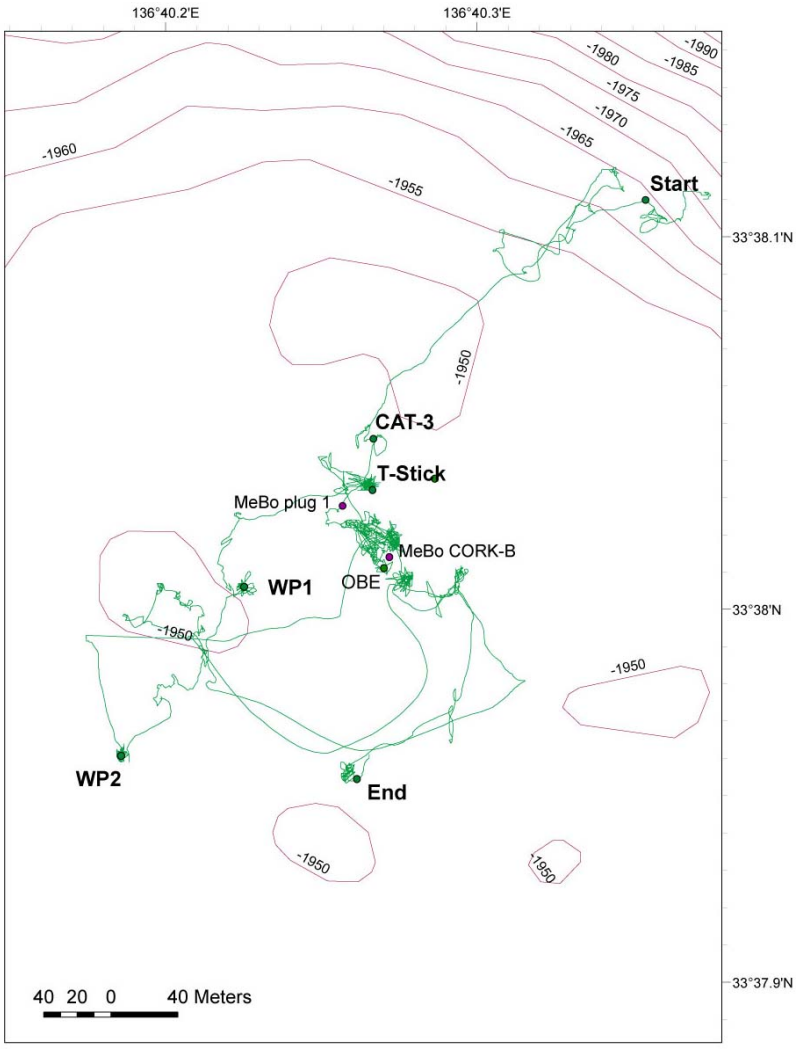

Figure 59: Track line of ROV Dive 321 on Kumano Basin mud volcano #3. WP1 – WP2 are marking T-stick measurements with sampling of two push cores.

WP1: T-stick-2 (GeoB 16767-6), push core 2 (GeoB 16767-7), and push core 15 (GeoB 16767-8).

WP2: T-stick-3 (GeoB 16767-9), push core 18 (GeoB 16767-10), and push core 30 (GeoB 16767-11).

OBE = MeBoCORK B bottom unit.

After a T-stick measurement (T-stick 1; GeoB16767) the location was left by moving the ROV to the southwest. The undulated sea bed morphology of the broad mud volcano summit did not allow a wider look over longer distances. This hilly structure is best documented in the image of the forward-looking sonar of the ROV (Fig. 60). Beside some exceptions mud volcanic ejecta like some clasts are not very often to see. After approximately 70 m survey close to sea floor the ROV landed in an area where no clams are seen. Two push cores (GeoB16767-7 and -8) were taken during the T-stick-2 (GeoB16767-6) measurement was performed. On the way with southwestern heading the ROV

stopped again after ca. 80 m distance. A final T-stick measurement (GeoB16767-9) was done and two addition push cores were sampled (GeoB16767-10 and -11).

During these dive activities data from MeBo CORK-B station were already downloaded by an acoustic modem and the data quality proved that not all functions of the bottom unit are working sufficiently. This lead to the plan to recover the bottom unit in order to check its performance during the remainder of the cruise and possibly deploy it again. After a detailed discussion with the master and the ship crew of RV *SONNE* a connecting wire with a hook system was launched with the heavy load by the wire of the ship and navigated close to the MeBoCORK B station. The ROV *QUEST* dove to the CORK again and disconnected the bottom unit from the MeBo rod and hooked the ship wire with the bottom unit of MeBoCORK B. After the ROV passed away the OBE was heaved from the sea floor and reached the deck at 13:27. The further plan to collect large clasts from the mud breccia was abandoned after the ROV encountered a hydraulic problem. Therefore the dive was finished after more than 11 hours sea floor operation. The ROV started to ascend at 13:28 UTC (Fig. 59).

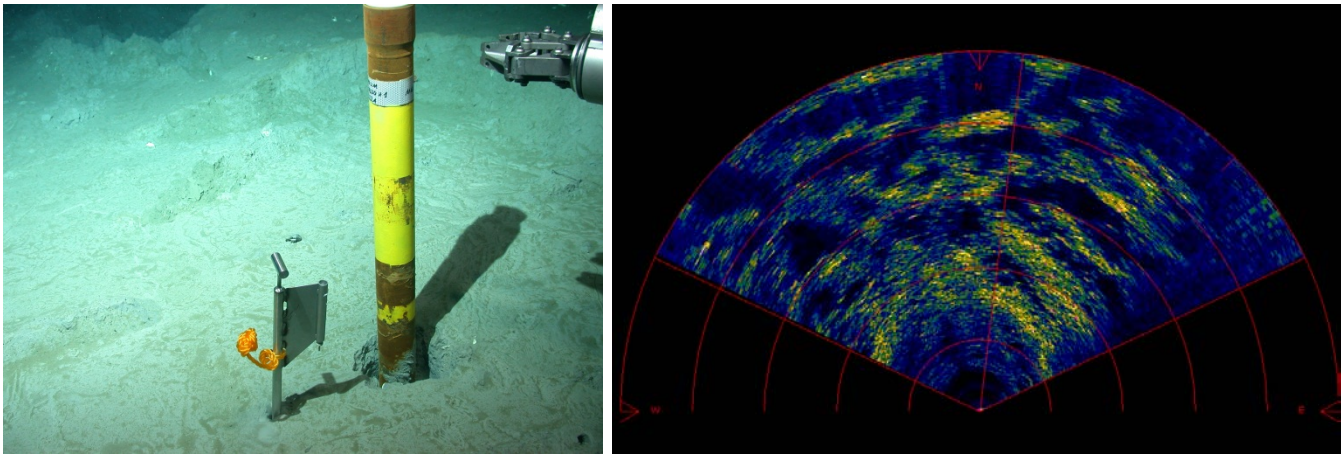

Figure 60: Deployment of MTL-stick close to MeBo Plug 1 (left). Screenshot of the forward-looking sonar Kongsberg DT MS1000 showing the hilly morphology in a sector up to 30 m from the ROV of the mud volcano close to MeBoPlug #1 (below right).

6.9. Observatories

(A. Kopf, S. Hammerschmidt, K. Kitada, T. Kimura, T. Fleischmann)

MeBoPlugs and MeBoCORKs

As already mentioned in sections 6.5 (MeBo deployments, Table 9) and 6.8 (ROV operations), a total of four observatories was set with MeBo, and in case of MeBoCORK B assisted by ROV. In general, operations were effortlessly carried out, in particular for MeBoPlug #1 and MeBoCORK A. Both systems were pre-installed on the uppermost, final drill rod, which was pushed down into the seafloor

so that only appx. 70-80 cm stuck out into the water column. Figure 61 illustrates how the situation looked like before MeBo took off.

When installing MeBoPlug #2 at station GeoB16728, we encountered some problems with drilling progress when hitting several indurated sand layers at appx. 17 mbsf (Table 9). Despite efforts to clean the hole with pressurised fluid, the string did not progress any deeper, so that the only option to install MeBoPlug #2 was to crew on the drill pipe with the MeBoPlug and leave it sticking out of the seafloor by appx. 2 – 2.5 meters. Despite this fragile pipe representing an obstacle, the MeBo take-off went well and the pipe was not bend or damaged.

Figure 61: MeBoPlug (left) and MeBoCORK B top hole assembly with black endcap (right) after installation with MeBo. Photos were taken iummediately before the seafloor drill rig takes off the ground. See text.

The majority of the other installations was also successful, e.g. for the autonomous CORK A (Fig. 55, right), the CORK B downhole assembly (Fig. 61, right), the bottom unit and hotstab (Fig. 58), or the MeBoPlugs, as sighted by TV-grab (see Fig. 60, left).

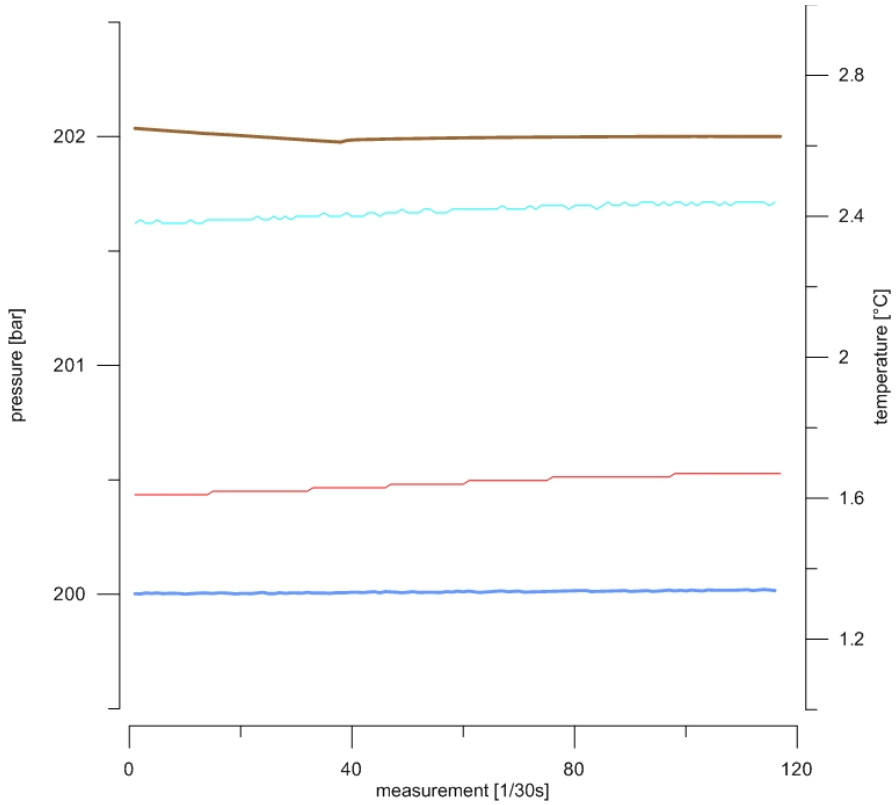

Figure 62: First data sets from MeBoCORK A as recovered by acoustic data transmission. Pressure curves are blue colours, T cirves are red/brown colours. Note the offset in borehole vs. reference pressure, which attests the successful deployment of the drop weight into the open hole.

The installation of MeBoCORK A at the crest of MV #4 represented no problems, and once the MeBo had taken off, we send an acoustic signal to unlatch the drop weight and lower the pore pressure tubing into the open bottom end of the otherwise cased drill hole. As can be seen from one of the first data sets downloaded from the CORK A via acoustic communication by develogic, the borehole pressure shows appx. 18 m higher pressure values than its seafloor counterpart (Fig. 62), which is in good agreement with the terminal depth of appx. 19 mbsf at this drill site.

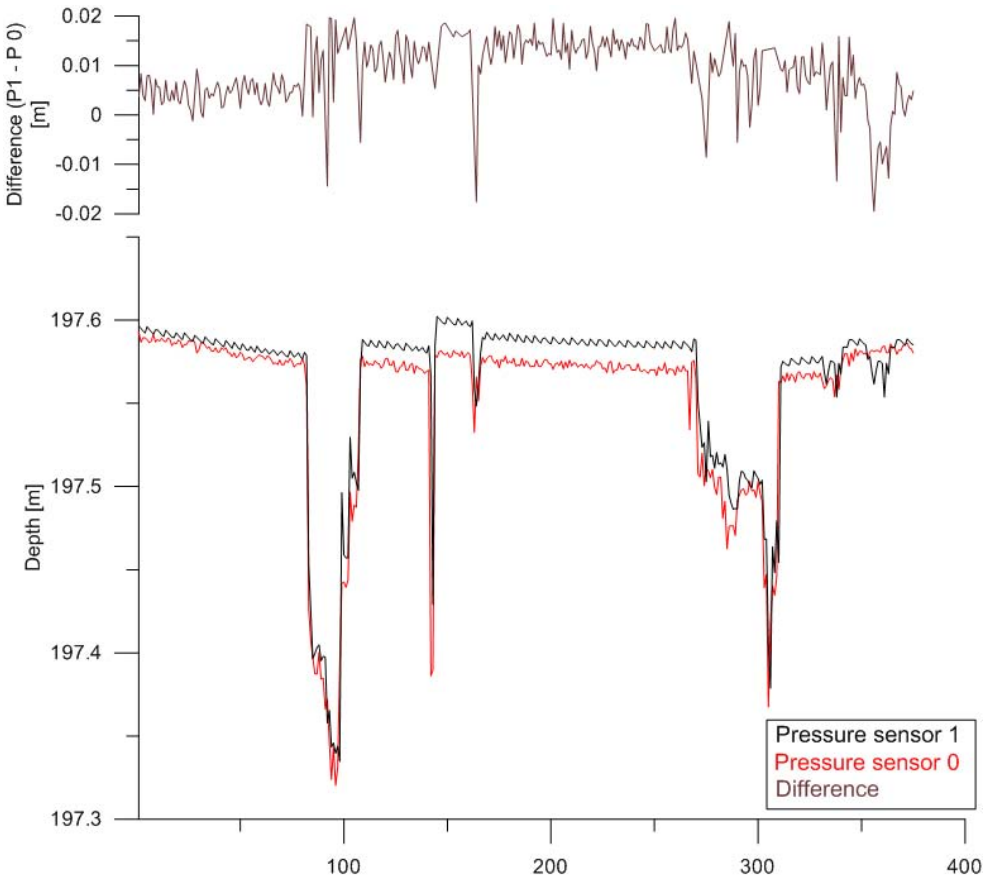

Figure 63: Data set covering the connection of MeBoCORK B with ROV *Quest*. For reasons to be explored, the borehole pressure is not any higher than the seafloor reference, suggesting a problem with the hotstab connection. Note that the vertical scale is in m * 10^{1} and that the horizontal unit is minutes.

At sites GeoB16711 (MeBo) / GeoB16767 (ROV), we had at first no problem untangling the hotstab of the seafloor unit of MeBoCORK B, take it to the MeBo drill rod, and plug the hotstab into its female counterpart (see section 6.8 above, and also Fig. 58, upper right/lower left). However, there was some uncertainty whether the tubing got caught and pinched during this operation, so that we unplugged the hotstab again and pushed it back in more safely a second time. The P records of seafloor reference and downward-looking (=borehole) P are shown in Figure 63. It can be seen that the differential pressures do not change much over the time of installation, which is unexpected given that the borehole is 33 mbsf and the drop weight should sit near TD of this hole. The only explanation for the P record measured is a leak somewhere inside the upper end of the female hotstab end of the drill string; all other sources of error, including the entire bottom unit, umbilical with tubes to hotstab and osmo-sampler, as well as the hotstab connector itself, are flawless.

SmartPlug piezometer

Given the unforeseen problems with the bottom unit of MeBoCORK B, and more so with the ROV "Quest 40m", we had no chance to re-install the bottom unit during leg SO222B. Instead, the

SmartPlug was redesigned to become a piezometer and was successfully installed by TV-grab at the crest of MV #4 (Station GeoB16789). Figure 64 shows the piezometer strapped to the TV-grab, with the releaser (white) right above it. The deployment was visually controlled via the camera system of the TV-grab sampler, and the release was activated once the piezometer was vertically stuck into the seabottom. When heaving the TV grab again, the SmartPlug instrument was sighted and it could be confirmed that the nstallation was successful. The instrument will remain in the seafloor for 2-3 years and is likely to be recovered by ROV during the same cruise necessary to recover the MeBoPlugs.

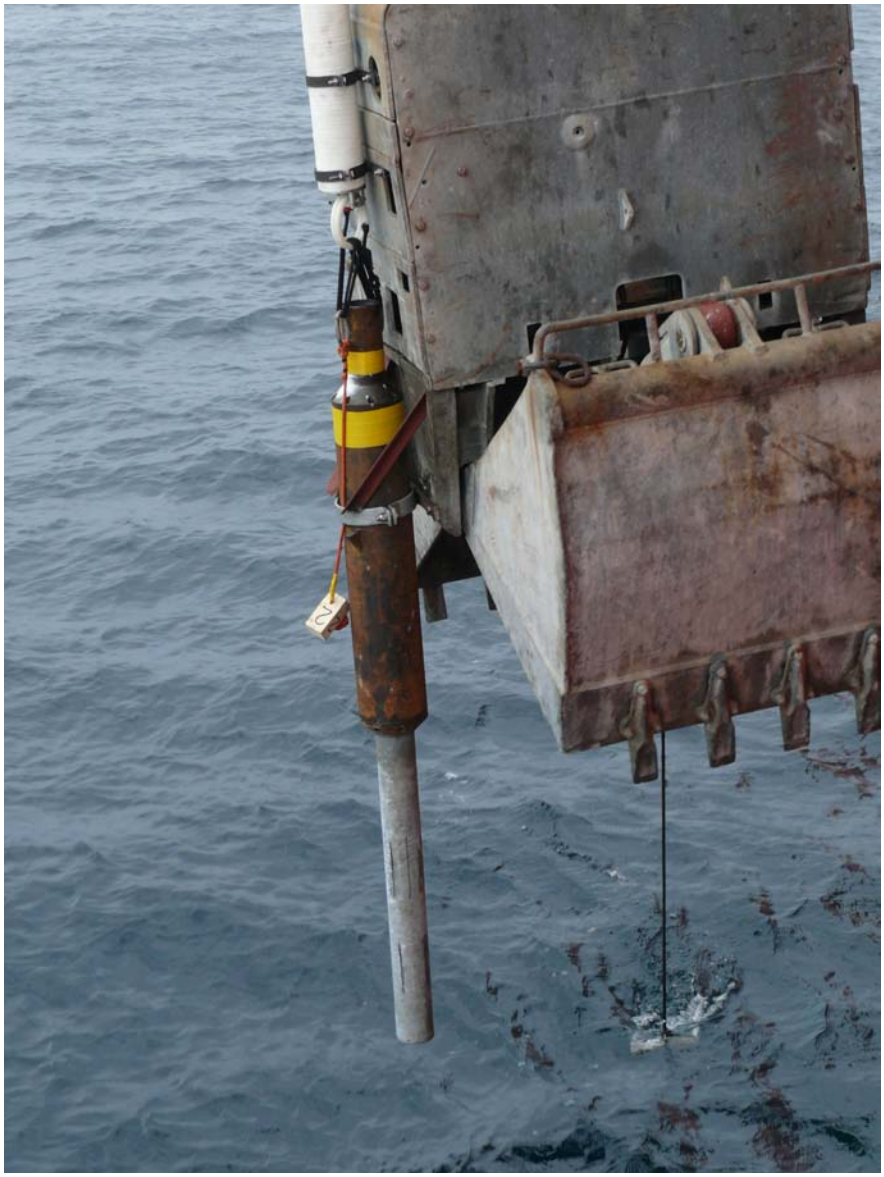

Figure 64: SmartPlug piezometer mounted to releaser and TV-grab when going overboard on MV#4.

6.10. TV grab

(T. Pape, A. Kopf, M.Tryon, A. Hüpers, J. Wei, G. Bohrmann, P. Geprägs, M. Belke-Brea)

During R/V *SONNE* cruise SO222, five TV-grab stations were performed (see Table 14) for different purposes. Four deployments have been used to survey and sample the sea floor for sediments and rocks. In additional, TVG-4 was used to deploy the SmartPlug piezometer (see section 6.9 observatories, and Fig. 64) on Mud Volcano KK #4.

Table 14: List of TV-grab stations.

Instr. No.	GeoB no.	Area	Date/UTC Time	Lat. / Long.	Depth (m)	Remarks
TVG 1	16713	MV #3	18 Jun - 06:17-08:28	33°38.048'N 136°40.228'E	1929	Sediment with large clast
TVG 2	16744	MV #10	28 Jun – 08:05-09:21	33°32.937'N 136°47.088'E	1854	No sample
TVG 3	16770	MV #2	9 Jul – 02:56-03:55	33°40.516'N 136°55.157'E	1965	No sample / stopped due to TVG problems
TVG 4	16789	MV #4	13 July – 08:13-08:15	33°39.384'N 136°38.043'E	1977	Deployment of SmartPlug
TVG 5	16793	MV #2	14 Jul - 11:10-12:30	33°40.542'N 136°55.279'E	2000	Seep sampled

TV-grab station GeoB 16713 on Mud volcano #3

Protocol: T. Pape
Scientists: A. Kopf, M. Tryon, A. Hüpers, J. Wei
Date: Monday, 18 June 2012
Start at the bottom: 06:11 UTC 33°38.019'N 136°40.251'E 1929 m water depth
Start ascend: 08:28 UTC 33°38.048'N 136°40.228'E 1930 m water depth
Total bottom time: 2 hours 17 minutes

Mud volcano KK #3 is around 1300 m in diameter and extends the sea floor nearly 100 m in height. The grab reached the sea floor in the northern center of the mud volcano and moved 50 m to the south and then approximately 100 m to east. The relative smooth seafloor and scattered mud clasts and dead clam shells were to see (Fig. 65, right). The density of the shells increased and MeBo Station GeoB16709 was seen and identified with the plug on top of the rod (MeBoPlug #1; see Fig. 65, left). Moving to the second Mebo station the topography became rougher. The TV-grab passed again the MeBoPlug #1 site. At 08:23 the grab was deployed over a large clast. The closing mechanisms of the

grab failed and a second attempt was necessary. The sample which come on deck contained many clasts which were stored for clasts analyses in the laboratory.

Figure 65: Frame grabs taken from the video of TV-grab-1 (GeoB16767-1). TV-grab passing MeBo station Plug 1 (left). Open clam shells from genus *Acharax* are lying on top of the sediment surface. Scale of weight lowered by the robe measures 20 cm in longitudinal axis.

TV-grab station GeoB16744 on Mud volcano #10

Protocol: T. Pape
Scientists: A. Kopf, M. Tryon, T. Pape, M. Lange
Date: Monday, 28 June 2012
Start at the bottom: 08:05 UTC 33°32.830'N 136°16.783'E 1846 m water depth
Start ascend: 09:21 UTC 33°32.937'N 136°47.088'E 1854 m water depth
Total bottom time: 1 hour 16 minutes

Mud volcano KK #10 has a diameter of 1100-1300 m is around 90 m in height. It was sampled by gravity cores and contained hydrate at least in core the catcher. The TV-grab started already on top of the volcano. No characteristic animals or clasts have been seen. After half an hour scattered clams were observed and later on large clasts have been found. On purpose was to check the Mebo drilling position on mud volcano 10. However, this goal was not reached. In the end the TV-grab was not deployed and was retrieved empty back to the ship's deck.

TV-grab station GeoB 16793 on Mud volcano #2

Protocol: Gerhard Bohrmann
Scientists: P. Geprägs, M. Belke-Brea
Date: Saturday, 14 July 2012
Start at the bottom: 11:10 UTC 33°40.567'N 136°55.420'E 2000 m water depth
Start ascend: 12:30 UTC 33°40.542'N 136°55.279'E 2000 m water depth
Total bottom time: 1 hour 20 minutes

Mud volcano #2 is around 700-800 m in diameter and extends the seafloor in 2010 m water depth only 10-15 m in height. Small differences in topography are not able to be recorded by the multibeam EM 120 of the ship, however, the mud volcano seems to have an undulated sea floor morphology including a more or less flat part in the center of the mud volcano. Several gravity cores taken during the cruise SO222 have shown that disseminated gas hydrates are present in the sediments of the mud volcano, which might be an indication for elevated fluid and gas discharge. Sampling an active seep site or an area containing visibly containing mud clasts were the goals of this TV-grab deployment.
We started the sea floor track of TVG in the eastern area of the mud volcano and moved slowly to the west using a heading of 270°. After 500 m we moved around 40 m to the south and then parallel to first track back to the east (Fig. 66). The first bottom sight showed a soft sediment covered sea floor with scattered single clam shells very few sea stars, seldom grabs, and other benthic animals which often could not be identified precisely enough.

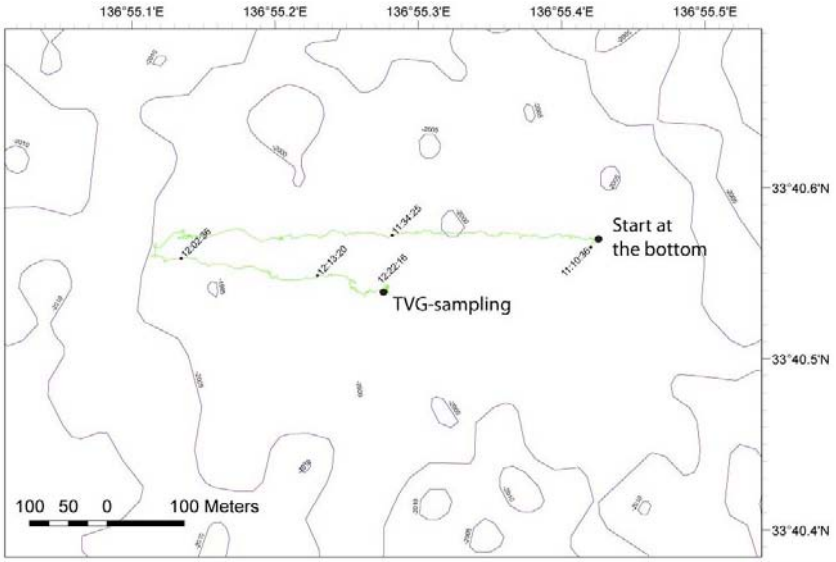

Figure 66: Track and sampling station of TVG-5 (GeoB16793) on the sea floor of mud volcano #2.

Only a few single clasts have been observed during the sea floor track. Coming to the center at around 11:34 we recognised more clams and traces of clam tracks (Fig. 67) as well as more fishes and often some small patches showing a lighter sediment color. On the southern track close to the same longitude the denser colonization by clams became more evident, and when we saw a dense field of *Calyptogena* clams (Fig. 67) at around 12:21 we deployed the grab directly into the clam field and closed the shovels. After the grab was retrieved to surface 2 tubes for pore water analyses were pushed from surface of the grab down into sediment. We collected mud clasts and the clam shells. Six *Calytogena* clams of around 12-15 cm length together with one *Acharax* clam (Fig. 68) were sampled

alive and were frozen in liquid nitrogen. More than 200 dead shells in many different sizes (Fig. 68) have been sampled from the TV-grab and were stored for detailed determination at home.

Figure 67: Frame grabs taken from the video of TV-grab-5 (GeoB16793). Traces on the sea floor caused by travelling clams outside of distinct seep sites (left). TV-grab view on a cold seep site, which is characterized by chemosynthetic clams. The field was sampled by the TV-grab just 15 seconds after this video image was taken. Scale of weight lowered by the robe measures 20 cm in longitudinal axis.

In addition to the clams, approximately 30 mud clasts, dark grey with diameters between 2-5 cm, were recovered from the grab as well. Similar to those in the earlier TVG-1 and from gravity and MeBo cores, the clast lithologies span over a wide range on grain sizes (mostly clay- and mudstones, but also fine sandstones) and different degrees of induration. The harder examples are most likely originating from the deeper portion of the Kumano basin sequence, or even the underlying accreted strata. Shore-based analyses including semi-quantitative XRD, illite crystallinity, and vitrinite reflectance.

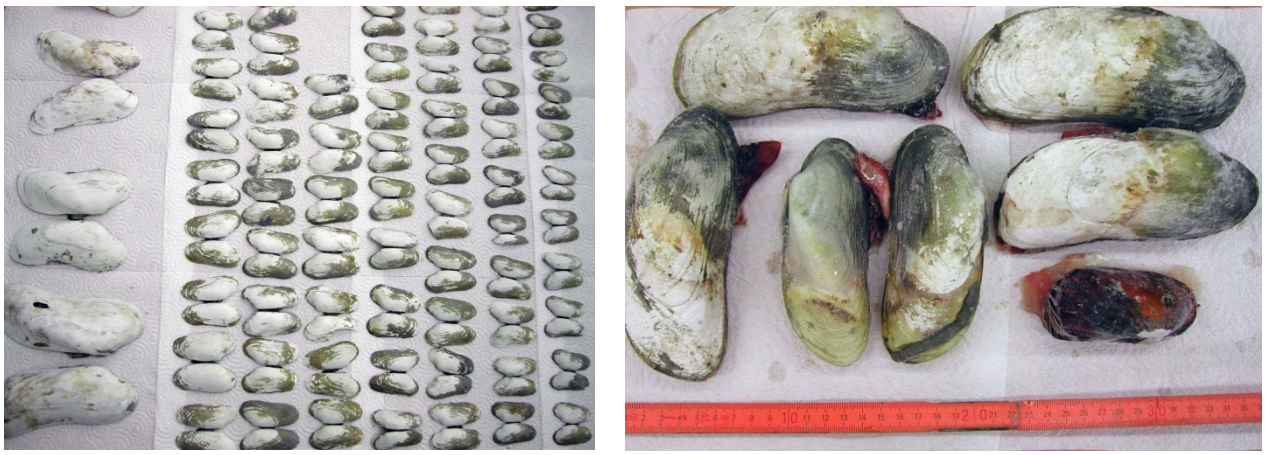

Figure 68: Clams recovered from the TVG-#5 (GeoB16793). Dead shells of *Calyptogena* (left); 6 *Calyptogena* clams and one *Acharax* have been alive (right).

7. References

Ando, M., 1975. Source mechanisms and tectonic significance of historical earthquakes along the Nankai Trough, Japan. *Tectonophysics*, 27: 119-140.

Ask, M., and Kopf, A., 2004. Rock mechanic characteristics of ODP Leg 186 claystones in the Japan Trench forearc, and their relationship to lithology, geologic structures, physical properties and seismicity. *Island Arc*, 13, 242-257.

Bebout, G.E., Ryan, J.G., Leeman, W.P., Bebout, A.E., 1999. Fractionation of trace elements by subduction zone metamorphism - effect on convergent margin thermal evolution. Earth Planet. Sci. Letts., 171: 63-81

Becker, K., Fisher, A.T., and Davis, E.E., 1997, The CORK experiment in hole 949C: Long-term observations of pressure and temperature in the Barbados accretionary prism, in T.H. Shipley et al., *Proc. ODP, Sci. Results*, 156: 247-252.

Becker, K., et al., 2004, Temperature and video logs from the upper oceanic crust, Holes 504B and 896A, Costa Rica rift flank: Implications for the permeability of upper oceanic crust, *Earth Planet. Sci. Lett.*, 222, 881-896.

Becker, K., and Davis, E.E., 2003, New evidence for age variation and scale effects of permeabilities of young oceanic crust from borehole thermal and pressure measurements, *Earth Planet. Sci. Lett.*, 201, 499-508.

Becker, K., and Davis, E.E., 2005. A review of CORK designs and operations during the Ocean Drilling Program. In Fisher, A. T., Urabe, T. , Klaus, A., and the Expedition 310 Scientists, Proc. IODP, 301: College Station TX)Integrated Ocean Drilling Program Management International, Inc.) doi:10.2204/iodp.proc.301.104.2005.

Bekins, B.A., and Screaton, E.J., in press, Pore Pressure and Fluid Flow in the Northern Barbados Accretionary Complex: A Synthesis, *in*: The Seismogenic Zone of Subduction Thrust Faults, edited by T. Dixon et al., Columbia University Press.

Behrmann JH, Lewis SD, Musgrave RJ, and Shipboard Scientific Party Leg 141 (1992) Proc. ODP, Init. Repts., 141, College Station, TX (Ocean Drilling Program): 709pp

Behrmann, J.H., Kopf, A., 1993. Textures and microfabrics in fine grained muds and mudstones from ODP Site 808, Nankai Accretionary Prism. Proc. ODP, Sci. Results, 131: 45-56.

Bennett, R.H., et al., 1985. In-Situ Undrained Shear Strengths and Permeabilities Derrived from Piezometer Measurements. In: Strength testing of Marine Sediments: Laboratory and In-Situ-Measurements. American Society for Testing and Materials ASTM STP 883, Philadelphia, 1985

Bjorlykke, K., Hoeg, K., 1997. Effects of burial diagenesis on stresses, compaction and fluid flow in sedimentary basins. *Mar. Petr. Geol*., 14/3: 267-276

Bredehoeft, J.D., 1967, Response of well-aquifer systems to Earth tides, *J. Geophys. Res.*, 72, 3075-3087.

Brenan, J.M., Shaw, H.F., Ryerson, F.J., Phinney, D.L., 1995. Mineral-aqueous fluid partitioning of trace elements at 900°C and 2 GPa: constraints on the trace element geochemistry of mantle and deep crustal fluids. *Geochim. Cosmochim. Acta*, 59: 3331-3350

Brown, K.M., et al., 2005, Correlated transient fluid pulsing and seismic tremor in the Costa Rica subduction zone, *Earth Planet. Sci. Lett.*, 238, 189-203.

Burrus, J., Bessis, F. and Doligez, B., 1987. Heat flow, subsidence and crustal structure of the Gulf of Lions (NW Mediterranean): a quantitative discussion of the classical passive margin model. In: Sedimentary Basins and Basin-Forming Mechanisms (C. Beaumont & A.J. Tankard, eds). *Mem. Can. Soc. Petrol. Geol.,* 12, 1–15.

Byerlee, J.D., 1978. Friction of rocks. *Pure and Applied Geophys.* 116, 615-626.

Chaumillon, E., Mascle, J., 1997. From foreland to forearc domains: new multichannel seismic reflection survey of th e Mediterranean Ridge accretionary complex (Eastern Mediterranean). Mar. Geology, 138: 237-259

Chronis, G., Lykousis, V., Anagnostus, C., Karageorgis, A., Stavrakakis, S., Poulus, S., 2000. Sedimentological processes in the southern margin of the Crete Sea (NE Mediterranean). Progress in Oceanography 46, 143-160

Cochrane, G., J.C. Moore, and H.J. Lee, 1996, Sediment pore-fluid overpressuring and its effect on deformation at the toe of the Cascadia accretionary prism from seismic velocities, in *Subduction top to bottom*, edited by G. Bebout, et al., Geophysical Monograph 96, American Geophysical Union: Washington, DC, United States, 57-64.

Cundall, P. A., Strack, O. D. L. 1979. A discrete numerical model for granular assemblies. *Géotechnique*,

29: 47-65

Dählmann, A., de Lange, G.J., 2003. Fluid-sediment interactions at Eastern Mediterranean mud volcanoes : a stable isotope study from ODP Leg 160. *Earth Planet. Sci. Letts.,* 212: 377-391.

Davis, E.E., and Becker, K., 1994, Formation temperatures and pressures in a sedimented rift hydrothermal system: Ten months of CORK observations, Holes 857D and 858G, in M.J. Mottl et al., *Proc. ODP, Init. Res.*, 139: 649-666.

Davis, E.E., and Becker, K., 2001, Using ODP boreholes for studying subseafloor hydrogeology: Results from the first decade of CORK observations, *Geosci. Can.*, 28, 171-178.

Davis, E.E., and Becker, K., 2002, Observations of natural-state fluid pressures and temperatures in young oceanic crust and inferences regarding hydrothermal circulation, *Earth Planet. Sci. Lett.*, 204, 231-248.

Davis, E.E., et al., 2001. An episode of seafloor spreading and associated plate deformation inferred from crustal fluid pressure transients, *J. Geophys Res.,* 106, 21953-21963.

Davis, E.E., et al., 2004, Hydrological response to a seafloor spreading episode on the Juan de Fuca ridge, *Nature*, 430: 335-338.

Davis, E.E., et al., 2006, A discrete episode of seismic and aseismic deformation of the Nankai Trough subduction zone accretionary prism and incoming Philippine Sea plate, *Earth Planet. Sci. Lett.*, 242, 73-84.

Davis, E.E. & Villinger, H.,2006. Transient formation fluid pressures and temperatures in the Costa Rica forearc prism and subducting oceanic basement: CORK monitoring at ODP Sites 1253 and 1255; *Earth Planet. Sci. Letters*, 245: 232–244.

Dayal, U., Allen, J.H., 1975. The effect of penetration rate on the strength of remolded clay and sand samples. Can. Geotech. J. 12:336–348.

Dewhurst, D.N., Yang, Y., Aplin, A., 1999. Permeability and fluid flow in natural mudstones. *Geol. Soc. London, Spec. Publ.* 158: 23-43

Deyhle, A., Kopf, A., 2001. Deep fluids and ancient pore waters at the backstop: Stable isotope systematics (C, B, O) of mud volcano deposits on the Mediterranean Ridge accretionary wedge. *Geology*, 29/11: 1031-1034.

Deyhle, A., Kopf, A., 2002. Strong B enrichment and anomalous $d^{11}B$ in pore fluids from the Japan Trench forearc. *Marine Geology* 183: 1-15.

Deyhle, A., Kopf, A., Aloisi, G., 2003. Boron and boron isotopes as a tracer for diagenetic reactions and depth of mobilization, using muds and authigenic carbonates from eastern Mediterranean mud volcanoes. In: Maltman, A.J., Van Rensbergen, P. & Hillis, R. (eds.) Subsurface sediment mobilisation. *Geol. Soc. London, Spec. Publications* 216, 493-505.

Deyhle, A., Kopf, A.J., 2005. The use and usefulness of boron isotopes in natural silicate-water systems. *Physics and Chemistry of the Earth*,30: 1038-1046.

Dia, A.N., Castrec-Rouelle, M., Boulègue, J., and Boudou, J.P., 1995. Major and trace elements and Sr isotope constraints on fluid circulations in the Barbados accretionary complex. Part 1: Fluid origin. *Earth Planet. Sci. Letts.*, 134: 69-85.

Dickens, G.R., Koelling, M., Smith, D.C., Schnieders, L., the IODP Expedition 302 Scientists, 2007. Rhizon Sampling of Pore Waters on Scientific Drilling Expeditions: An Example from the IODP Expedition 302, Arctic Coring Expedition (ACEX). Scientific Drilling 4, 22-25.

Elliot, T., Plank, T., Zindler, A., White, W., Bourdon, B.,1997. Element transport from slab to volcanic front at the Mariana arc. *J Geophys Res* 102: 14,991-15,019.

Emeis, K.-C., Robertson, A.H.F., Richter, C., Shipboard Scientific Party, 1996. Proc. ODP, Init. Repts., 160, College Station, TX (Ocean Drilling Program), 972pp.

Expedition 308 Scientists, 2005, Overpressure and fluid flow processes in the deepwater Gulf of Mexico: slope stability, seeps, and shallow-water flow, *IODP Prel. Rept.,* 308, doi:10:2204/iodp.pr.308.2005

Fisher, A.T., K. Becker, and E.E. Davis, 1997, The permeability of young oceanic crust east of the Juan de Fuca ridge, as determined using borehole thermal measurements, *Geophys. Res. Lett*., 24, 1311-1314.

Foucher, J.-P., Henry, P., and Harmegnies, F., 1997, Long-term observations of pressure and temperature in hole 948D, Barbados accretionary prism, *in* Shipley, T.H. et al. (eds.), Proc. ODP, Sci. Results, 156: 239-245.

Ge S., and E.J. Screaton, 2005, Modeling seismically induced deformation and fluid flow in the Nankai subduction zone, *Geophys. Res. Lett.*, 32, doi:10.1029/2005GL023473.

Gieskes, J.M., Gamo, T., Brumsack, H., 1991. Chemical methods for interstitial water analysis aboard Joides Resolution, ODP Technical Note, College Station, TX, p. 60.

Grevemeyer, I., Kopf, A.J., Fekete, N., Kaul, N., Villinger, H.W., Heesemann, M., Wallmann, K., Spiess, V., Gennerich, H.-H., Müller M., and Weinrebe, W., 2004. Fluid flow through active mud dome Mound

Culebra offshore Nicoya Peninsula, Costa Rica: evidence from heat flow surveying. *Marine Geology*, 207:145-157

Guangzhi, T., 1996. *Low-Temperature Geochemistry*. Bejing, China (Science Press), 216pp.

Hammerschmidt S, Davis EE, Kopf A (in press) Fluid Pressure and Temperature Transients Detected at the Nankai Trough Megasplay Fault: Results from the SmartPlug Borehole Observatory, Tectonophysics

Hayward N., G.K. Westbrook, and S.Peacock, 2003, Seismic velocity, anisotropy, and fluid pressure in the Barbados accretionary wedge from an offset vertical seismic profile with seabed sources, *J. Geophys. Res*., 108, doi:10.1029/2001JB001638.

Hedberg, H., 1974. Relation of methane generation to undercompacted shales, shale diapirs and mud volcanoes. *AAPG Bull*., 58: 661-673

Heesemann, M., Villinger, H., Jannasch, H.W., Kastner, M. & 301T scientists, 2006. Long-term temperature measurements in holes 1253A and 1255A off Costa Rica, ODP Leg 205. In: Morris, Villinger, H.W., Klaus, A., et al., *Proc. ODP, Sci. Results.*, 205: College Station, TX (Ocean Drilling Program).

Henry, P., Le Pichon, X., Lallemant, S., Lance, S., Martin, J., Foucher, J.-P., Fiala-Medioni, A., Rostek, F., Guilhaumou, N., Pranal, V., Castrec, M., 1996. Fluid flow in and around a mud volcano field seaward of the Barbados accretionary wedge: results of the Manon cruise. Journal of Geophysical Research 101, 20297-20323.

Higgins, G.E., Saunders, J.B., 1974. Mud volcanoes – Their nature and origin. *Verhandlungen der Naturforschenden Gesellschaft Basel*, 84: 101–152

Hüpers, A., A. Kopf, 2009. The thermal influence on the consolidation state of underthrust sediments from the Nankai margin and its implications for excess pore pressure, *Earth Planet. Sci. Letts.* 286: 324-332.

Hüpers, A., S. Kreiter, A. Kopf, The role of temperature on pre-consolidation stress determination for the projected sedimentary underthrust sequence at the Nankai margin *Marine Petroleum Geology* 27 (7), 1565-1571, doi:10.1016/j.marpetgeo.2010.03.014.

Hüpers, A., Bach, W., Zabel, M., A. Kopf, in press. Effects of experimental hydrothermal consolidation on pore water chemistry: implications for the alteration of underthrust sediments. *Geochimica Cosmochimica Acta*

Husen, S., Kissling, E., 2001, Postseismic fluid low after the large subduction earthquake ofAntofagasta, Chile. *Geology,* 29, 847-850.

Hubbert, M., Rubey, W.W., 1959. Role of fluid pressure in mechanisms of overthrust faulting: I. Mechanics of fluid-filled porous solids and its application overthrust faulting. *GSA Bull*., 70: 115-160

Ichinose, G., et al., 2003, Rupture process of the 1944 Tonankai earthquake (Ms 8.1) from the inversion of teleseismic and regional seismograms, *J. Geophys. Res.*, 108, doi:10.1029/2003JB002393.

Inagaki, F., and cruis eparticipants, 2009. CK09-01 *Chikyu* training cruise Leg. 1 - Kumano Mud-Volcano Drilling: A Window to the Deep-Biosphere. Unpubl. JAMSTEC Report, 29pp.

IODP, 2001, Earth, oceans and life, Integrated Ocean Drilling Program Initial Science Plan: IWG, Washington, 110 p.

Ito, Y., and Obara, K., 2006, Dynamic deformation of the accretionary prism excites very low frequency earthquakes, *Geophys. Res. Lett.*, 33, doi:10.1029/2005GL025270.

Jannasch, H.W., et al., 2003, CORK-II: Long-term monitoring of fluid chemistry, fluxes, and hydrology in instrumented boreholes at the Costa Rica subduction zone, *in* Morris, J.D., Villinger, H.W., Klaus, A., et al., *Proc. ODP, Init. Repts.*, 205: College Station, TX (Ocean Drilling Program).

Johnson, M.C., Plank, T., 1999. Dehydration and melting experiments constrain the fate of subducted sediments. *Geochemistry, Geophysics, Geosystems - G* ^{3} 1:paper1999GC000014

Karig, D.E., 1993. Reconsolidation tests and sonic velocity measurements of clay-rich sediments from the Nankai Trough. In: Hill et al., *Proc. ODP, Sci. Res.* 131: 247-260.

Kastner, M., et al., 2005, Continuous Chemical and Fluid Flux Monitoring in Two Distinct Fluid Flow Systems at the Costa Rica Subduction Zone, *Eos Trans. AGU, 86*(52), Fall Meet. Suppl.

Kastner M., K. Becker, E. E. Davis, A. T. Fisher, H. W. Jannasch, E. A. Solomon, C. G.Wheat, 2006. New Insights Into the Hydrogeology of the Ocean Crust through Long-Term Monitoring, *Oceanography*, 19 (4), 30-42.

Kinoshita, M., Tobin, H., Ashi, J., Kimura, G., Lallement, S., Screaton, E.J., Curewitz, D., Masago, H., Moe, K.T., and the Expedition 314/315/316 Scientists, 2009. *Proc. IODP,* 314/315/316: Washington, DC (Integrated Ocean Drilling Program Management International, Inc.). doi:10.2204/iodp.proc.314315316.2009

Kikuchi, M., M. Nakamura, and K. Yoshikawa, 2003. Source rupture processes of the 1944 Tonankai earthquake and the 1945 Mikawa earthquake derived from low-gain seismograms, *Earth, Planets & Space*, 55: 159-172.

Kopf, A., Robertson, A.H.F., Clennell, M.B., and Flecker, R., 1998. Mechanisms of mud extrusion on the Mediterranean Ridge Accretionary Prism. Geo-Marine Letters, 18: 97-114.

Kopf, A., Klaeschen, D., and Mascle, J., 2001. Extreme efficiency of mud volcanism in dewatering accretionary prisms. *Earth Planet. Sci. Letters*, 189/3-4: 295-313.

Kopf, A.J., 2002. Significance of mud volcanism. *Reviews of Geophysics*, 40/2, 52pp. [DOI 10.1029/2000RG000093]

Kopf, A.J., and Deyhle, A., 2002. Back to the roots: Source depths of mud volcanoes and diapirs using boron and B isotopes. Chem. Geology, 192: 195-210.

Kopf, A., and Brown, K.M., 2003. The stress state of the Nankai and Barbados subduction thrusts. *Marine Geology* 202: 193-210.

Kopf, A., Delisle, G., Faber, E., Panahi, B., Aliyev, C.S., Guliyev, I., 2010. Long-term *in situ* monitoring at Dashgil mud volcano, Azerbaijan: A link between seismicity, pore pressure transients and methane emission. *Int. J. Earth Sciences*, 99, Supplement 1, 227-240, DOI: 10.1007/s00531-009-0487-4

Kopf, A., Araki, E., Toczko, S. et al., 2011. NanTroSEIZE Stage 2: Riserless Observatory - 2. IODP Prel. Rept., 332. doi:10.xxxx/iodp.pr.332.2011

Kopf, A., Bartsch, C., Castellino, J., Fleischmann, T., Haas, S., Ioakim, C., Kirsch, K., Kufner, S.K., Tryon, M.D., Wiemer, G., 2011 (in prep.). REPORT AND PRELIMINARY RESULTS OF POSEIDON CRUISE P410: MudFlow (Mud volcanoes and fluid flow in the Mediterranean Ridge Accretionary Complex), *Berichte aus dem Fachbereich Geowissenschaften der Univ. Bremen*, No.

Lallemand S.E., Schnurle P., Malavieille J., 1994. Coulomb theory applied to accretinary and non-accretionarywedges - possible causes for tectonic erosion and/or frontal accretion. *J. Geophys. Res*., 99: 12033-12055

Lavrushin, V.U., Polyak, B.G., Prasolov, R.M., Kamenskii, I.L., 1996. Sources of material in mud volcano products (based on isotopic, hydrochemical, and geological data). *Lithology Min. Resources,* 31/6: 557-578Mellors R., Kilb D., Aliyev, A., Gasamov A., Yetirmishli, G., 2007. Correlations between Earthquakes and Large Mud Volcano Eruptions. *J Geophys Res*, 112, B04304, doi:10.1029/2006JB004489

Lunne, T., Robertson, P.K., Powell, J.J.M., 1997. Cone penetration testing in geotechnical practice. Spon Press, London.

Lunne, T., 2010. The CPT in offshore soil investigations – a historic perspective. In: Mitchell et al (eds) CPT'10, Huntington Beach, California.

Mazzullo, J.M., Meyer, A., and Kidd, R.B., 1988. New sediment classification scheme for the Ocean Drilling Program. *In* Mazzullo, J.M., and Graham, A.G. (Eds.), *Handbook for shipboard sedimentologists.* ODP Tech. Note, 8:45–67. doi:10.2973/odp.tn.8.1988.

Mitchell, J.K., 1976. Fundamentals of Soil Behavior. Wiley New York.

Miyazaki, S., and Heki, K., 2001, Crustal velocity field of southwest Japan: Subduction and arc-arc-collision, *J. Geophys. Res*., 106, 4305-4326.

Moore, G.F., Park, J.-O., Bangs, N.L., Gulick, S.P., Tobin, H.J., Nakamura, Y., Sato, S., Tsuji, T., Yoro, T., Tanaka, H., Uraki, S., Kido, Y., Sanada, Y., Kuramoto, S., and Taira, A., 2009. Structural and seismic stratigraphic framework of the NanTroSEIZE Stage 1 transect. *In* Kinoshita, M., Tobin, H., Ashi, J., Kimura, G., Lallemant, S., Screaton, E.J., Curewitz, D., Masago, H., Moe, K.T., and the Expedition 314/315/316 Scientists, *Proc. IODP,* 314/315/316: Washington, DC (Integrated Ocean Drilling Program Management International, Inc.). doi:10.2204/iodp.proc.314315316.102.2009

Moore, J.C., Saffer, D., 2001. Updip limit of the seismogenic zone beneath the accretionary prism of southwest Japan: An effect of diagenetic to low-grade metamorphic processes and increasing effective stress. *Geology*, 29: 183-186

Morgan, J.K., and M.V.S. Ask , 2004, Consolidation state and strength of underthrust sediment and evolution of the décollement at the Nankai accretionary margin: Results of uniaxial reconsolidation experiments, *Jour. Geophys. Res*. *109*, B03102, doi:10.1029/2002JB002335.

Morris J.D., Leeman W.P., Tera F.,1990. The subducted component in island arc lavas: Constraints from Be isotopes and B-Be systematics. Nature 344: 31-36.

Munsell Color Company, Inc., 1991. *Munsell Rock Color Charts:* Baltimore, MD (Munsell).

Obara, K., et al., 2004, Episodic slow slip events accompanied by non-volcanic tremors in southwest Japan subduction zone, *Geophys. Res. Lett.*, 31, doi:10.1029/2004GL020848.

Obara, K., and Ito, Y., 2005, Very low frequency earthquakes excited by the 2004 off the Kii peninsula earthquakes: A dynamic deformation process in the large accretionary prism, *Earth Planets & Space*, 57, 321-326.

Ogawa, Y., Miyata, Y., 1985. Vein structure and its deformational history in the sedimentary rocks of the Middle America Trench slope off Guatemala, Deep Sea Drilling Project Leg 84. *DSDP Init. Rept*., 84: 811-829

Orcutt, B., Wheat C.G., Edwards K.J., 2010. Subseafloor ocean crust microbial observatories: development of FLOCS (FLow-through Osmo Colonization System) and evaluation of borehole construction materials. Geomicrobiol J 27: 143–157.

Plank, T., Langmuir, C.H., 1998. The chemical composition of subducting sediment and its consequences for the crust and mantle. *Chem. Geol.* 145: 325-394.

Rice, J. R., 1992, Fault stress states, pore pressure distributions, and the weakness of the San Andreas fault, *in* Fault Mechanics and Transport Properties of Rocks, B. Evans, T. F. Wong (eds.), pp. 475-503, Academic, San Diego, CA.

Robertson, P.K., 2009. Interpretation of cone penetration tests - a unified approach. Can Geotech J 46: 1337-1355.

Roeloffs, E.A., 1996, Poroelastic techniques in the study of earthquake-related hydrologic phenomena, *Adv. Geophys*., 37, 135-195.

Rogers, G. & Dragert, H., 2003. Episodic tremor and slip on the Cascadia subduction zone: the chatter of silent slip, *Science*, 300, 1942-1945.

Rothwell, R.G. 1989. *Minerals and Mineraloids in Marine Sediments: an Optical Identification Guide*. London: Elsevier.

Saffer, D.M., E.A. Silver, A.T. Fisher, H. Tobin, and K. Moran, 2000, Inferred pore pressures at the Costa Rica subduction zone: Implications for dewatering processes, *Earth Planet. Sci. Lett*., *177*, 193-207.

Saffer, D.M., and Bekins, B.A., 2002, Hydrologic controls on the mechanics and morphology of accretionary wedges and thrust belts*, Geology, 30*, 271-274.

Saffer, D.M., 2003, Pore pressure development and progressive dewatering in underthrust sediments at the Costa Rican subduction margin: Comparison with Northern Barbados and Nankai*, J. Geophys. Res*., 108 (B5), 2261, doi: 10.1029/2002JB001787.

Saffer, D.M., and McKiernan, A.W., 2005, Permeability of underthrust sediments at the Costa Rican margin: Scale dependence and implications for dewatering, *Geophys. Res. Lett., 32,* doi:10.1029/2004GL021388.

Saffer, D.M., Araki, E., Byrne, T., McNeill, L., Eguchi, N., Moe, K.T., Toczko, S. and the Expedition 319 Scientists, 2010. Proc. IODP, Initial Reports 319: Washington, DC (Integrated Ocean Drilling Program Management International, Inc.).

Sakai, H., Gamo, T., Ogawa, Y., Boulegue, J., 1992. Stable isotopic ratios and origins of the carbonates associated with cold seepage at the eastern Nankai Trough. *Earth Planet. Sci. Lett.*, 109: 391–404

Screaton, E.J., D.M. Saffer, P. Henry, S. Hunze, and Leg 190 Shipboard Scientific Party, 2002,Porosity loss within underthrust sediments of the Nankai accretionary complex: Implicationsfor overpressures, *Geology,* 30, p. 19-22.

Screaton, E.J., et al., 2005, Numerical Modeling of Steady State Pore Pressures and CoseismicPressure Changes at the Nankai Margin off the Kii Peninsula, Japan, *Eos Trans. AGU, 86*(52),Fall Meet. Suppl.

Screaton, E.J., D.R. Wuthritch, S.J. Dreiss, 1990, Permeabilities, fluid pressures, and flowrates in the Barbados ridge complex, *J. Geophys. Res., 95*, 8997-9007.

Seeberg-Elverfeldt, J., Schluter, M., Feseker, T., Kolling, M., 2005. Rhizon sampling of porewaters near the sediment-water interface of aquatic systems. Limnology and Oceanography: Methods 3, 361-371.

Shepard, F.P., 1954. Nomenclature based on sand-silt-clay ratios, Journal of Sedimentary Research, September 1954, v. 24, pp. 151-158,

Shipboard Scientific Party, 2002. Leg 195 summary. *In* Salisbury, M.H., Shinohara, M., Richter, C., et al., *Proc. ODP, Init. Repts.,* 195: College Station, TX (Ocean Drilling Program), 1–63. doi:10.2973/odp.proc.ir.195.101.2002

Stegmann, S., Moerz, T., Kopf, A., 2006. Initial Results of a new Free Fall-Cone Penetrometer (FF-CPT) for geotechnical *in situ* characterisation of soft marine sediments. *Norwegian Journal of Geology*, 86/3: 199-208.

Stegmann, S., Strasser, M., Anselmetti, F.S., Kopf, A., 2007. Geotechnical *in situ* characterisation of subaquatic slopes: The role of pore pressure transients versus frictional strength in landslide initiation. *Geophysical Research Letts.*, 34/7, doi:10.1029/2006GL029122.

Stegmann, S., Kopf, A., 2007. Marine deep-water Free-fall CPT measurements for landslide characterisation off Crete, Greece (Eastern Mediterranean Sea). Part 1: A new 4000 m cone penetrometer. Lykousis, V., Sakellariou, D., Locat, J. (eds.), Submarine Mass movements and their consequences. Advances in Natural and Technological Hazards Series, Springer, 171-177.

Steiner, A., L'Heureux, J.S., Kopf, A., Vanneste, M., Longva, O., Lange, M., Haflidason, H., 2012. An in-situ free-fall piezocone penetrometer for characterizing soft and sensitive clays at Finneidfjord, northern Norway. In: Yamada Y et al (eds) Submarine mass movements and their consequences, vol. 31, Advances in natural and technological hazards research. Springer, Dordrecht, 99–109.

Strasser, M., Moore, G.F., Kimura, G., Kitamura, Y., Kopf, A.J., Lallemant, S., Park, J.O., Screaton, E.J., Su, X., Underwood, M.B., Zhao, X., 2009. Origin and evolution of a tsunamigenic splay fault. *Nature Geosciences* 2 (9): 648-652.

Tanioka, Y., Satake, K., 2001, Detailed coseismic slip distribution of the 1944 Tonankai earthquake estimated from tsunami waveforms, *Geophys. Res. Lett.*, 28, 1075-1078.

Tobin, H., Kinoshita, M., 2007. The IODP Nankai Trough Seismogenic Zone Experiment. *Scientific Drilling*, Spec. issue 1: 39-41

Tobin, H.J., Kinoshita, M., Ashi, J., Lallemant, S., G. Kimura, Screaton, E., Moe, K.Y., Masago, H., D. Curewitz, and the Expedition 314/315/316 Scientists, 2009. NanTroSEIZE Stage 1 Expeditions 314, 315 and 316: First drilling program of the Nankai Trough Seismogenic Zone Experiment offshore the Kii Peninsula, Japan. *Scientific Drilling*, 8: 4-17.

Trehu, A., P. Long, M. Torres, G. Bohrmann, and Leg 204 Scientific Party (2004), Three-dimensional distribution of gas hydrate beneath southern Hydrate Ridge: Constraints from ODP Leg 204, Earth Planet. Sci. Lett., 222, 845– 862.

Tryon, M.D., Brown, K.M., Dorman, L., Sauter, A., 2001. A new benthic aqueous flux meter for very low to moderate discharge rates. *Deep Sea Research* Pt. I, 48: 2121-2146

Tryon, M.D., K.M. Brown, M. Torres 2002. Fluid and chemical flux in and out of sediments hosting methane hydrate deposits on Hydrate Ridge, OR, II: Hydrological processes, *Earth Planet. Sci. Lett.,* 201(3-4), 541-557.

Tryon, M.D. 2009. Monitoring aseismic tectonic processes via hydrologic responses: An analysis of log-periodic fluid flow events at the Costa Rica outer rise, *Geology*, 37(2), 163-166.

Tryon, M.D., Wheat, C.G., Hilton, D.R., 2010. Fluid sources and pathways of the Costa Rica erosional convergent margin. *Geology, Geophysics, and Geosystems (G-Cubed)*, doi:10.1029/2009GC002818

Underwood, M.B. (ed.), 1993. Thermal Evolution of the Tertiary Shimanto Belt, Southwest Japan: An Example of Ridge-Trench Interaction. GSA Special Paper, 273: 172 pp.

Verma, S.P., Pandarinath, K., Santoyo, E., 2008. SolGeo: A new computer program for solute geothermometers and its application to Mexican geothermal fields. Geothermics 37, 597-621.

Villinger, H., Davis, E. E., 1987. A new reduction algorithm for marine heat flow measurements, Journal of Geophysical Research, 92 (B12), 846-856.

Vrolijk, P., Miller, T., and Gooch, M.J., 1998, Hydrostatic consolidation tests of undeformed, clay-rich samples from the Barbados accretionary prism, Leg 156, *in:* Moore, J.C., Klaus, A., et al. (eds.), Proc. ODP., Init. Repts., 171A: 107-116.

Wang, K., and Davis, E.E., 1996, Theory for the propagation of tidally induced pore pressure variations in layered subseafloor formations, *J. Geophys. Res.*, 101, 11483-11495

Wentworth, C.K., 1922. A Scale of Grade and Class Terms for Clastic Sediments, The Journal of Geology , Vol. 30, No. 5 (Jul. - Aug., 1922), pp. 377-392

Wheat CG, Jannasch HW, Kastner M, Hulme S, Cowen J, Edwards K, Orcutt BN, Glazer B (2010) Fluid Sampling from Oceanic Borehole Observatories: Design and Methods for CORK Activities (1990-2010). ODP Proc 327

You, C.-F., Spivack, A.J., Smith, J.H. & Gieskes, J.M., 1993. Mobilization of boron at convergent magins: Implications for boron geochemical cycle. *Geology*, 21: 207-210

You, C.-F., Castillo, P.R., Gieskes, J.M., Chan, L.H., Spivack, A.J., 1996. Trace element behavior in hydrothermal experiments: Implications for fluid processes at shallow depths in subduction zones. *Earth Planet. Sci. Letts*., 140, 41-52

You, C.F., Gieskes, J., 2001. Hydrothermal alteration of hemi-pelagic sediments: experimental evaluation of geochemical processes in shallow subduction zones. Applied Geochemistry 16, 1055-1066.

Zervas, D., Nichols, G.J., Hall, R., Smyth, H.R. , Lüthje, C. and Murtagh, F., 2009. SedLog: a shareware program for drawing graphic logs and log data manipulation, Computers & Geosciences, 35, 2151-2159.

8. Acknowledgements

We thank Master Oliver Meyer and his officers on the bridge for their cooperation, and outstanding support during complex operations, in particular with MeBo and ROV *Quest*. Special thanks go also to entire crew of R/V *Sonne* for their friendly support and efficient technical assistance with the various devices used.

The cruise in Japanese waters, and in particular in close proximity to seafloor cables such as DONET and other communication lines, would not have been possible with the diplomatic skills and generous support of Fumoi Inagaki. Cooperation by other colleagues in Japan as well as the various governmental organisations providing permissions is also acknowledged.

We thank ORI and JAMSTEC for sending experts to participate into the cruise, and also providing survey data and unpublished information that helped preparation of cruise SO222. We are particularly indebted to Fumio Inagaki, who hosted German colleagues on a parallel expedition using D/V *Chikyu* to mud volcano #5.

Partners at MARUM Bremen (Goetz Ruhland, Volker Diekamp) have also provided crucial help with expedition planning, logistical decisions, and post-cruise demobilisation. Additionally, Klaus Bohn is thanked for his repeated professional logistical assistance.

Thanks go also to the German Ministry for Research and Education (BMBF) and German Science Foundation (DFG) for providing the funds to realise cruise SO222 with large seagoing gear and costly long-term monitoring technology.

9. Appendices

9.1. Station list

9.2. Lithologs and shear strength data

9.3. Core photographs and MSCL

9.4. Weekly reports to PtJ / BMBF (in German)

9.1 Station list

GeoB station	Campaign	Area	Device	Date	Time	Latitude	Longitude
GeoB16701-1	SO 222 A		CTD	14.06.12	07:32	33°38.309	136°30.699
GeoB16701-2	SO 222 A		Calibration	14.06.12	09:40	33°38.5	136°30.39
GeoB16702-1	SO 222 A	MV#3 and MV#5	Parasound	14.06.12	12:58	33°38.28	136°30.68
GeoB16703-1	SO 222 A	MV#3 crest	GC 6 m	14.06.12	21:14	33°37.9900	136°40.2187
GeoB16303-2	SO 222 A	MV#3	Calibration	14.06.12	23:06	33°37.968	136°40.249
GeoB16704-1	SO 222 A	MV#3 N-E base wedge	GC 6 m	15.06.12	04:47	33°38.225	136°40.469
GeoB16705-1	SO 222 A	MV#3	HF	15.06.12	07:37	33°37.836	136°39.876
GeoB16706-1	SO 222 A	MV #6, MV #8 and MV #9	Parasound	15.06.12	15:24	33°36.95	136°38.96
GeoB16707-1	SO 222 A	MV #8 crest	GC 6 m	15.06.12	21:57	33°36.272	136°33.363
GeoB16708-1	SO 222 A	Japan Kumano Basin	GC 6 m	16.06.12	00:42	33°37.989	136°33.439
GeoB16709-1	SO 222 A	MV #3	MeBo	16.07.12	04:06	33°38.039	136°40.244
GeoB16710-1	SO 222 A	MV #3 MeBo Location	CPT	17.06.12	05:30	33°38.09	136°40.244
GeoB16710-2	SO 222 A	MV #3 MeBo Location	CPT	17.06.12	07:18	33°37.948	136°40.151
GeoB16710-3	SO 222 A	MV #3 MeBo Location	CPT	17.06.12	07:54	33°37.850	136°40.063
GeoB16710-4	SO 222 A	MV #3 MeBo Location	CPT	17.06.12	08:41	33°37.855	136°39.968
GeoB16711-1	SO 222 A	MV #3	MeBo	17.06.12	10:50	33°38.03	136°40.28
GeoB16712-1	SO 222 A	MV #3 crest	GC 6 m	18.06.12	05:09	33°38.039	136°40.244
GeoB16713-1	SO 222 A	MV #3 crest	TV-grab	18.06.12	15:41	33°38.039	136°40.244
GeoB16714-1	SO 222 A		Parasound	18.06.12	11:09	33°35.697	136°38.374
GeoB16715-1	SO 222 A	MV #10	Parasound	20.06.12	22:10	33°48.00	136°40.00
GeoB16716-1	SO 222 A	MV #10 crest	GC 6 m	21.06.12	02:07	33°32.824	136°16.880
GeoB16716-2	SO 222 A	MV #10 crest	GC 6 m	21.06.12	04:06	33°32.824	136°16.880
GeoB16717-1	SO 222 A		GC 6 m	21.06.12	06:02	33°32.90	136°16.96
GeoB16718-1	SO 222 A	KK #10	HF	21.06.12	08:00	33°32.606	136°17.015
GeoB16719-1	SO 222 A		Parasound	21.06.12	14:30	33°33.01	136°17.06
GeoB16720-1	SO 222 A	MV #8	GC 6 m	22.06.12	07:20	33°36.144	136°33.453
GeoB16721-1	SO 222 A	MV #9	GC 6 m	22.06.12	09:25	33°37.926	136°33.519
GeoB16722-1	SO 222 A	MV #4	GC 6 m	22.06.12	11:47	33°39.374	136°38.011
GeoB16722-2	SO 222 A	MV #4	GC 6 m	22.06.12	13:30	33°39.428	136°37.988
GeoB16723-5	SO 222 A	MV #4 N-flank	GC 6 m	22.06.12	15:35	33°39.503	136°38.017
GeoB16724-1	SO 222 A	MV #4	HF	22.06.12	17:40	33°39.538	136°38.016
GeoB16725-1	SO 222 A	MV #4	GC 6 m	23.06.12	00:00	33°39.328	136°38.051
GeoB16726-8	SO 222 A	MV #4 N-flank	GC 6 m	23.06.12	01:58	33°39.538	136°38.033
GeoB16727-1	SO 222 A	MV #4 ridge	GC 6 m	23.06.12	04:05	33°40.212	136°38.584
GeoB16728-1	SO 222 A	MV #4	MeBo	23.06.12	05:51	33°39.56	136°38.04
GeoB16729-11	SO 222 A	MV#4 mud ridge	GC 6 m	24.06.12	00:32	33°40.109	136°38.574
GeoB16730-1	SO 222 A	MV#4 crest	CPT	24.06.12	02:14	33°39.379	136°38.012
GeoB16731-1	SO 222 A	MV #3 NE	GC 6m	24.06.12	07:09	33°38.236	136°40.525
GeoB16732-1	SO 222 A	MV #3 NE	MeBo	24.06.12	09:17	33°38.20	136°40.48
GeoB16733-1	SO 222 A	MV #9	HF	25.06.12	20:05	33°38.188	136°33.284
GeoB16734-1	SO 222 A	MV #9	GC 6 m	26.06.12	02:12	33°38.157	136°33.456
GeoB16735-1	SO 222 A	MV #3	GC 6 m	26.06.12	05:04	33°38.242	136°40.437
GeoB16736-1	SO 222 A	MV #4 crest	GC 6 m	26.06.12	07:21	33°39.348	136°38.024
GeoB16736-2	SO 222 A	MV #4 crest	GC 6 m	26.06.12	09:13	33°39.351	136°38.008
GeoB16737-1	SO 222 A	MV #4 top	MeBo	26.06.12	11:04	33°39.350	136°38.040
GeoB16738-1	SO 222 A	MV buried	GC 6 m	27.06.12	02:38	33°37.155	136°22.829
GeoB16739-1	SO 222 A	MV buried	GC 6 m	27.06.12	04:36	33°36.777	136°22.183
GeoB16740-1	SO 222 A	MV #10 top	GC 6 m	27.06.12	06:58	33°32.853	136°16.986
GeoB16741-1	SO 222 A	MV #10 top	MeBo	27.06.12	09:17	33°32.870	136°16.91
GeoB16742-1	SO 222 A	MV #10 E crest	GC 6 m	27.06.12	22:35	33°32.917	136°17.025
GeoB16743-1	SO 222 A	MV #10	GC 6 m	28.06.12	00:30	33°32.866	136°16.883
GeoB16744-1	SO 222 A	MV #10 top	TV-grab	28.06.12	04:30	33°32.869	136°16.956
GeoB16745-1	SO 222 A	Western MV-area	HF	28.06.12	13:14	33°34.330	136°33.25
GeoB16746-1	SO 222 A	MV #5 top	GC 6 m	29.06.12	01:26	33°40.593	136°34.002
GeoB16747-5	SO 222 A	MV #5 top	GC 6 m	29.06.12	03:14	33°40.673	136°34.015
GeoB16748-1	SO 222 A	MV #5 top W	GC 6 m	29.06.12	04:59	33°40.492	136°33.916
GeoB16749-1	SO 222 A	MV #6 caldera	GC 6 m	29.06.12	06:50	33°41.037	136°33.669
GeoB16750-1	SO 222 A	MV #6 caldera	GC 6 m	29.06.12	08:20	33°41.093	136°33.571
GeoB16751-1	SO 222 A	MV #7	GC 6 m	29.06.12	10:19	33°44.127	136°34.046
GeoB16752-1	SO 222 A	Easter MV area	HF	04.07.12	09:10	33°42.700	136°37.863
GeoB16753-1	SO 222 A	MV #4 top	ROV	05.07.12	01:00	33°39.517	136°37.990
GeoB16754-2	SO 222 A	MV #4 N-flank	GC 6 m	05.07.12	14:59	33°39.489	136°38.038
GeoB16755-1	SO 222 A		Parasound	05.07.12	17:18	33°39.62	136°38.14
GeoB16756-1	SO 222 A	MV #11 NE top	GC 6 m	05.07.12	23:41	33°23.272	136°42.431
GeoB16757-1	SO 222 A	MV #11 top	GC 6 m	06.07.12	02:39	33°23.292	136°42.389
GeoB16758-2	SO 222 A	Background	GC 6 m	06.07.12	05:44	33°28.113	136°39.978
GeoB16759-3	SO 222 A	MV #12	GC 6 m	06.07.12	07:42	33°31.326	136°39.885
GeoB16760-1	SO 222 A		HF	06.07.12	11:33	33°25.280	136°41.943
GeoB16761-1	SO 222 A		Parasound	06.07.12	17:33	33°21.78	136°40.97
GeoB16762-6	SO 222 A	MV #12	GC 6 m	06.07.12	23:54	33°31.337	136°39.882
GeoB16763-1	SO 222 A		GC 6 m	07.07.12	04:05	33°39.995	136°53.012
GeoB16764-1	SO 222 A	MV #2	GC 6 m	07.07.12	06:15	33°40.548	136°55.334
GeoB16765-1	SO 222 A		Parasound	07.07.12	11:30	33°44.517	136°44.548
GeoB16766-1	SO 222 A		HF	07.07.12	15:44	33°39.338	136°40.907
GeoB16767-1	SO 222 A	MV #3	ROV	08.07.12	00:34	33°38.026	136°40.351
GeoB16768-1	SO 222 A	MV #4	ROV	08.07.12	11:20	33°38.02	136°40.28

GeoB16769-1	SO 222 A	MV #3 to MV #2	HF	08.07.12	16:55	33°38.351	136°30.649
GeoB16770-1	SO 222 A	MV #2	TV-grab	09.07.12	02:16	33°40.553	136°55.225
GeoB16771-1	SO 222 A	MV #2	GC 6 m	09.07.12	05:17	33°40.496	136°55.409
GeoB16772-1	SO 222 A	MV #2	GC 6 m	09.07.12	07:40	33°40.518	136°55.195
GeoB16773-1	SO 222 A	MV #2	CPT	09.07.12	10:17	33°40.649	136°55.214
GeoB16774-1	SO 222 A	MV #2	HF	09.07.12	14:56	33°40.793	136°56.247
GeoB16775-1	SO 222 A	MV #2	ROV	10.07.12	00:24	33°40.57	136°55.45
GeoB16776-1	SO 222 A	MV #2	CAT meter	10.07.12	02:28	33°40.582	136°55.318
GeoB16777-1	SO 222 A	MV #2	CPT	10.07.12	05:00	33°40.65	136°55.20
GeoB16778-1	SO 222 A		Parasound	10.07.12	07:13	33°40.63	136°55.19
GeoB16778-2	SO 222 A		HF	10.07.12	10:06	33°39.273	136°46.283
GeoB16779-1	SO 222 A		CTD	11.07.12	10:00	33°39.37	136°38.05
GeoB16780-1	SO 222 A	MV #13	GC 6 m	11.07.12	03:30	33°46.115	136°54.886
GeoB16781-1	SO 222 A	MV #13	GC 6 m	11.07.12	05:10	33°46.105	136°54.865
GeoB16782-1	SO 222 A	MV #13	GC 6 m	11.07.12	06:43	33°46.100	136°54.775
GeoB16782-2	SO 222 A	MV #14	GC 6 m	12.07.12	08:06	33°46.118	136°54.769
GeoB16783-1	SO 222 A	MV #13	Parasound				
GeoB16784-1	SO 222 A	MV #13 top	HF	11.07.12	10:50	33°46.718	136°54.831
GeoB16785-1	SO 222 A	MV #3 top	CAT meter	12.07.12	01:14	33°38.014	136°40.25
GeoB16785-2	SO 222 A	MV #3 top	GC 6 m	12.07.12	06:17	33°38.213	136°40.427
GeoB16786-1	SO 222 A	Kumano Basin	Parasound	12.07.12	07:37	33°38.02	136°40.29
GeoB16787-1	SO 222 A	MV #4 top	ROV	12.07.12	06:14	33°39.37	136°37.97
GeoB16788-1	SO 222 A	MV #2	GC 6 m	13.07.12	02:00	33°40.515	136°55.335
GeoB16788-2	SO 222 A	MV #2	GC 6 m	14.07.12	03:44	33°40.525	136°55.264
GeoB16789-1	SO 222 A	MV 4 top	TV-grab / Smart Plug	13.07.12	07:10	33°39.384	136°38.043
GeoB16790-1	SO 222 A	Kumano Basin	HF	13.07.12	13:00	33°35.341	136°26.245
GeoB16791-1	SO 222 A	MV #14	HF	14.07.12	02:00	33°40.665	136°25.128
GeoB16791-2	SO 222 A	MV #14	GC 6 m	14.07.12	03:50	33°40.66	136°25.13
GeoB16792-1	SO 222 A	Northern ridge	HF	14.07.12	06:02	33°40.504	136°26.966
GeoB16793-1	SO 222 A	MV #2	TV-grab	14.07.12	11:10	33°40.57	136°55.426
GeoB16794-1	SO 222 A	Kumano Basin	HF	14.07.12	17:23	33°26.502	136°58.522
GeoB16795-1	SO 222 A	Kumano Basin	Parasound	15.07.12	07:11	33°11.01	136°24.18

9.2 Lithologs and shear strength data

9.3 Core photographs and MSCL

9.4 Weekly reports to PtJ / BMBF (in German)

IMPORTANT NOTE:
Chapters 9.2 – 9.4 only appear in the electronic version as part of
"Berichte des Fachbereichs Geowissenschaften der Universität Bremen"

From report No. 289 onwards this series is published under the new title:
Berichte aus dem MARUM und dem Fachbereich Geowissenschaften der Universität Bremen
A complete list of all publications of this series from no. 1 to 292 (1986 – 2012) was printed at last in issue no. 292.

No. 289 – Mohtadi, M. and cruise participants (2012). Report and preliminary results of RV SONNE Cruise SO 223T. TransGeoBiOc. Pusan – Suva, 09.09.2012 – 08.10.2012. 47 pages.

No. 290 – Hebbeln, D., Wienberg, C. and cruise participants (2012). Report and preliminary results of R/V Maria S. Merian cruise MSM20-4. WACOM – West-Atlantic Cold-water Corals Ecosystems: The West Side Story. Bridgetown – Freeport, 14 March – 7 April 2012. 120 pages.

No. 291 – Sahling, H. and cruise participants (2012). R/V Heincke Cruise Report HE-387. Gas emissions at the Svalbard continental margin. Longyearbyen – Bremerhaven, 20 August – 16 September 2012. 170 pages.

No. 292 – Pichler, T., Häusler, S. and Tsuonis, G. (2013). Abstracts of the 3rd International Workshop "Research in Shallow Marine and Fresh Water Systems". 134 pages.

No. 293 – Kucera, M. and cruise participants (2013). Cruise report of RV Sonne Cruise SO-226-3. Dip-FIP - The extent and structure of cryptic diversity in morphospecies of planktonic Foraminifera of the Indopacific Warm Pool. Wellington – Kaohsiung, 04.03.2013 - 28.03.2013. 39 pages.

No. 294 – Wienberg, C. and cruise participants (2013). Report and preliminary results of R/V Poseidon cruise P451-2. Practical training cruise onboard R/V Poseidon - From cruise organisation to marine geological sampling: Shipboard training for PhD students on R/V Poseidon in the Gulf of Cádiz, Spain. Portimao – Lisbon, 24 April – 1 May 2013. 65 pages.

No. 295 – Mohtadi, M. and cruise participants (2013). Report and preliminary results of R/V SONNE cruise SO-228, Kaohsiung-Townsville, 04.05.2013-23.06.2013, EISPAC-WESTWIND-SIODP. 107 pages.

No. 296 – Zonneveld, K. and cruise participants (2013). Report and preliminary results of R/V POSEIDON cruise POS448. CAPRICCIO – Calabrian and Adriatic Past River Input and Carbon ConversIOn In the Eastern Mediterranean. Messina – Messina, 6 – 23 March 2013. 47 pages.

No. 297 – Kopf, A. and cruise participants (2013). Report and preliminary results of R/V SONNE cruise SO222. MEMO: MeBo drilling and in situ Long-term Monitoring in the Nankai Trough accretionary complex, Japan. Leg A: Hong Kong, PR China, 09.06.2012 – Nagoya, Japan, 30.06.2012. Leg B: Nagoya, Japan, 04.07.2012 – Pusan, Korea, 18.07.2012. 121 pages.